PROGRAMA DE DOCTORADO EN
INVESTIGACIÓN BIOMÉDICA

TESIS DOCTORAL:

Identification of a new mechanism for preserving lysosomal functional integrity upon oxidative stress.

Presentada por Raquel Pascua Maestro para optar al grado de Doctora por la Universidad de Valladolid

Dirigida por:

Dra. María Dolores Ganfornina Álvarez

Dr. Diego Sánchez Romero

To Mateo

Nothing in life is to be feared, it is only to be understood (Marie Curie)

SUMMARY

Environmental insults such as oxidative stress (OS) damage cell membranes. Lysosomes are particularly sensitive to membrane permeabilization since their functions require stable membrane-dependent proton gradients. The Lipocalin Apolipoprotein D (ApoD) is a lipid binding protein endowed with antioxidant capacity. Astrocytes secrete ApoD to help neurons cope with the challenge.

In this thesis we perform a comprehensive analysis of ApoD intracellular trafficking and demonstrate its role in lysosomal pH homeostasis upon paraquat-induced OS. We demonstrate that ApoD is endocytosed and targeted to a subset of vulnerable lysosomes in a stress-dependent manner, it is functionally stable in lysosomes, and its presence is sufficient and necessary for them to recover from OS-induced lysosomal alkalinization, both in astrocytes and neurons.

We also demonstrate that extracellular vesicles (EVs) with ApoD transfer between different cells exist *in vitro* cultures. This thesis characterizes different ApoD positive EVs involve in the glia-neuron communication.

Furthermore, ApoD function ensures processes as diverse as cell survival upon oxidative stress, adequated compaction of myelin (by controlling glycolipid recycling processes), or proper phagocytic activity. We will describe its role in these processes.

The crucial role of ApoD within the lysosome leds us to study the potential effects of ApoD on neurodegenerative diseases of different origins: proteinopathic neurodegeneration in Type I Spinocerebellar Ataxia and a particularly devastating Lysosomal storage disease (LSD), the Niemann Pick type A disease (NPA). While oxidative stress induces an accelerated entry of ApoD into the lysosomal compartment of healthy cells, such accelerated targeting is lost in the diseased cells, contributing to the vulnerability of lysosomes. We demonstrate that exogenously added ApoD is able to significantly reduce lysosomal permeabilization and NPA-promoted lysosomal alkalinization, resulting in a significant increase in cell survival.

Our results uncover previously unknown ApoD biological properties (location and transport) and funtions, which allows us to better understand the biological processes that it is involved and open therapeutic opportunities to repair lysosomes in pathological situations.

RESUMEN

El estrés oxidativo (OS) daña las membranas celulares. Los lisosomas son particularmente sensibles a la permeabilización de la membrana ya que sus funciones requieren gradientes de protones estables dependientes de la membrana. La lipocalina Apolipoproteína D (ApoD) es una proteína de unión a lípidos dotada de capacidad antioxidante. Los astrocitos secretan ApoD para ayudar a las neuronas a afrontar el desafío.

En esta tesis, realizamos un análisis exhaustivo del tráfico intracelular de ApoD y demostramos su papel en la homeostasis del pH lisosomal sobre el OS inducido por paraquat. Demostramos que ApoD se endocita y se dirige a un subconjunto de lisosomas vulnerables de una manera dependiente del estrés, es funcionalmente estable en los lisosomas, y su presencia es suficiente y necesaria para que se recuperen de la alcalinización lisosómica inducida por OS, tanto en astrocitos como neuronas.

También demostramos que existe transferncia de vesículas extracelulares (EV) con ApoD entre diferentes células de cultivos *in vitro*. Esta tesis caracteriza diferentes EVs ApoD positivos implicados en la comunicación glia-neurona.

Además, la función ApoD garantiza procesos tan diversos como la supervivencia celular sobre el estrés oxidativo, la compactación adecuada de la mielina (controlando los procesos de reciclado de glucolípidos) o una actividad fagocítica adecuada. Describiremos su papel en estos procesos.

El papel crucial de ApoD dentro del lisosoma nos permite estudiar los efectos potenciales de ApoD en enfermedades neurodegenerativas de diferentes orígenes: como la neurodegeneración proteinopática en la Ataxia Espinocerebelosa Tipo I (SCA1) y una enfermedad de almacenamiento Lysosomal (LSD) particularmente devastadora, la enfermedad Niemann Pick tipo A (NPA). Mientras que el estrés oxidativo induce una entrada acelerada de ApoD en el compartimiento lisosomal en las células sanas, tal objetivo se pierde en las células enfermas, lo que contribuye a la vulnerabilidad de los lisosomas. Demostramos que la ApoD agregada exógenamente es

capaz de reducir significativamente la permeabilización y la alcalinización lisosomal promovida por NPA, dando como resultado un aumento significativo en la supervivencia celular.

Nuestros resultados descubren propiedades biológicas (ubicación y transporte) y funciones de ApoD previamente desconocidas, lo que nos permite comprender mejor los procesos biológicos en los que está involucrada y abrir oportunidades terapéuticas para reparar los lisosomas en situaciones patológicas.

INDEX

ABBREVIATIONS

[ ]	Concentration
»	Wavelength
3-MA	3-Methyladenine
4-HNE	4-Hydroxynonenal
AOBS	Acousto-optical beam splitter
AOTF	Acousto-optic tunable filter
AP	Autophagosome
ApoD	Apolipoprotein D
ApoE	Apolipoprotein E
ASM	Acid sphingomyelinase
ATXN1	Ataxin 1
bhApoD	Bacterial human Apolipoprotein D
BSA	Bovine serum albumin
BSG	Basigin
CAT	Catalase
CAV	Caveolin
CCD	Charge-coupled device
CD81	Cluster of Differentiation 81
CDS	Coding DNA sequence
CM	Conditional medium
CNS	Central Nervous System
Cox	Cyclooxygenase
cPLA2	Cytosolic Phospholipase A2

CQ	Chloroquine
Cy3/5	Cyanine Dyes 3/5
DAPI	4 ',6-diamino-2-fenilindol
DHA	Docosahexaenoic acid
DiI	1,1'-Dioctadecyl-3,3,3',3'-Tetramethylindocarbocyanine Perchlorate
DMEM	Dulbecco's Modified Eagle's medium
DMF	Dimethylformamide
DMSO	Dimethyl sulfoxide
DNA	Deoxyribonucleic acid
DRM	Detergent-resistant membrane
DTT	Dithiothreitol
EBSS	Earle's Balanced Salt Solution
ECL	Enhanced chemiluminescence
EE	Early endosomes
EEA1	Early endosome antigen 1
EM	Electron Microscopy
ERK	Extracellular Signal-regulated Kinase
Et-OH	Etanol
EVs	Extracellular vesicles
FBS	Fetal bovine serum
Gal3	Galectin-3
Gal4	Galactose-induced gene 4
GFAP	Glial fibrillary acidic protein

GFP	Green fluorescent protein
GLaz	Glial Lazarillo
gmr	Glass multiple reporter promoter element
hApoD	Human Apolipoprotein D
HDL	High density lipoproteins
HEK293T	Human embryonic kidney cell line
HEPES	Hydroxyethyl piperazineethanesulfonic acid
HOPS	Homotypic fusion and protein sorting
HRP	Horseradish peroxidase
ICQ	Intensity correlation quotient
ILVs	Intraluminal vesicles
ILVs	Intraluminal vesicles
IPL	Intraperiodic line
IREG	Regularity index
JNK	Junk protein
kDal	KiloDalton
KO	Knock out
L	Lysosome
LAMP-1	Lysosomal-associated membrane protein 1
LAMP-2	Lysosomal-associated membrane protein 2
Lcn2	Lipocalin-2
LE	Late endosome
LELC	Late endosomal-lysosomal compartment
l-Glut	L-glutamine

LLME	L-leucyl-L-leucine methyl ester
L-pH	Lysosomal pH
LPL	Lipoprotein lipase
LPL	Lipoprotein lipase
LRO	Lysosomal related organelles
LS	Low serum
LSDs	Lysosomal Storage Diseases
LUTs	Pseudocolor Image Look-Up Tables
MAA	*Maackia amurensis*
Mag	Myelin Associated Glycoprotein
Mbp	Myelin basic protein
MD	Membrane domains
MES	2-(N-Morpholino)ethanesulfonic acid
Mito	Mitochondria
mRNA	Messenger RNA
MTT	3-(4,5-dimethylthiazol-2-yl)-2,5-diphenyltetrazolium bromide
MVBs	Multivesicular bodies
MVs	Microvesicles
Neu1	Sialidase 1
Neu3	Neuraminidase 3
Nlaz	Neural Lazarillo
NOS	Nitric oxide synthases
NPA	Niemann Pick disease type A

NPD	Niemann Pick disease
NTA	Nanoparticle tracking analysis
OS	Oxidative stress
P/S	Penicillin-Streptomycin
P/S/A	Penicillin-Streptomycin-Amphoterycin B
PB	Phosphate buffer
PBS	Phosphate-buffered saline
PCA	Principal component analysis
PFA	Phosphate-buffered formaldehyde
PMSF	Fluoride phenylmethylsulfonyl
PNS	Periferal Nervous System
poly-Q	Polyglutamine
PQ	Paraquat
PVDF	Polyvinylidene difluoride
RA	Retinoic acid
RE	Recycling endosome
RER	Endoplasmic reticulum
RNAi	Interfering RNA
ROIs	Regions of interest
ROS	Reactive oxygen species
SCA1	Type I Spinocerebellar Ataxia
SEM	Standard error of the mean
SER	Smooth endoplasmic reticulum
SH-SY5Y	Human neuroblastoma cell line

SM	Sphingomyelin
SOD	Superoxide dismutase
TBS	Tris-buffered saline
TEM	Transmission Electron Microscopy
TGN	Trans-Golgi network
TNF±	Tumor necrosis factor alpha
UAS	Upstream Activation Sequence
VLDL	Very low density lipoproteins
WT	Wild type

Introduction

1. Apolipoprotein D.

    1.1 The neuroprotective role of Apolipoprotein D.

    1.2 Oxidative stress: its effects on the nervous system.

    1.3 The role of lipids in the function of ApoD.

    1.4 Evidences of ApoD intracellular trafficking.

2. The cellular trafficking of membrane-asociated proteins: a complex network of vesicles.

    2.1 The Lysosomes.

    2.2 Biogenesis and function of extracellular vesicles.

3. Lysosomal storage diseases.

The general objective of this thesis is to decipher the mechanism of action of the neuroprotective protein Apolipoprotein D (ApoD). For this purpose, it is necessary to know ApoD subcellular trafficking and its role under oxidative stress conditions. For this reason, this introduction will describe, on the one hand, the structural and molecular characteristics of ApoD. Next, the existing evidences of the neuroprotective function of ApoD will be shown, and the bases of oxidative stress as an important parameter to be taken into account. On the other hand, the most important aspects related to intra and intercellular trafficking, to understand the context in which this work has been done. Finally, a review of the neurodegenerative diseases in which the ApoD intervention has been studied will be made.

1. Apolipoprotein D.

ApoD is a lipid binding protein of the Lipocalin family first known as part of bloodstream lipoprotein particles [1] where it is associated with high density lipoproteins (HDL) and in a lesser proportion very low density lipoproteins (VLDL) [2-4]. Due to its location in HDL, ApoD was initially considered as a member of the Apolipoprotein group. However, based on the prediction of its tertiary structure from its sequence [5] it was included in the family of Lipocalins.

Lipocalins are typically small (160-230 amino-acid residues) extracellular proteins [6]. The Lipocalins belong to a set of families mainly defined by its structural homology. The Lipocalin fold consists of a ²-barrel, forming a cup or calyx, with a central cavity that serves as a ligand-binding site [7]. This cavity, or pocket, is usually

outlined by apolar amino acids and is ideal for binding small hydrophobic compounds [8, 9]. Many Lipocalins present N- and/or O-linked glycosylation, and glycosylation residues range from none to six. Glycosylation is known to confer different properties and functional properties [10, 11]. Their functions cannot be completely understood without taking into account their ligands [12-14].

The hApoD mature protein, after secretory signal peptide removal, is composed by 169 amino acids [15]. hApoD has been crystallized and its structure solved [14]. The wide calyx of ApoD allows the binding of hydrophobic molecules of different nature. Some molecules that ApoD can bind are progesterone, arachidonic acid [16], retinol, retinoic acid [17], and sphingomyelin [18].
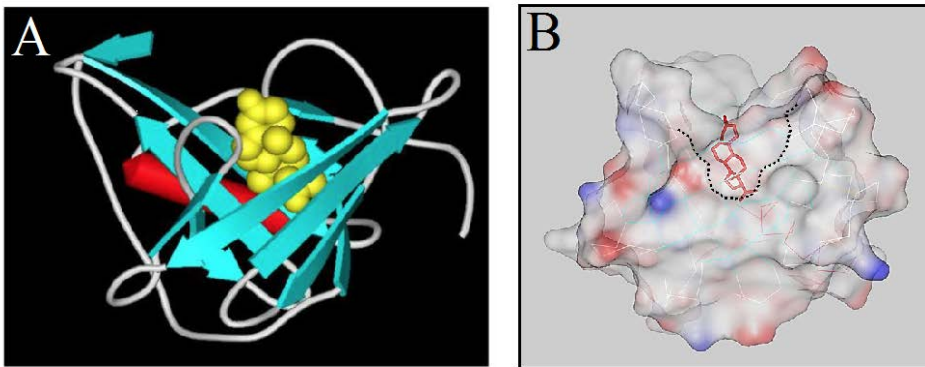
Figure 1. Three-dimensional structure of the hApoD. A. *The β-barrel is shown in blue, formed by 8 β-sheets, and the ±-helix is shown in red. ApoD bound to progesterone (in yellow). Code in the Protein Data Bank (PDB: 2HZQ).* **B**. *Same structure represented as surface accessible to the solvent.*

hApoD has different glycosylation sites and two different glycosylation patterns have been reported: in plasma and in apocrine secretions, such as saliva or sweat. Its molecular weight varies between 19 and 32 kDal, depending on the degree of glycosylation [19, 20].

In humans, ApoD mRNA has been detected in adrenal glands, pancreas, kidneys, placenta, spleen, lungs, ovaries, testes, brain and peripheral nerves [3, 5]. In the mouse, the expression of ApoD is observed mainly in the central nervous system (CNS),

specifically in the spinal cord, brain and cerebellum [21] but also in the peripheral nervous system (PNS).

In the CNS, ApoD is expressed by glial cells, specifically by astrocytes and oligodendrocytes [22, 23], from embryonic and postnatal development to aging [24, 25]. In the PNS, ApoD is expressed under normal conditions by fibroblasts [26] and by Schwann cells [27, 28]. Neuronal expression of ApoD has been described in the CNS during development [22, 29], but not in peripheral axons.

In Drosophila melanogaster, ApoD homologs, called Lazarillo, are expressed in neurons (Nlaz) and glia (Glaz) [30-32]. This indicates that the expression of ApoD in the nervous system is evolutionarily conserved. NLaz, like ApoD, binds *in vitro* retinoic acid and sphingomyelin [12]. On the other hand, GLaz is found in the longitudinal glia of the developing ventral nerve cord of the central nervous system (CNS), and in specific glial precursors during late stages of embryogenesis [32-34]. The study of GLaz and ApoD experimental data discloses a number of points in common, which will synergically lead to a better understanding of their biological function.

1.1 The neuroprotective role of Apolipoprotein D.

In humans, ApoD is up-regulated in many pathological situations, including schizophrenia [35], Alzheimer's [36], and Parkinson's disease [37]. Additionally, ApoD levels are altered in several types of cancers [38] and lysosomal disease [39].

ApoD is one of the few genes consistently over-expressed in the aging brain, and in all neurodegenerative and psychiatric diseases tested so far [40]. In addition, it is remarkable the high levels of ApoD expression during development [41].

APOD-KO mice of the C57BL / 6J strain were generated by homologous recombination. The wild allele was substituted by a null one due to the insertion of the neomycin phosphotransferase (Neo) gene in exon 6 of the ApoD gene. They show an increase in lipid peroxidationin the brain, lower resistance to Paraquat (PQ), and failures in behavioral tests; a decrease in locomotor and exploratory activity and memory deficit [42]. The lack of ApoD generates a basal oxidative stress that causes

an increase in the expression of genes related to the oxidative stress response (GFAP) and an abnormal expression of them in response to the oxidation induced by PQ [43].

Protecting and pro-survival functions for ApoD keep accumulating both in animal models and in cell systems, revealing a functional pleiotropy that connects nervous system response to oxidative stress, recovery after injury, brain aging, or diverse forms of neurodegeneration.

GLaz expression level has been experimentally altered in Drosophila using genetic tools [6]. Due to GLaz ability to deal with oxidative stress, the effect of GLaz over-expression has been studied in the context of flies that model human neurodegenerative diseases. One example is the Drosophila retinal degeneration model on a poly-Q triggered disease, the Type I Spinocerebellar Ataxia (SCA1), a polyglutamine disease characterized by the expansion by repetition of CAG and loss of CAT in the coding region of the ataxin-1 gene (SCA1). In this model [44], photoreceptors accumulate nuclear inclusions of the human protein. Protein aggregates can impair axonal transport, alter transcription factors and block protein quality control systems [45]. The induction of autophagy has protective effects in models of polyglutamine diseases [46].

It has proved to be part of the endogenous transcriptional protective response against poly-Q-based neurodegeneration. GLaz overexpression rescues neurodegeneration. GLaz gain-of-function in this model promotes clearance of ubiquitinated proteins, reduces the accumulation of the autophagy cargo receptor p62 and thereby reduces apoptotic cell death. GLaz enters the degenerating neurons by endocytosis and promotes the resolution of autophagy, increasing its flow and helping to clear poly-Q-induced protein aggregates [33].

1.2 Oxidative stress: its effects on the nervous system.

The most important phenotypes of the ApoD-KO mouse have been shown in situations of oxidative stress. Oxidative stress in biological systems is an imbalance between the production of reactive oxygen species and the mechanisms responsible for eliminating them or repairing the damage they generate. ROS (reactive oxygen species) are highly destructive products of aerobic metabolism [47].

Oxidative stress is closely related to a wide variety of neurodegenerative diseases, including age-related disorders. In particular, lipid peroxidation is a source of damage present in many neurodegenerative diseases, including Alzheimer's disease and other types of dementia, Parkinson's disease, Huntington's disease, Niemann-Pick diseases, etc. [48]. Levels of lipid peroxidation in various organs, including the brain, increase with aging [49].

Elevated levels of oxidized proteins also correlate with diseases associated with age and disease progression [50]. Oxidation inactivates enzymes affecting a wide variety of biochemical processes while the accumulation of unusable oxidized proteins endangers cellular functions and viability [51].

For the study of the mechanisms involved in oxidation, drugs and compounds that induce the formation of ROS are used. Paraquat is one of the most widely used compounds (1,2-dimethyl 4-4-bipyridinium). PQ is a non-selective ROS-generating herbicide. The toxicity mechanism of PQ [52] would be controlled by SOD (Fig. 2).
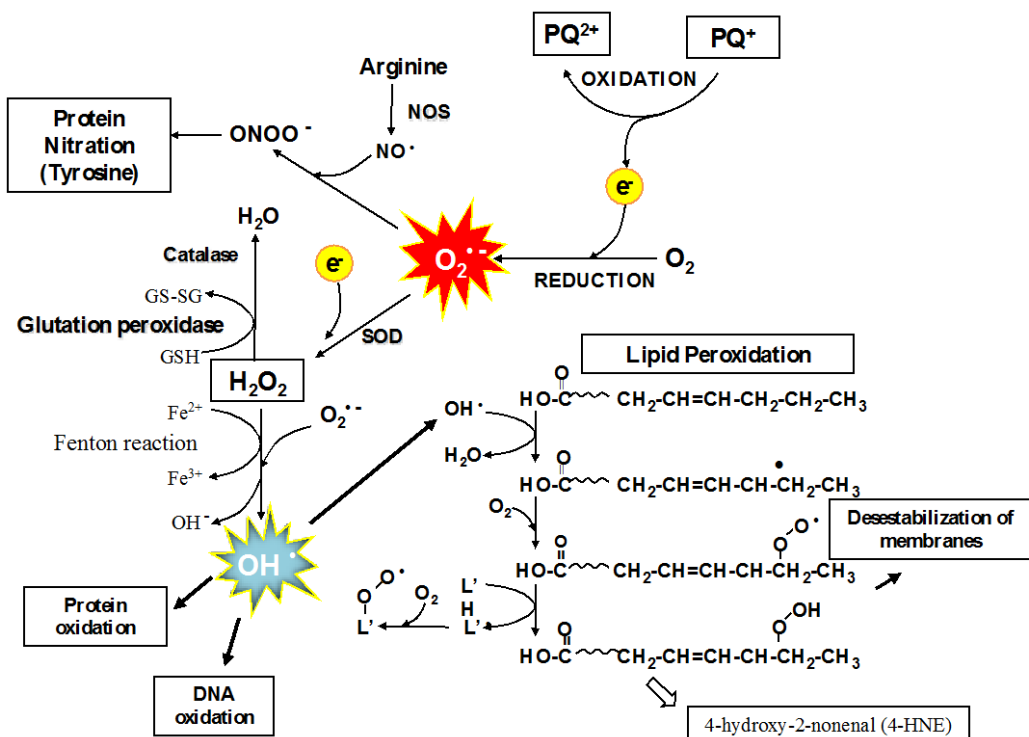
Figure 2. Diagram of molecular and cellular consequences of Paraquat treatment. Paraquat is oxidized causing the reduction of O_2 to superoxide anion. This anion can cause the nitration of proteins through the oxidation of nitric oxide (NO^-) (radical generated by nitric oxide synthases (NOS) from the amino acid arginine). Superoxide dismutase (SOD) has the capacity to transform the superoxide anion into hydrogen peroxide that in turn can be transformed into H_2O by the action of catalase or hydroxyl anion, through the Fenton reaction. The hydroxyl anion produces the oxidation of proteins, lipids and DNA (modified from [53]).

Endogenously, one of the proteins that are up-regulated under oxidative stress caused by PQ exposure is Apolipoprotein D (ApoD) [42].

1.3 The role of lipids in the function of ApoD.

In addition to the control of lipid peroxidation, many connections between ApoD and lipids are often established. In fact, the addition of ApoD has recently been described for the antioxidant activity of lipids and Alzheimer's disease. ApoD is able to reduce hydroperoxieicosatetraenoic acids to their hydroxy derivatives, a process that can contribute to the antioxidant function of ApoD [54].

On the other hand, the fatty acid composition in the brain of these mice without ApoD is altered. Specifically, they present an increase in palmitic acid (16:00) and stearic acid (18:00) and also in polyunsaturated fatty acids such as linoleic acid (18: 2), eicosadienoic acid (20: 2) and DHA (22: 6) [35]. The lack of ApoD is associated with a decrease in the activity of lipoprotein lipase (LPL), an increase in triglycerides and hyperinsulinemia [46].

A model of damage in the mouse peripheral nerve reveals that the lack of ApoD increases the duration and magnitude of the inflammatory response by delaying regeneration. Also, the absence of ApoD alters the thickness of the myelin sheath decreasing the speed of electrical conduction of neurons [55, 56]. ApoD-KO myelin is less hydrophobic than WT myelin. The most direct cause of the anomalous hydrophilicity and uncompacted outer leaflet in ApoD-KO myelin would be a deficit in glycocalyx removal [57]. A clear increase in sialic acid content was observed in ApoD-KO nerves [57]. This process is carried out in lysosomes, a key organelle in the role of ApoD.

The lack of ApoD also modifies the signaling between Schwann cells and macrophages, the phagocytosis activator Galectin-3 and the levels of lysophosphatidylcholine and arachidonic acid after damage indicating that ApoD favors the initiation of phagocytosis and promotes the degradation of myelin [56, 57].

1.4 The ApoD intracellular trafficking.

ApoD is internalized by different cell types including astrocytes and neurons [29, 58-60], not being described its subcellular trafficking yet. It was described that basigin (BSG, CD147); is very likely the ApoD receptor [58]. BSG is a multifunctional cell surface transmembrane glycoprotein. However, the exact mechanisms of interaction between ApoD and BSG remain to be determined.

In our laboratory it has been discovered that ApoD behaves as a peripheral membrane protein associated to detergent-resistant membrane (DRM) domains in a stable and independent of species manner [61]. Lipid rafts, membrane domains, or detergent-resistant membranes (DRM), are some of the names they have received. Multiple functions of the membrane domains have been suggested, especially the generation and maintenance of polarity, membrane trafficking and signal transmission [62, 63]. Specifically ApoD appears linked to membrane domains extracted by Triton X-114 characterized as cellular membrane domains rich in gangliosides.

This relationship between ApoD and lipid rafts, a membrane domain involved in a large number of signaling processes, could condition cell fate.

2. The cellular trafficking of membrane-asociated proteins: a complex network of vesicles.

In eukaryotic cells, the system of network of vesicles reaches a remarkable development and it is there where a great part of the vital reactions are carried out. The endoplasmic reticulum, the Golgi apparatus, the endosomes and the lysosomes belong to the endomembrane system of the cell, together with the nuclear envelope. As a result of the resulting cell compartimentalization, the molecules travel throught exchange vesicles between compartments [64].

The internal membrane system, besides forming the nuclear envelope, constitutes a complex network of canals called endoplasmic reticulum, responsible for the synthesis of many proteins and cellular lipids [65]. Lipid droplets are formed from an increasing accumulation of esterified lipids between the two monolayers of the smooth endoplasmic reticulum (SER) membrane. When they reach a critical size, this cluster of lipids separates and remains free in the cytosol surrounded by the outer monolayer of the reticulum membrane [66].

The rough endoplasmic reticulum (RER) connects with other membranes that form groups of superposed sacs that constitute the Golgi apparatus, where many of the modifications of proteins such as glycosylation are produced. From here, the molecules migrate in exocytosis vesicles towards the plasma membrane, where they will merge by spreading the content to the extracellular space. The Golgi apparatus also produces vesicles that contain enzymes needed for cellular digestion. They are called lysosomes [67].

Other vesicles with very different functions are the peroxisomes, where essential peroxides are generated in the oxidation of fatty acids and in the synthesis of certain membrane lipids [68]. Membranous organelles that present certain autonomy are the mitochondria, which perform the oxidative metabolism [69].

The endocytic pathway consist of highly dynamic membrane compartments (Fig.3) involved in the internalization of extracellular ligands or celular components, their recycling to the plasma membrane, and /or their degradation [70]. One of the compartments of the endocytic pathway are early endosomes (EE), that matures into late endosomes [71] by changes in form, size, content and pH [72].
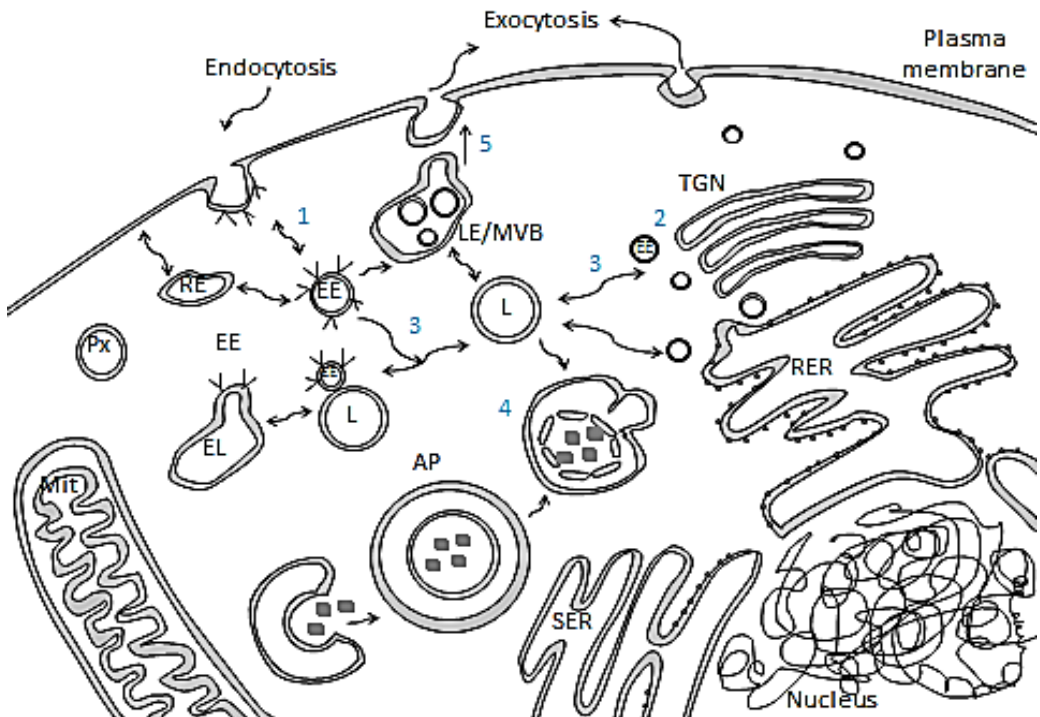
Figure 3. The cellular trafficking of membrane-asociated proteins. Lysosomes (L) are terminal compartments of the endocytic and autophagic pathways (autophagosome AP). Newly synthesized lysosomal proteins are delivered to them from the trans-Golgi network (TGN) via early endosomes (EE), recycling endosomes (RE), and late endosomes/multivesicular bodies (LE/MVB). Following lysosome fusion with late endosomes to form an endolysosome (EL).

Early endosomes would be formed by the convergence and fusion of endocytosis vesicles. This would occur in the vicinity of the plasma membrane (step 1-Fig. 3). Later they would move towards the cellular interior. During their journey they mature, becoming recycled endosomes, producing vesicles back to the plasma membrane, and later late endosomes / multivesicular body, which receive vesicles from the Golgi apparatus (step 2-Fig. 3), and send others back to the Golgi apparatus. Eventually they would become lysosomes or merge with them (step 3-Fig. 3) [73]. The lysosomes can be fused with an autophagosome, double membrane organelle. In this way, cytoplasmic material will be degraded along with the internal membrane of the autophagosome, in the process of autophagy (step 4-Fig. 3) [74].

So all the types of endosomes described are only states of a continuous maturation process [75]. Sometimes multivesicular bodies, instead of becoming lysosomes, fuse with the plasma membrane releasing their internal vesicles into the extracellular space (step 5 Fig. 3). These released vesicles are called exosomas [76].

2.1 The Lysosomes.

Lysosomes are a key and fundamental element of the cell. Lysosomes are acidic intracellular vesicles surrounded by a simple membrane, and located in the cytoplasm, that provide an optimal physicochemical milieu for enzymatic activities, most of them catabolic, which need to be controlled. It contains hydrolytic enzymes, proteins that control the internal pH and proteins that transport the initial or final products of digestion inside or outside the lysosome. Lysosomes were once considered the end point of endocytosis, simply used for macromolecule degradation. They are now recognized to be dynamic organelles, able to fuse with a variety of targets and to be formed again after fusion events.

Lysosomes are structures common to all animal cells (except red blood cells), although their content, their enzymes and their size (between 0.1-1.2 μm) vary between cell types and between lysosomes in the same cell. More than 40 lysosomal enzymes with hydrolytic activity at acid pH have been identified. The lysosomal membrane keeps these destructive enzymes separate from the rest of the cell as well as generating and controlling the optimal conditions for maximum effectiveness. A transmembrane protein, the vacuolar proton pump [V-ATPase], transports protons from the cytosol into the lysosome until a pH of around 4.8 is established [77]. At this pH, lysosomal enzymes can degrade proteins, lipids and other molecules. The proteins of the lysosome membrane are highly glycosylated making them resistant to degradation. [78]. The material that can no longer be degraded or cannot return to the cytosol forms the so-called residual bodies; if they are not exocytosed, they accumulate in the lysosomes becoming markers of cellular aging. An example of these residual bodies is the accumulations of lipofuscin: fluorescent aggregates of proteins, lipids and oxidized metals [79].

Among the proteases present in the lysosome, cathepsins are noteworthy. They can cut proteins by a cysteine, serine or aspartyl residue and are involved in several pathways of cell death and lysosomal membrane damage [80].

Other important lysosomal enzymes are neuraminidases. They have been classified as lysosomal (Neu1), cytosolic (Neu2), plasma membrane (Neu3), and mitochondria/lysosomal (Neu4) [81]. These proteins are involved in numerous metabolic processes such as cell adhesion, membrane fusion and fluidity. Neu1 initiates the intralysosomal hydrolysis of sialo-oligosaccharides, -glycolipids, and -glycoproteins by removing their terminal sialic acid residues.

LAMP proteins are abundant, ubiquitous proteins that coat the lysosome membrane and protect it from the action of lysosomal hydrolases. One of them, LAMP2 is necessary for autophagy mediated by chaperones, and its expression improves tissue function in aging models. LAMP proteins represent a cholesterol binding site controlling the availability of cholester and facilitating the export of cholesterol from lysosomes [82].

Recently, three types (or three states) of lysosomes have been defined: Conventional lysosomes that maintain the classic intracellular digestive function; a type of lysosome that fuses with the plasma membrane and secretes its content in the extracellular medium; and a third type of lysosome that would exert both functions, fusing with the plasma membrane and repairing their damaged areas [83]. The study of lysosomes has expanded its definition from being only digestive vesicles to an important part of cellular homeostasis given its involvement in multiple processes such as secretion, membrane repair, cell signaling or energy metabolism [84-87].

Lysosomes are key elements in the recycling of cellular components by autophagy since they are responsible for the correct outcome of the autophagic process. Likewise, they are centers for obtaining essential materials either by intracellular digestion of material ingested by endocytosis (such as cholesterol extraction from LDL) or by phagocytosis [88]. Therefore, the maturation of the lysosome is the point of intersection between the secretion pathway, the endocytic and autophagic pathway, through which extra and intracellular material is internalized, signaled and recycled.

In addition, lysosomes participate in the perception of the metabolic state of the cell and participate in a regulated exocytosis. We can also find lysosomal related organelles, which can be related to lysosomes by their molecular composition and physiological characteristics, or are directly modified lysosomes, such as for example lamellar bodies [89].

2.2 Biogenesis and function of extracellular vesicles.

Nervous sytem function relies on a complex set of cell types interacting and communicating among them. Besides membrane interactions that underlie adhesion and neural circuit plasticity, and secretion of signaling molecules and neurotransmitters involved in synaptic function, the discovery of extracellular vesicles (EVs) produced by most cells [90], including all neural cell types, opens up a new mechanism of signal transmission [91, 92] that is changing our understanding of how glia and neurons communicate [93-95].

Furthermore, EVs molecular composition of lipids, carbohydrates, proteins and nucleic acids [96-98] is cell type and physiological state-specific [99, 100], which makes them candidates as biomarker tools in many human diseases [101, 102]. Particularly important in brain illnesses is the potential therapeutic use of EVs, given their demonstrated bypass of the blood-brain barrier [103, 104]. In this regard, EVs purposedly loaded with neuroprotective molecules [105, 106] are a promising therapy for neurodegenerative disorders [91, 107, 108].

In this regard, two main groups have been identified: endosome-derived vesicles named exosomas and plasma membrane-shedding vesicles called ectosomes or microvesicles (MVs) (Fig 4). Other known Evs are apoptotic bodies [109] ranging from 1 to 5 μm, containing cellular portions undergoing apoptosis [110, 111], so they will not be treated in this section.
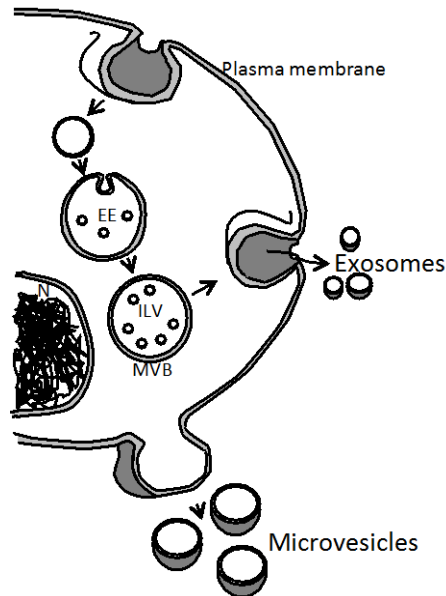
Figure 4. Biogenesis and release of extracellular vesicles. *Extracellular vesicles can be broadly classified into 2 main classes:* ***A.*** *Exosomes that are formed within the endosomal network and released upon fusion of multi-vesicular bodies with the plasma membrane.* ***B.*** *Microvesicles or ectosomes that are produced by outward budding and fission of the plasma membrane EE: early endosome; MVB: multi-vesicular body; ILVs: intraluminal vesicles; N: Nucleus. (modified by [112]).*

All EVs present important differences but share some characteristics. Moreover, the size is another of the main differences among the different types of EVs. MVS are vesicles with a diameter size that ranges from 100 to 1000 nm and exosomes ranging between 40 and 100 nm. Hewever, all EVs contain proteins, lipids and nucleic acids and also share some markers such as Annexin V, CD81 or CD9 in the case of exosomes and MVs [40]. Nevertheless, their specific composition depends on the cell type of origin and the state of them, which is revealed by proteomic analysis in large scale of EVs from various cell types [99].

Late endosomes accumulate intraluminal vesicles (ILVs) that are formed by inward budding of the late endosome membrane, at the same time some cytoplasmic molecules are engulfed. Because of the morfological features of the late endosomes, they are generally referres to as multivesicular bodies (MVBs). The MVBs, could merge with the plasma membrane and consequent reléase of ILVs to the extracellular

medium, which are then called exosomas [113, 114]. Other vesicles, MVs formed by regulated release of outward budding of the plasmic membrane [110, 111] (Fig. 4).

3. Lysosomal diseases: Lysosomal storage diseases.

The stability of lysosomal membrane is a key factor determining cell survival-death signaling [115], and its composition is essential for an efficient lysosomal enzymatic activity [116]. Reactive oxygen species (ROS) compromise lysosomal integrity due to membrane lipid peroxidation [115, 117]. An increase in ROS can cause permeabilization of the membrane, the release of cathepsins to the cytosol and apoptosis is induced [118].

Because of the critical role of its luminal pH, the alkalinization of lysosomes due to proton leakage is thought to contribute to many pathologies [119], and compensatory responses or therapeutic manipulations that restore lysosomal pH would result in clear benefits [120]. Interestingly, not all lysosomes are equally sensitive to oxidative stress or have the same luminal pH [117, 121].

Moreover, lysosomal dysfunction is known to underlie the pathogenic mechanisms of neurodegenerative disorders, such as Alzheimer's, Parkinson's and Huntington's diseases as well as physiological aging [122, 123].

Lysosomal storage diseases (LSDs) are monogenic disorders caused by mutations in genes encoding lysosomal enzymes that are responsible for metabolizing a broad spectrum of cellular substrates. However, recent evidence indicates that deficient degradation in LSDs also derives from alterations in endosomal and autophagosomal pathways, which flow into the lysosomal system.

Table 1. Summary of Human LSDs.

Lysosomal Storage Disease in Humans		
Type	**Examples**	**Implicated protein**
Carbo-hydrate storage diseases	Manosidosis, Galactosyalidosis, Mucopolysacharidosis, Pompe disease, etc.	Glucosidases, cathepsins, sulfatases, glucuronidases, etc.
Neurami-nidosis	Salla's disease	Sialic acid transporter (SLC17A5)
Sphingo-lipidosis	Niemann Picktype A and B	ASM (Acid Sphingomyelinase)
	Fabry's disease	±-Galactosidase
	Niemann Pick type C and D	NPC1 (C), NPC2 (D)
	Globoid Cell Leukodystrophy	Galactosylceramidase (GALC)
	Metachromatic Leukodystrophy	Arylsulfatase A
	Fucosidosis	±-L-fucosidase
Ganglio-sidosis	GM1 gangliosidosis I	²-galactosidase
	Sandhoff disease	²-Hexosaminidases
	Tay Sachs disease (GM2 gangliosidosis)	²-Hexosaminidase A
Muco-lipidosis	Mucolipidosis Type IV	Transient Receptor Potential-Mucolipin 1
Ceroid lipofuscinosis	Batten Disease	Ceroid-lipofuscinosis, neuronal 3 (CLN3)
	Neuronal cerois lipofuscinosis	Progranulin (PGRN/CLN11)
	Infantile neuronal ceroid lipofuscinosis	Palmitoyl-protein thioesterase 1(PPT1)

Niemann Pick disease type A (NPA) is a lipid storage disorder with an autosomal recessive inheritance and occurrs by defect of the SMPD1 gene encoding sphingomyelinase (ASM). This enzyme catalyzes sphingomyelin (SM) conversion into ceramide in lysosomes. As a result of ASM deficiency, cells from NPA patients accumulate SM in lysosomes and plasma membrane, leads to the accumulation of SM in liver and neurons [124], which in turn causes tissue dysfunction or damage [125, 126].

The disease has a severe neurological affectiont that leads to early death. In mice lacking ASM (acid sphingomyelinase knockout mice, ASMko), which are a model for NPA [127] several pathophysiological characteristics of patients with NPA can be

observed [128]. ASM - / - mice are normal at birth but the rapid progression of the disease causes them motor alterations from 2 months of age that end in ataxia and early death around 8 months [129]. ASM deficiency has consequences for different types of brain cells. In the case of the cerebellum, there is a marked degeneration of the Purkinje neurons of the granular layer, with a specific temporal and spatial pattern [130]. Because of this, ASM - / - mice show motor alterations at an early age that result in a lack of response to stimuli and ataxia [130].

Environmental insults such as oxidative stress can damage cell membranes, particularly the membranes of lysosomes. Within the nervous system, cell types in the defense line, such as astrocytes, secrete ApoD to help neurons face the challenge. EVs could be responsible for this transit. A lysosomal activity of ApoD, together with the ability to bind to lipids, the ability of overexpression in oxidative stress makes ApoD a perfect candidate for the treatment of various lysosomal diseases.

Aim of the thesis

The aim of this thesis is is to understand the biological processes where ApoD are involved, and decipher the mechanism by which ApoD exerts its neuroprotective functions. To accomplish this general plan, five specific objectives were carried out:

1. Characterization of ApoD subcellular localization and transit through different cell compartments in response to stress in the nervous system.

2. Analysis of how ApoD affects established protection processes put forward by glial cells against stress.

3. Characterization of ApoD transit between different cells of the nervous system in response to stress.

4. Analysis of how the lysosomal function of ApoD has other biological implications in physiological parameters of glial cells that express ApoD.

5. Evaluation of the possible therapeutic effect of ApoD in different neurodegenerative diseases.

Materials and Methods

Cell culture and treatments

The cell lines used in this work were obtained from Sigma-Aldrich, ATCC and Coriell Institute for Medical Research (Camden, NJ, USA). Cells were grown at 37°C in humidity-saturated atmosphere containing 5% CO_2. Culture conditions and reagents are summarized in Table 2. The culture medium was replaced twice a week, and cells were subcultured at 90% confluence. For co-cultures, cells were counted with Countess Automated Cell Counter (Invitrogen).

Table 2. Culture conditions and reagents.

Cell culture	Type	Cultured medium	Supplements
1321N1	Human astrocytoma cell line	DMEM (Lonza)	5% heat-inactivated FBS
			1% l-Glut (final concentration 2 nM)
			1% P/S/A (final concentration: 100 U/ml penicillin, 100 U/ml streptomycin, 0.25 µg/ml amphoterycin B)
SH-SY5Y[1]	Human neuroblastoma cell line	DMEM supplemented with 4.5 g/l glucose (LONZA)	10% heat-inactivated FBS
			1% l-Glut (final concentration 2 nM)
			1% P/S (final concentration: 100 U/ml penicillin, 100 U/ml streptomycin)
HEK293T	Human embryonic kidney cell line	DMEM supplemented with 4.5 g/l glucose (LONZA)	10% heat-inactivated FBS
			1% l-Glut (final concentration 2 nM)
			1% P/S/A (final concentration: 100 U/ml penicillin, 100 U/ml streptomycin, 0.25 µg/ml amphoterycin B)

U87 Wt and clone #8 BSG-null[2]	Human Glioblastoma cell lines	DMEM (Gibco)	10% heat-inactivated FBS
			1% l-Glut (final concentration 2 nM)
			1% P/S (final concentration: 100 U/ml penicillin, 100 U/ml streptomycin)
Fibroblast[3]	Primary skin cells	Optimem supplemented with GlutaMax-I (Gibco)	10% heat-inactivated FBS
			1% l-Glut (final concentration 2 nM)
			1% P/S/A (final concentration: 100 U/ml penicillin, 100 U/ml streptomycin, 0.25 µg/ml amphoterycin B)

[1]-SH-SY5Y cells differentiation was achieved by culture on collagen-treated plates with medium supplemented with 3% FBS and Retinoic acid (10 µM). A 72h differentiation period was allowed before experiments.

[2]-U87 clone #8 BSG-null U87 and A549 BASIGIN expressing cell lines were transfected with the plasmid ZFN designed by Sigma-Aldrich (CKOZFN1227-1KT, CompoZr Custom ZFN) targeting exon 2 of BSG as previously described [131, 132].

[3]-Primary skin fibroblasts from unaffected individuals (AG7323 and GM00969) and NPA patients carrying mutations in exon 2 of the SMPD1 gene (GM13205 with deletion of a cytosine in codon 330, and GM00112 with T-C transition in the nucleotide 905) were used. AG7323 and GM13205 cells were used for immunocytochemistry and immunoblot, and GM00969 and GM00112 to study lysosomal functionality.

For the exogenous addition of ApoD, human ApoD purified from breast cystic fluid [18] or recombinant human ApoD from *E. coli* (ProSpec) were added (10 nM) to the cell cultures for 2 h. For long-term treatment (7 days), media was replaced every 48-72 h with freshly added ApoD.

Cells treated with Paraquat (PQ; Sigma; 500 µM; 1-24 h), Sphingomyelin (SM; Sigma; 40 µM; 24 h-7 d), Chloroquine (CQ; Sigma; 20 µM; 1 h), Rapamycine (Rap; LC Laboratories; 2 µM; 2 h), and 3-Methyladenine (3-MA; Sigma; 5 mM; 2 h) were cultured in phenol red-free DMEM supplemented with 4.5 g/l glucose (LONZA), 1% L-glutamine, 1% P-S, and 0.2% charcoal stripped FBS. This medium without additives was used as our low-serum (LS) condition. Sphingomyelin was dissolved in ethanol.

The expression constructs used in this work (pcDNA3.1-ApoD; pHSVer-GA; pHSVGA-cox8; pCDNA3.1-tgoGAm) were transiently transfected into cell lines using Lipofectamine LTX reagent (Invitrogen) according to the manufacturer's protocol.

EV-free medium: FBS was EV-depleted by ultracentrifugation, and added (5%) to phenol red-free DMEM with 25 mM HEPES, 4.5 g/l glucose, 1% L-glutamine and 1% PS.

Astrocyte-derived media collection: Cells were cultured in phenol red-free DMEM with 25 mM HEPES, 4.5 g/l glucose, 5% FBS, 1% L-glutamine and 1% PS. Cells were plated onto cultured flasks and incubated at 37ºC in 5% CO_2 with 90–95% humidity for 72 h before the culture medium was collected by centrifugation at $1500 \times g$ for 30 min at 4°C. The supernatant was filtered through a 0.22 µm membrane prior to vesicle isolation by differential ultracentrifugation. The collected culture medium was immediately frozen at -80°C for further vesicle isolation.

To label membranous organelles and organelles of the phagocytic-endocytic pathway [endosomes, lysosomes and multivesicular bodies (MVB)] we used Vybrant-DiI or Dextran-Alexa488 respectivelly following the manufacturer's specifications (Molecular Probes). Cells were incubated with the dye solution for 48 h. After removing the culture medium and performing three 5 min washes with PBS, cells were incubated overnight and then sub-cultured alone or in diferent co-culture formats (see below). Cells remained in co-culture during 48 h before performing flow cytometry or fluorescence microscopy analyses to test for transfer of vesicles between astrocytes and neurons. Two types of co-cultures were used: cells were subcultured to experimental plates in a 50:50 proportion (mixed cultures), or separated by a 0.4 µm pore membrane (Transwell plates, Corning Inc.) to avoid direct cell-cell contact.

Primary astrocyte cell cultures

ApoD-KO mice were generated by homologous recombination [42] maintained in positive pressure-ventilated racks at 25±1°C with 12 h light/dark cycle, fed *ad libitum* with standard rodent pellet diet (Global Diet 2014; Harlan Inc., Indianapolis, IN, USA), and allowed free access to filtered and UV-irradiated water. In order to avoid

potential maternal effects of ApoD, and to generate WT and ApoD-KO mice of homogeneous genetic background, the experimental cohorts used in this study are the F1 generation of homozygous crosses of ApoD −/− and ApoD +/+ littermates born from heterozygous crosses of an ApoD-KO line backcrossed for over 20 generations into the C57BL/6J background.

We used neonatal (0-1 days old) mice of two genotypes: ApoD-KO and their WT littermates. Experimental procedures were approved by the University of Valladolid Animal Care and Use Committee, and followed the regulations of the Care and the Use of Mammals in Research (European Commission Directive 86/609/CEE, Spanish Royal Decree ECC/566/2015).

Primary astrocyte cell cultures were previously described [60]. For the dissection of the neonatal mouse brain cortex, first we must anchor the head with a needle bent by the snout, remove the skin by cutting through the midline of the head and anchor with two needles the pieces of skin on each side. Then we need to eliminate the skull without damaging the brain. For this we make three cuts: a cross section with the microdissection scissors in the middle of the cerebellum, followed by a section through the sagittal suture to the olfactory bulb between the eyes and another cross section at the height of the olfactory bulb. Finally, with two microsurgical forceps (sharp tip) we move the skull apart with a lateral movement and upwards of the parietal bones. Cerebral cortices and part of the diencephalon (at the height of the 1st and 2nd ventricle) were quickly extracted with a microspatula. We collect it by making a movement from back to front.

Their meninges removed by rolling on a sterile filter paper, and pieces of cortex placed in Earle's Balanced Salt Solution (EBSS) containing 2.4 mg/ml DNAse I and 0.2 mg/ml bovine serum albumin (BSA). Tissue was minced with a surgical blade; centrifuged (200 g, 2 min); incubated with 10 mg/ml trypsin for 15 min at 37ºC (incubation terminated by 10% FBS addition); mechanically dissociated with a Pasteur pipette and centrifuged (200 g, 5 min). The last two steps were repeated, and the resulting cells were resuspended in DMEM with 10% FBS, 1% L-glutamine, 1% P-S-A. Cells were plated onto culture flasks and incubated at 37ºC in 5% CO_2 with 90–95%

humidity, and the culture medium was replaced weekly. Cell cultures were used for experiments after two subculture steps, when >99% of cells are astrocytes and the rest of cell types have died [53, 60].

MTT-viability assay

Primary astrocytes cultured with astrocyte-derived conditioned medium were subjected to the MTT (3-(4,5-dimethylthiazol-2-yl)-2,5-diphenyltetrazolium bromide) colorimetric assay as previuouly described [23]. After MTT exposure for 3 h, cells were incubated in isopropanol with 10% Triton X-100, and the solubilized formazan was measured by spectrophotometry using the SOFTmax Pro microplate reader (Molecular Devices). Absorbance was measured at »=570 nm after subtracting the »=690 nm background.

Isolation, fractionation and analysis of astrocyte-derived EVs

To isolate EVs, the stored samples were centrifuged at $10,000 \times g$ for 30 min and the supernatant was ultra-centrifuged at $100,000 \times g$ for 75 min. The resulting pellet was washed with an excess of phosphate-buffered saline (PBS), and ultra-centrifuged again at $100,000 \times g$ for 60 min. The pellet was resuspended in cold PBS and stored at -80°C.

EVs size distribution and concentration were analyzed using a NanoSight LM10 system equipped with a fast video capture and particle-tracking software. Vesicles are visualized by light scattering using a light microscope with a Nanoparticles tracking analysis (NTA) software that tracks Brownian motion of individual vesicles. NTA post-acquisition settings were kept constant for all samples, and each video was analyzed to calculate the median vesicle size and concentration estimate [38]. We also characterized EVs by Western Blot and Transmission Electron Microscopy (TEM).

Glia-derived EVs were fractionated in a continous 0.25-2 M sucrose density gradient [37]. The sample was ultracentrifugated for 16 h at 210.000 x g, 4ºC in a SW40 Ti rotor. Fractions (1 ml) were collected from top to botton by using an autodensity-flow gradient fractionator (Labconco). Subsequently, each fraction was diluted in 20 mM HEPES (pH 7.4), and centrifugated 1 h at 110.000 x g, 4ºC, in a

TLA-110 rotor to obtain the sample. Finally, pellets were resuspended in PBS and stored at -80ºC. Additionally, the reactive index was measured with a refractometer (Abbe 2WAJ, PCE Americans, Inc.) to estimate the density value.

Immunocytochemistry and immunochemistry

Cells attached to poly-L-lysine (Sigma) treated coverslips were fixed with 4% phosphate-buffered formaldehyde (methanol free) (Polysciences, Inc.). Following washes in phosphate-buffered saline (PBS), the cells were blocked and permeabilized. Cells were incubated overnight at 4ºC or for 1 h at room temperature with the primary antibodies summarized in Table 3.

Table 3. Primary antibodies used to immunocytochemistry and immunochemistry.

Antibody	Company	Source	Permeabilization	Block	Concentration
Rabbit serum anti-human ApoD	Abyntek Biopharma against purified ApoD [12] or generated by Dr. C. López-Otin	4% PFA in PBS	Tween-20 (0.1%)	1% non-immune goat serum	24.45 µg/ml
Goat serum anti-mouse ApoD	Santa Cruz Biotechnology	4% PFA in PBS	Tween-20 (0.1%)	1% non-immune FBS	1 µg/ml
Mouse serum anti-clathrin LCA	Santa Cruz Biotechnology	4% PFA in PBS	Tween-20 (0.1%)	1% non-immune goat serum	1 µg/ml
Mouse serum anti-caveolin-1	Santa Cruz Biotechnology	4% PFA in PBS	Tween-20 (0.1%)	1% non-immune goat serum	1 µg/ml
Goat serum anti-catalase	Santa Cruz Biotechnology	4% PFA in PBS	Tween-20 (0.1%)	1% non-immune FBS	1 µg/ml
Mouse serum anti-EEA1	BD Biosciences	4% PFA in PBS	Tween-20 (0.1%)	1% non-immune goat serum	1.25 µg/ml
Mouse serum anti-LC3	MBL	4% PFA in PBS	Tween-20 (0.1%)	1% non-immune goat serum	1 µg/ml

Rat monoclonal anti-Galectin-3	American Type Culture Collection, ATCC	4% PFA in PBS	Tween-20 (0.1%)	1% non-immune goat serum	1 µg/ml
Goat serum anti-4HNE	Alpha Diagnostic	4% PFA in PBS	Tween-20 (0.1%)	1% non-immune FBS	0.5 µg/ml
Mouse monoclonal anti-human Lamp-2 *	DSHB	4% PFA in PBS	0.1% saponin in PBS	1% BSA	2.65 µg/ml
Rat monoclonal anti-mouse Lamp-2	DSHB	4% PFA in PBS	0.1% saponin in PBS	1% BSA	1.95 µg/ml
Mouse-serum anti-human CD147 (basigin, BSG)	Thermo scientific	4% PFA in PBS	Tween-20 (0.1%)	1% non-immune goat serum	5 µg/ml
Mouse-serum anti Fyn	Santa Cruz Biotechnology	4% PFA in PBS	Tween-20 (0.1%)	1% non-immune goat serum	1 µg/ml
Rabbit-serum anti Neu1	Santa Cruz Biotechnology	4% PFA in PBS	Tween-20 (0.1%)	1% non-immune goat serum	1 µg/ml
Rabbit-serum anti Neu3	Santa Cruz Biotechnology	4% PFA in PBS	Tween-20 (0.1%)	1% non-immune goat serum	1 µg/ml
Rabbit-serum anti CD81	Gene Tex	4% PFA in PBS	Tween-20 (0.1%)	1% non-immune goat serum	5.4 µg/ml
Rabbit-serum anti CD63	BD Biosciences	4% PFA in PBS	Tween-20 (0.1%)	1% non-immune goat serum	1.25 µg/ml
Biotin-conjugated MAA-Lectin	Y Labs	4% PFA in PBS	No permeabilization	1% non-immune goat serum	5 µg/ml

Mouse monoclonal anti-human Lamp-2 antibody is very sensitive to low concentrations of methanol that can appear in fixatives and sealants.

Cy5, Cy3 (Abcam), Alexa Fluor® 594/488 (Jackson Labs) or DyLight® 405 (Thermo Scientific)-conjugated IgGs were used as secondary antibodies (1.5 µg/ml) for fluorescence immunocytochemistry. All antibodies, both primary and secondary, are dissolved in blocking solution. After washes in PBS, the preparations were mounted with EverBrite™ Mounting Medium with DAPI, and sealed with CoverGrip™ Coverslip Sealant (Biotium).

To carry out immunocytochemistry in non-permeabilized conditions, it is very important to avoid contact with fixatives with methanol, as well as with any detergent (Tween-20 or saponin). You should work with fresh samples and fresh solutions prepared on the day.

Nerve and brain samples were fixed by immersion in 4% formaldehyde overnight at 4ºC. The tissues were washed thoroughly in phosphate buffered saline (PBS), and either embedded in paraffin following standard procedures or cryoprotected and frozen in Tissue-Tek (Sakura). Paraffin sections (4 µm), performed with a rotary microtome (Microm), or Cryostat (Microm) sections (10 µm) were mounted on Polysine Slides (Menzel-Gläser) and dried or stored at -20ºC respectively.

Paraffin sections were dewaxed in xylene and rehydrated through ethanol series in PBS. Endogenous peroxidase was inactivated with H_2O_2 (0.9%) for 5 min in the dark before HRP immunohistochemisty. Paraffin and cryostat sections were blocked in 1% normal goat/bovine serum. When needed, the sections were permeabilized with Triton X-100 (0.25%) or Tween-20 (0.2%). Labelings with Biotin-conjugated MAA-Lectin were performed in cryostat sections in the absence of detergents.

Teased nerve fibers were obtained from 4% formaldehyde fixed mouse sciatic nerves as described [133, 134].

Immunoblot analysis

Cell lysates, or culture media (either directly or concentrated 20x by filter centrifugation with 10 KDa cut-off Centricon YM-10; Millipore), or isolated EVs, were analyzed to detect ApoD by immunoblot. Proteins were transferred to PVDF membranes using standard procedures, and exposed to primary antibody described in

Table 4 and followed HRP-conjugated secondary antibody (Santa Cruz Biotechnology). An HRP-conjugated anti-² -actin antibody (Sigma) was used to normalize protein loads. Membranes were developed with ECL reagents (Millipore), and the signal was visualized with a high sensitivity CCD camera (VersaDoc; BioRad). The integrated optical density of the immunoreactive protein bands was measured in images taken within the linear range of the camera, avoiding signal saturation.

Table 4. Primary antibodies used to Immunoblot analysis.

Antibody	Source	Block	[ ] Antibody
Rabbit serum anti-human ApoD	Abyntek Biopharma against purified ApoD [12], or generated by Dr. C. López-Otin	5% Milk	4.89 µg/ml
Goat serum anti-mouse ApoD	Santa Cruz Biotechnology	5% Milk	0.2 µg/ml
Mouse serum anti-caveolin-1	Santa Cruz Biotechnology	5% Milk	0.2 µg/ml
Mouse serum anti-flotillin-1	BD Biosciences	5% Milk	0.25 µg/ml
Mouse monoclonal anti-human Lamp-2	DSHB	1% BSA	2.65 µg/ml
Rabbit-serum anti CD81	Gene Tex	5% Milk	1.08 µg/ml

Ligand binding assay by tryptophan fluorescence titration

These methods were performed as previously described [18, 34]. Fluorescence measurements were conducted with a Shimadzu RF-5301PC spectrofluorometer in a quartz cuvette (105.251-QS, 3-mm path length; Hellma). Temperature was held at $22\pm0.1°C$. Excitation wavelength was 295 nm (selective for tryptophan residues). Emission was recorded at 327-400 nm with slit width set at 5 nm. Purified human ApoD was diluted to 0.5 µM with 10 mM phosphate buffer (binding at pH 7.0), or 30 mM sodium citrate (binding at pH 5.1). The ligand retinoic acid (RA) was dissolved in dimethylformamide (DMF; Sigma). The mixture was equilibrated for 3 min in the dark before the fluorescence was recorded.

The fluorescence spectrum in the presence of ligand was subtracted from DMF baseline obtained mixing the protein with the same amounts of carrier without ligand. Binding was assayed with RA 5 μM (1:10, protein:ligand concentration) and a DMF final concentration of 0.005%.

Image acquisition and analysis

Labeled cells were visualized with an Eclipse 90i fluorescence microscope (Nikon) equipped with a DS-Ri1 (Nikon) digital CCD camera. Images were acquired under the same conditions of illumination, diaphragm and condenser adjustments, exposure time, background correction and color levels.

Confocal images were obtained with a 63x oil immersion objective (HCX PL Apo CS NA=1.4; Leica) attached to a confocal DMI 6000B microscope with a TCS SP5 confocal system (Leica) equipped with AOBS and AOTF systems. Fluorophores were excited with WLL laser (Leica) and a 405 line (Leica) controlled by LAS AF software (Leica). Emissions were collected with the AOBS system and three spectral detectors. Laser power and detection gains were set by scanning control samples labeled with secondary antibody alone. We ensured to obtain similar dynamic ranges in our images, and adjusted gain and offset using LUTs. In this manner, bleedthrough can be neglected. Negative control images showed very weak and homogeneous background. We obtained confocal sections under constant conditions to minimize image acquisition variation. Images were stored as 1024x1024 pixels and 8-bit TIFF files.

Z-series (xyz scan) were performed. The number of z-stacks was determined by observing the limits of the cell membrane. The focus plane was set to be 3 μm beneath the section surface. The optimal value of the step size was calculated for the wavelength used to fulfill the Nyquist theorem. The optical section thickness was 0.772 μm. Besides, images were taken with a 4x zoom, reducing field size. Pixel size corresponded to $0.06*0.06*0.3777$ μm^3. Scanning was performed with a 1.0 Airy unit pinhole size.

Images were processed with a Gaussian Blur filter [Sigma (Radius): 1.00], to facilitate object detection, and analyzed with the Colocalization Indices plug-in [135]

and the 3D Object Counter tool using the FIJI software. To analyze triple-colocalization experiments we used the Image Calculator and 3D Object Counter tools of FIJI.

A principal component analysis (PCA) was performed on the 54 different variables per cell retrieved from our image analysis to reduce its dimensionality. Nine components were found with informative value, and three of them explained over 55% of the data variability (not shown). Intensity correlation quotient (ICQ) [136] variables were heavily represented in the first component. Pixel overlap proportions, and number and volume of objects were also of interest. Thus, we run a second PCA with 11 variables defined in table 5. ICQ (variables 1-3) and Pixel Overlap (variable 4) presented the largest weight in component 1 (accounting for 31.5% of variability), and relative Overlaps (variables 5-7) were the most important for component 2 (explaining 21.3% of variability) (Fig. 13A). The first component score of this PCA was used to assess for global statistical differences due to the experimental conditions (Fig. 13B). Only EEA1 and Lamp2 showed significant variation between control and PQ condition (Two-way ANOVA, Holm-Sidak post-hoc method, $p < 0.05$).

Table 5. Definition of the variables used in the second PCA analysis.

Number	Variable	Definition
1	ApoD ICQ	ICQ is the Intensity Correlation Quotient [136], which ranges from -0.5 to 0.5. It measures whether the staining patterns are randomly distributed (ICQ = 0), dependent on each other (0 <ICQ <0.5) or segregated (0> ICQ> -0.5).
2	Marker ICQ	
3	Colocalization ICQ	
4	Global pixel overlap	Overlap' is the Manders's Overlap Coefficient [137], ranges from 0 to 1 and is the proportion of pixels of different colors that overlap.
5	ApoD pixel overlap	
6	Marker pixel overlap	
7	Proportional pixel overlap	

8	Number of ApoD objects	Set of voxels with a homogeneous intensity and that are so close that they form the same entity.
9	Number of marker objects	
10	Volume marker objects	Surface of a marker object in voxels.
11	Volume ApoD objects	

This multivariate analysis helped us to focus on two main colocalization variables relative to ApoD signal (1 and 5; arrows in Fig. 13A) and the number and volume of ApoD-positive objects (variables 8 and 11) to understand the dynamics of ApoD trafficking in the cell. It also helps us to focus on the PQ-dependent changes, since most variables covariate between control and LS conditions (not shown).

Lysosomal pH measurement

Lysosomal pH was measured using the dye LysoSensor Yellow/Blue DND-160 (Life Technologies) as described [138-141]. As a ratiometric dye, the LysoSensor readout is independent of concentration. Moreover, because it is membrane permeable, its readout is representative of a broad range of lysosomes in comparison with a dextran-tagged probe that reaches lysosomes by endocytosis. Experimental parameters such as incubation time and dye concentration have been set to minimize variation and to give the best signal-to-noise ratio [141].

LysoSensor ratiometric excitation analysis for lysosomal pH in cell populations. Procedure.

1. Cell seeding in fluorometer plate. Cells were grown to >80% confluence in black 96-well plates (NUNC). The amounts of cells and culture medium are described in the table 6.

Table 6. The amounts of cells and culture medium used to measure lysosomal pH in fluorometer plate.

Plate	cm²	culture medium (ml)	# cells in confluence
96 well	0.32	0.35	10000

2.   Dye loading

After removal of medium and washes with PBS, cells were incubated for 3 min with 2 µM LysoSensor Yellow/Blue in isotonic solution (Dye loading solution). Dye loading and incubation steps were carried out at room temperature in the dark. After 3 min, cells were rinsed three times in isotonic solution, and then incubated with either additional isotonic solution (for experimental cells) or with pH calibration buffers (for the standard curve).

➤ Isotonic solution: NaCl, 105 mM; KCl, 5 mM; HEPES-Acid, 6 mM; Na-HEPES, 4 mM; NaHCO$_3$, 5 mM; mannitol, 60 mM; glucose, 5 mM; MgCl$_2$, 0.5 mM; CaCl$_2$, 1.3 mM; pH adjusted to 7.4.

➤ Complete isotonic solution (100 ml, prepared fresh): 50 ml 2x stock + 180 µl glucose 50% + 10.92 ml mannitol 10% + dH$_2$O up to 100 ml.

➤ Dye loading solution: 2 µM LysoSensor (7.2 µl LysoSensor 1mM stock + 3.6 ml Complete isotonic solution).

3.   Calibration curve

Absolute pH levels were obtained by calibrating lysosomal pH against the signal obtained in the calibration standards.

Cells present in calibration wells were incubated with 15 µM monensin and 30 µM nigericin (SIGMA), which are proton-cationophores that permeabilize the lysosomal membrane to Na$^+$ and K$^+$, respectively. These ionophores added in solutions with pH 4.0, 4.5, 5.0, 5.5 and 6.0, force lysosomes to equilibrate with those pH values (Fig. 5).

➤ pH calibration buffers: 20 mM MES (2-(N-Morpholino)ethanesulfonic acid), 110 mM KCl and 20 mM NaCl. 5 ml of stock calibration buffer were adjusted to pH 4.0, 4.5, 5.0, 5.5 and 6.0 by adding 1 N NaOH.

➤ Monensin intermediate solution (6.25 mg/ml (9.31 µM)): 8.75 µl stock calibration buffer with adjusted pH + 1.25 µl of Monensin stock (50 mg/ml prepared in MetOH).

➤ Nigericin intermediate solution (12.5 mg/ml (16.73 µM)): 7.31 µl stock calibration buffer with adjusted pH + 2.69 µL of Nigericin stock (50 mg/ml prepared in

MetOH).

> Complete permeabilization solution (1.204 ml, prepared fresh): 1.2 ml stock calibration buffer + 2 µl of Monensin intermediate solution (Final concentration = 15 µM) + 2 µl of Nigericin intermediate solution (Final concentration = 30 µM).

Our conditions contain no serum in the isotonic solution. If the experiment requires maintaining cells in the presence of serum all the time, including time of measurement, we add the appropriate amount to isotonic solution and perform the standard curve in the same conditions.
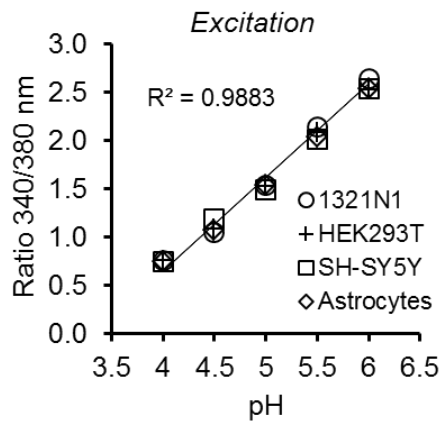
Figure 5. LysoSensor ratiometric excitation analysis for lysosomal pH in cell populations*. Calibration curves obtained from excitation spectra (ratio 340/380 nm) for the cell types used in this work after forcing lysosomal pH to equilibrate with known extracellular pH.*

4.   Fluorescence measurements

Fluorescence was measured with a GENios Pro Fluorometer and recorded using the XFluor4GENiosPro software package (TECAN). Lysosomal pH was determined from the ratio of excitation light at 340 nm and 390 nm (F340/F390 nm, 535 nm emission) [120]. Mean light levels at both excitation wavelengths were integrated over 2000 µs and recorded for each well. This step was repeated after 5 ms for each sample. The final calculated pH represents the mean of six measurements taken strictly within the 12 min following dye removal, as LysoSensor generates lysosomal alkalinization with longer incubation times.

LysoSensor confocal emission spectra analysis for single lysosomal pH.

1.   Cells were grown to < 50% confluence in µ-slide 8 well poly-L-lysine treated (Ibidi). The amounts of cells and culture medium are described in the table 7.

Table 7. The amounts of cells and culture medium used to measure lysosomal pH with confocal.

Plate	cm^2	culture medium (ml)	# cells in confluence
8 well	2.20	0.2 ml	50000-75000

2.   Dye loading

For LysoSensor staining, cells attached to poly-L-lysine coverslips were washed in warm isotonic solution, and incubated with isotonic solution or pH calibration buffers. After removal of medium and washes with PBS, cells were incubated for 3 min with 2 µM LysoSensor Yellow/Blue in isotonic solution. Dye loading and incubation steps were carried out at room temperature in the dark. After 3 min, cells were rinsed three times in isotonic solution, and incubated with either additional isotonic solution or with pH calibration buffers.

3.   Fluorescence measurements

Confocal fluorescence images were obtained by exciting at 405 nm and the emission collected at 420-700 nm (» scan (xyz)) taking two averaged images every 10 nm. A white field image was taken in the confocal microscope (Fig. 7D, step 4).

4.   Fluorescence analysis

Using the LAS AF Lite software (LEICA), we created regions of interest (ROI) for each lysosome and their emission spectra were obtained. Each spectrum was fitted to a five parameters Weibull's equation (Fig 6A). The emission 470/524 nm ratio was then calculated for each lysosome. The lysosomal pH values were determined from the standard curve generated with the pH calibration samples (Fig. 6B).
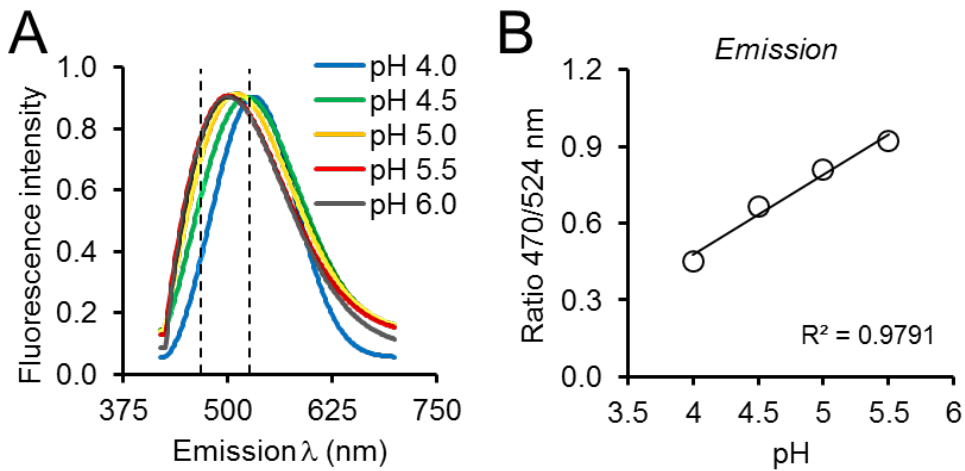
***Figure 6. Calibration curves of LysoSensor confocal Fluorescence. A.** Representative fluorescence emission spectra of single lysosomes in confocal sections, fitted to a five-parameter Weibull function, after equilibrating lysosomal pH to different extracellular pH. Dashed lines point to the pH values (470 nm/524 nm) selected to calculate the ratio. **B.** Calibration curve for 1321N1 cells confocal emission spectra from single lysosomes.*

LysoSensor confocal emission spectra analysis for single lysosomal pH combined with immunocytochemistry.

When a marker needs to be detected after lysosomal pH measures, we use µ-slide 8 wells poly-L-lysine treated (Ibidi), so that fixation and antibody labelling can be performed after the in vivo measure of single lysosome pH.

1. Immunocytochemistry.

Cells were fixed and permeabilized. Immunocytochemistry was then performed to detect ApoD in lysosomes, and each cell was position-identified to overlap ApoD to the LysoSensor signal.

2. Fluorescence measurements

Confocal fluorescence images were obtained by exciting at 405 nm, and the emission collected at 420-700 nm to detect LysoSensor and at the appropriate wavelength to detect ApoD. A white field image was taken in the confocal microscope. (Fig. 7 steps 5-7).

3.   Fluorescence analysis.

Images were analyzed with FIJI, and the Image Calculator tool was used to estimate the proportion of ApoD-positive and ApoD-negative lysosomes.
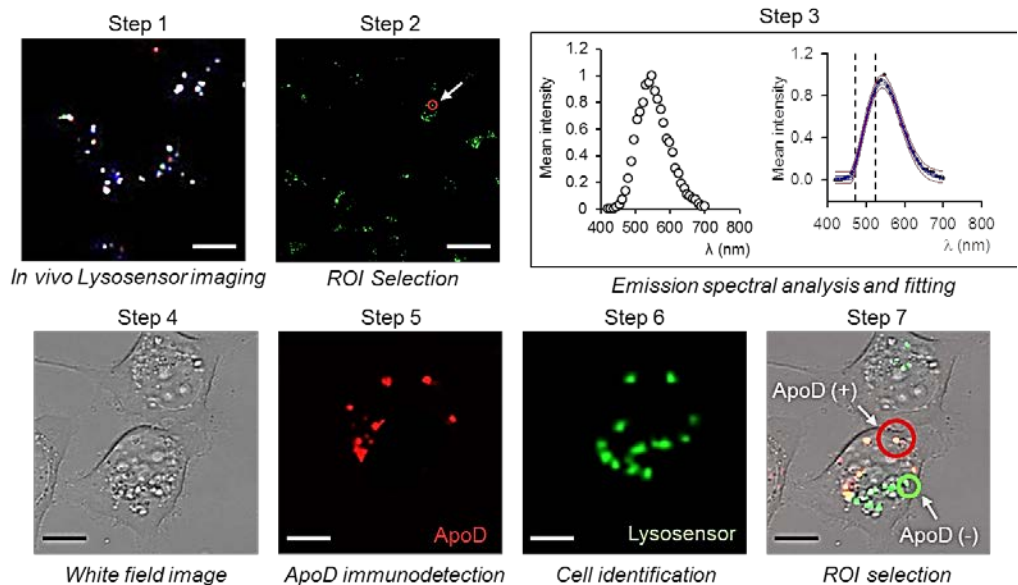
Figure 7. LysoSensor confocal emission spectra analysis for single lysosomal pH. *Schematic representation of the protocol devised to measure single lysosome pH combined with ApoD labeling. Steps: 1) In vivo imaging; 2) ROI; 3) LysoSensor spectra analysis and non-linear regression fitting; 4) White field image before cell fixation; 5) Native ApoD immunodetection; 6) Cell identification (guided by bright-field image); 7) Selection of ApoD positive/negative lysosomes for analysis. Calibration bars: 10 μm.*

Electron microscopy methods

1321N1 cells, under control or PQ conditions, destined for pre-embedding immunogold labelling of ApoD, were fixed in 4% formaldehyde and 0.3% glutaraldehyde in 0.1 M phosphate buffer (PB) pH 7.4 for 30 min at 4ºC. Following washes in 0.1 M PB, the cells were blocked with 0.1% cold water fish skin gelatin and permeabilized with Tween-20 (0.5%) in Tris-buffered saline (TBS; 20 mM Tris-HCL, 150 mM NaCl). Samples were incubated for 48 h at 4ºC with rabbit serum anti-human ApoD primary antibody in blocking solution. Samples were later washed and incubated with ultra-small gold-conjugated goat anti-rabbit secondary antibodies

(EMS, Electron Microscopy Sciences) in PBS for 48 h at 4ºC. After several washes with PBS, samples were post-fixed in 2% glutaraldehyde in PBS for 20 min, washed and the ultra-small gold particles were silver enhanced for 20 min at room temperature with AURION R-Gent SE-EM (Silver Enhancement for Electron Microscopy) (EMS, Electron Microscopy Sciences) following the manufacturer's indications. Later, samples were post-fixed with 0.5% OsO_4 in PBS for 20 min at 4ºC and washed with PBS, dehydrated through a graded series of ethanol and embedded in Epoxy EMbed-812 resin (EMS, Electron Microscopy Sciences). Ultrathin sections were obtained with an Ultracut E ultramicrotome (Reichert/Leica), contrasted with uranyl acetate and lead citrate, and analyzed using a JEOL JEM-1011 HR electron microscope with a CCD Gatan ES1000W camera with iTEM software.

EV preparations destined to cryo-electron microscopy were directly adsorbed onto glow-discharged holey carbon grids (QUANTIFOIL, Germany). Grids were blotted at 95% humidity and rapidly plunged into liquid ethane with the aid of VITROBOT (Maastricht Instruments BV, The Netherlands). Vitrified samples were imaged at liquid nitrogen temperature using a JEM-2200FS/CR transmission electron microscope (JEOL, Japan) equipped with a field emission gun and operated at an acceleration voltage of 200 kV.

Flow cytometry

Cells cultured for 48 hours after labelling with Vybrant-DiI or Dextran-Alexa 488 were lifted with 500 of Triple (TrypleTM Select, Gibco Life Technologies) after removal of the culture medium and whashes with PBS. Suspended cells were analyzed in a FACS Canto II flow cytometer (Beckton Dickinson). DiI signal was collecetd with the "PE" detector (BP585/42) and Alexa 488 was detected with the "FITC" channel (BP530/30) after excitation with 488 nm laser. Data was processed with Kaluza Analysis software v.1.3 (Beckman Coulter).

Myelin endocytosis and degradation assay

Myelin isolation and labeling were previously described [134, 142]. Myelin was extracted from the brain of 2-month-old mice [134, 143], a method based on

discontinuous gradient centrifugation of sucrose.

Mice were anesthetized with CO_2 and subsequently euthanized by cervical dislocation. Once extracted, the brain was homogenized in 0.3 M sucrose with 20 mM Tris-HCl (pH 7.45), 1 mM EDTA (ethylenediaminetetraacetic acid), 1 mM DTT (dithiothreitol), and 0.2 mM PMSF (fluoride phenylmethylsulfonyl) in a Potter homogenizer (Sartorius). The homogenized tissue suspension in 0.3 M sucrose was placed on 0.83 M sucrose (1:1 ratio) and centrifuged for 30 min at 75000 g and 4ºC (Ultracentrifuge Beckman Optima L-100 XP, SW40 rotor, Ultra-ClearTM 12.5 ml tubes). The myelin band formed at the interface between sucrose solutions (0.3 M / 0.83 M) was collected and washed with a hypotonic solution (0.2 M Tris-HCl) and centrifuged for 15 min at 75000 g and at 4°C. Subsequently, the sample was subjected to low speed centrifugation cycles (12000 g, 15 min and 4ºC) in order to eliminate cytoplasmic and microsomal contaminants. The resulting myelin was resuspended in PBS and stored at -20°C.

The amount of myelin obtained was determined by measuring the total amount of protein in the sample using Micro BCA Protein Assay Kit (Pierce). The test was carried out according to the manufacturer's instructions, but it was necessary to solubilize the sample in PBS with 2% SDS due to the large amount of lipids present. In this assay the protein used for the standard curve (bovine serum albumin, BSA), was also prepared in PBS with 2% SDS.

For myelin labeling, 1,1'-Dioctadecyl-3,3,3',3'-Tetramethylindocarbocyanine Perchlorate (DiI, SIGMA) was used. One mg/ml of myelin protein was incubated for 30 min at 37°C with 12.5 µg / ml of DiI in dimethyl sulfoxide (DMSO). Excess DiI was washed with sterile PBS and removed by centrifugation (20 min at 24000 g). The myelin labeled with DiI was stored in aliquots at -20°C [134].

Fluorescence microscopy was used to visualize myelin uptake by astrocytes. For this purpose, 2.5×10^5 cells were cultured on 12 mm coverslips at 37°C in 5% CO_2. Cells were incubated with 5 µg of DiI-labeled myelin (10 µg/ml) for three days. After incubation, non-endocytosed and unbound myelin was removed by washing twice with PBS, and cells were grown at 37°C for 2 or 6 days.

Cells were fixed in 4% formaldehyde in PBS, washed in PBS and mounted with EverBrite™ Mounting Medium with DAPI. DiI-labeled particles were visualized with a fluorescence microscope as described above. Number and size of myelin particles ingested by cultured astrocytes were measured from thresholded images with FIJI.

Fly lines and maintenance

Flies were grown in a temperature-controlled incubator at 25°C, 60% relative humidity, under a 12 h light–dark cycle. They were fed on wet yeast 84 g/l, NaCl 3.3 g/l, agar 10 g/l, wheat flour 42 g/l, apple juice 167 ml/l, and propionic acid 5 ml/l. Fly females were used in all experiments. We used the line gmr:GAL4 to drive transgenes expression to the eye photoreceptors. UAS:hATXN1^{82Q} was used to trigger the neurodegenerative phenotype [44], combined with UAS:GLaz [33] and/or UAS:Dor-RNAi [144]. Recombination of two of the elements present in the second chromosome (gmr:GAL4 and UAS:GLaz) was required to obtain some of the experimental combinations. Two independent lines were used.

Drosophila eye external morphology

Flies were anesthetized with CO_2 and frozen for 10 min at −20°C. Their bodies were immobilized on dual adhesive tape, and their heads set up to have an eye parallel to the stereomicroscope objective. Fly eyes were photographed with a Nikon DS-L1 digital camera, in a Nikon SMZ1000 stereomicroscope equipped with a Plan Apo WD70 objective. Fly eyes were illuminated with a homogeneous fiber optic light (20 W; KL 200, Zeiss). A white balance was performed on the background white surface. Additional settings include a 6x optical zoom in the stereomicroscope that results in a final resolution of 1.85 µm/pixel. Image files were saved in Tiff format. We maintained the same illuminating conditions and camera settings between experiments, as differences among pictures of the same stack may introduce undesired artifacts that would hamper the discrimination capacity of analysis [61].

Local intensity maxima were obtained with the FIJI program, and nearest neighbor distances were calculated for each ommatidium. A regularity index (IREG) was estimated as described [145], and a percent recovery was calculated considering 0%

the average degenerated eye and 100% the control wildtype eye. Samples of 20–35 flies (3 days old) per condition and genotype were used to calculate the mean ± SEM regularity index. We have used the FIJI plugin FLEYE for a semiautomated analysis of fly eye pictures [145].

Statistical analysis

Statistical analyses were performed with SPSS v.19 (IBM) and SigmaPlot v.11.0 (Systat) softwares. A p value < 0.05 was used as a threshold for significant changes. The tests used for each experiment are stated in figure legends.

Results

Chapter 1: Astroglial ApoD traffics through endocytic pathways, concentrates in the late endosomal-lysosomal compartment and is subsequently transported to either autophagosomes or plasma membrane.

Chapter 2: ApoD controls lysosomal functional integrity and stabilizes their pH.

Chapter 3: ApoD-enriched astroglial-derived extracellular vesicles mediate neuroprotection upon oxidative stress.

Chapter 4: In addition to cell survival, ApoD affects biological processes in which optimal lysosomal function is important for glial cells.

Chapter 5: Lysosomal ApoD function rescues cells from neurodegenerative diseases of different origins.

In this work, we describe ApoD subcellular trafficking and its role in lysosomal pH homeostasis under oxidative stress conditions. We demonstrate that ApoD is endocytosed and targeted to lysosomes in a stress-dependent manner, it is functionally stable in this acidic environment, and actively helps to maintain lysosomal pH gradients both in astrocytes and in neurons. Our analysis also reveals ApoD as a specific marker for a subset of lysosomes vulnerable to oxidation. Moreover, ApoD travels from the astrocytes to the neurons in EVs to protect them. We also report a role for this Lipocalin in lysosomal-dependent biological processes such as neurodegeneration-triggered autophagy, myelin phagocytosis and glycocalyx removal required to complete myelin compaction. Finally we will analyze the role that ApoD plays in neurodegenerative diseases of different origin and if it could be a good therapy to treated them.

CHAPTER 1: **Astroglial ApoD traffics through endocytic pathways, concentrates in the late endosomal-lysosomal compartment and is subsequently transported to either autophagosomes or plasma membrane.**

1.1 Astroglial ApoD is a secreted protein, uses canonical secretion pathways, and interacts with particular subdomains of plasma membrane.

1.2 ApoD endocytosis occurs in a Basigin-independent manner.

1.3 Astroglial ApoD traffics through clathrin and caveolin-dependent endocytic pathways, and concentrates prominently in the late endosomal-lysosomal compartment (LELC).

1.4 ApoD is transiently enriched in the LELC upon oxidative stress, and is subsequently transported to autophagosomes.

1.5 LELC is a "functional niche" for ApoD.

Among the catalog of oxidative stress-responsive genes is the Lipocalin Apolipoprotein D (ApoD), an extracellular lipid binding protein endowed with antioxidant capacity. The protecting role of ApoD is known at the organism level, and many of its downstream effects, including optimization of autophagy upon neurodegeneration, have been described. However, we still cannot assign a cellular mechanism to ApoD that explains how this protection is accomplished. Here we performed a comprehensive analysis of ApoD intracellular trafficking describing ApoD subcellular localization in astroglial cells upon different oxidative stress stimuli.

1.1 Astroglial ApoD is a secreted protein, uses canonical secretion pathways, and interacts with particular subdomains of plasma membrane.

We studied ApoD subcellular localization by detecting the native protein in astroglial cells (1321N1), avoiding transfections that could alter its physiological trafficking. As expected for a Lipocalin, 1321N1 cells secrete ApoD to the culture medium (Fig. 8A). Also, in ApoD-transfected HEK293T cells, extracellular ApoD is detected with a stable accumulation in the culture medium over time (Fig. 8B). However, no significant co-localization was observed with endoplasmic reticulum (RER; Fig. 8C) and only borderline values were obtained within the Golgi apparatus (Fig. 14A,G) of 1321N1 cells. A rapid passage through RER and Golgi in astroglial cells might render ApoD concentration below detection levels in those organelles, a hypothesis supported by the apparent ApoD-RER co-localization obtained when ApoD is overexpressed in HEK293T cells (Fig. 8D).
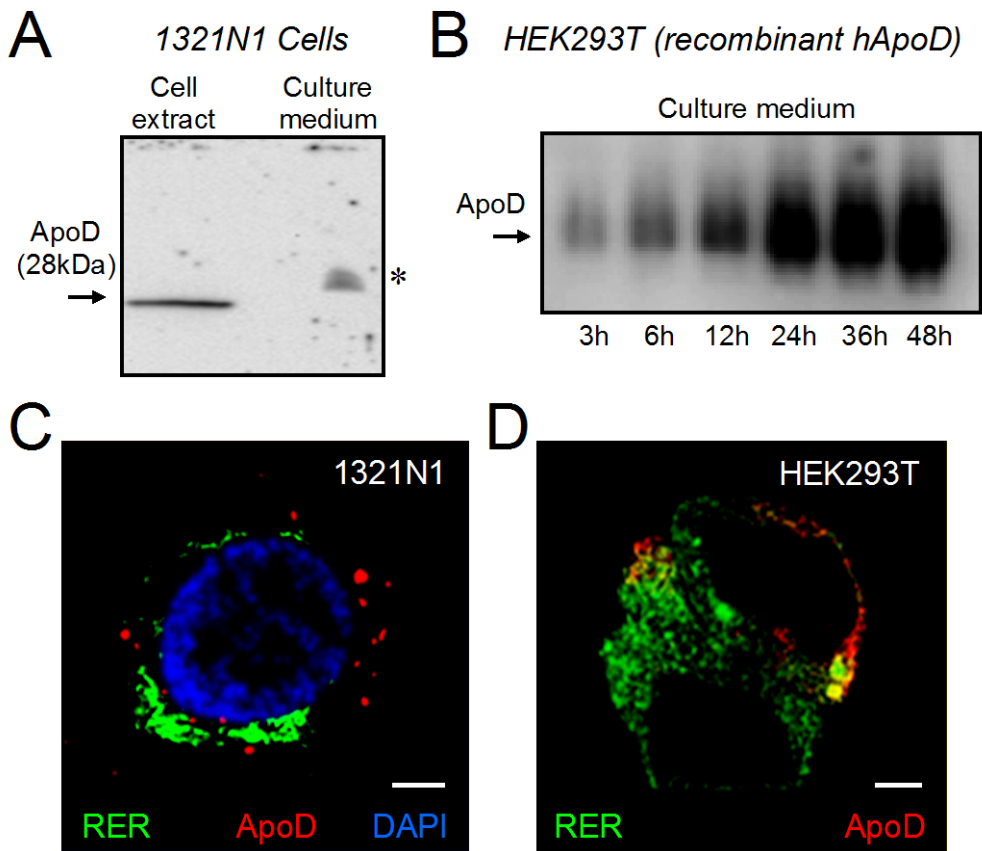
Figure 8. ApoD is a secreted protein and uses canonical synthesis and secretion pathways. A. *Immunoblot analysis of native hApoD expressed by 1321N1 astroglial cells, detected both in cell extracts (arrow) and in concentrated (20x) culture medium (asterisk). Apparent molecular weight is disrupted by the excess presence of serum Albumin in the concentrated medium. **B.** Time course of ApoD accumulation in the culture medium of HEK293T cells transfected with a hApoD expression plasmid (no concentration of media required). **C.** Representative confocal microscopy section of a 1321N1 cell transfected with a RER-targeted GFP expression plasmid (using the Calreticulin signal sequence). Native ApoD is detected by immunocytochemistry. **D.** Co-localization of hApoD with RER in HEK293T cells co-transfected with a RER-targeted GFP construct and a hApoD plasmid (see Methods). Calibration bars in C-D: 5 μm.*

We evaluated ApoD colocalization in control, low serum (LS) and treatment with the oxidative stress-inducing agent paraquat (PQ) at 2 and 24 hours after stimulus. Our co-localization studies, performed in conditions of membrane permeabilization (see

Methods), uncovered that ApoD signal was also present in a peripheral dotted pattern (Fig. 9A). By performing ApoD immunolocalization in non-permeabilized conditions, we confirmed that this labeling is due to ApoD presence at the extracellular side of the plasma membrane (Fig. 9B).

An object-based analysis of the ApoD signal located on the plasma membrane at 2 and 24 h of PQ treatment (Fig. 9C) shows two phases, which might be indicative of different cell biological processes: (i) An initial phase with increased number and size of ApoD objects. (ii) Small, but still abundant, membrane-associated ApoD aggregates at 24 h. These areas could be detergent-resistant membranes (DRMs), also known as lipids rafts. The presence of ApoD in DRMs has already been described [61]. Interestingly, the DRMs present hApoD, Lamp2, Flotillin, and Caveolin as markers (Fig. 9E). That is why we wanted to study the localization pattern of the lysosomal marker Lamp2 in the membrane.

Performing Lamp2 immunolocalization in non-permeabilized conditions, we also confirmed the presence of Lamp2, a lysosomal marker at the same extracellular side (Fig. 9E-F, arrowheads in panel). During the 2 h of PQ treatment, the Lamp2-positive objects increased in size (Fig. 9D) which indicates a progressive enrichment of Lamp2 in the membrane with the PQ treatment.

Then, we studied separately if the ApoD objects were homogeneously distributed or there were groupings in different areas of the cell membrane. We observe that there are no differences in both markers with treatment in the distances of the different objects of both markers. This may indicate that the vesicles fuse with the membrane at sites with a similar composition.
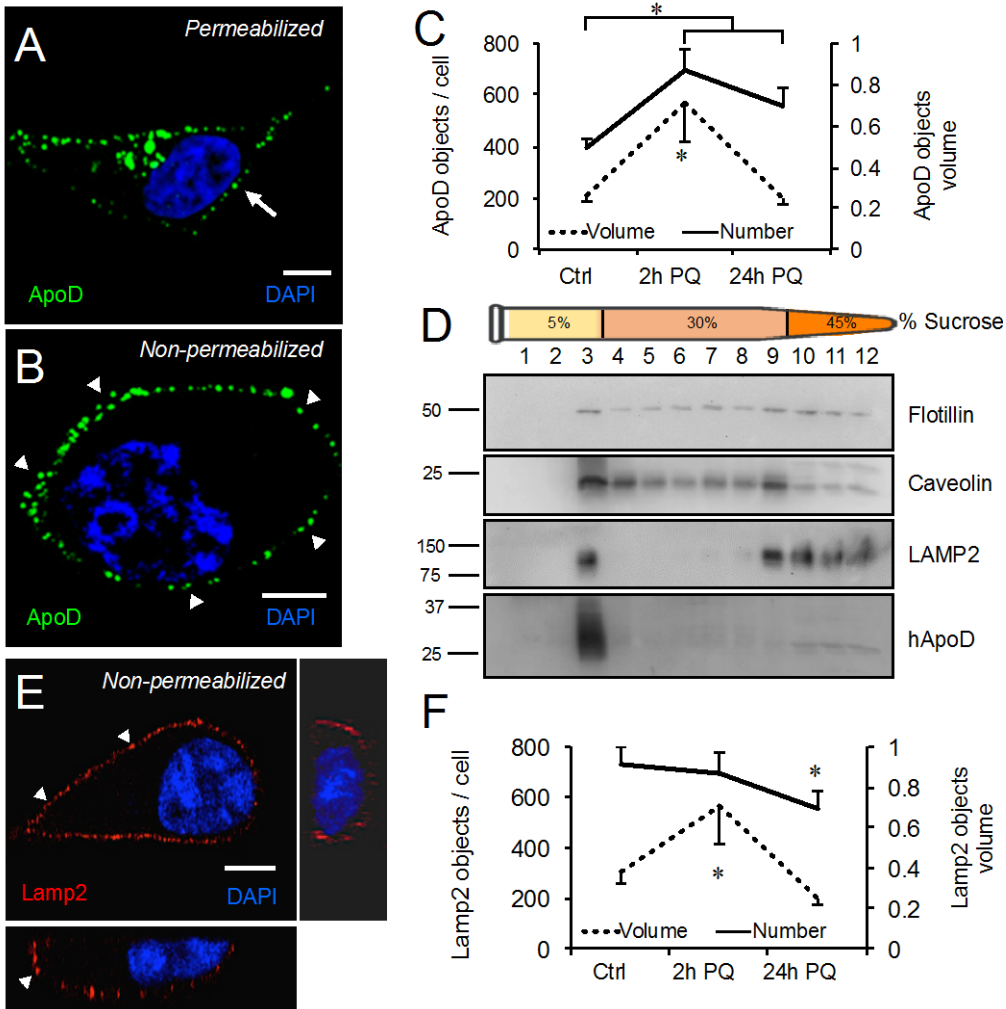
Figure 9. ApoD is located in the plasma membrane in particular detergent-resistant membrne domains. A-B. *Representative confocal sections of ApoD signal in permeabilized (A) and non-permeabilized (B) 1321N1 cells.* **C.** *The number and volume of ApoD positive membrane objects significantly differ with time of PQ treatment (500 µM). Object volume was measured by the number of pixels/voxel.* **D.** *Fractionation on a discontinuous sucrose gradient of 1321N1 membrane preparations after Triton-X114 solubilization. Lamp2, Flotillin, hApoD and Caveolin are detected in the low density fractions containing membrane domains resistant to Triton-X114. ApoD is almost exclusively present at the interface between 5% and 30% sucrose.* **E.** *Representative confocal section of Lamp2 signal in non-permeabilized 1321N1 cells.* **F.** *The number and volume of Lamp2 positive membrane objects significantly differ with time of PQ treatment (500 µM). Object volume was measured by the number of pixels/voxel. Statistical*

differences in C and F were assessed by ANOVA on Ranks (p<0.001) with Tukey post-hoc method (p<0.05, denoted by asterisks within variables). Calibration bars in A, B and E: 5 μm.

1.2 ApoD endocytosis occurs in a Basigin-independent manner.

ApoD internalization has been reported recently to be related to an interaction with the transmembrane protein Basigin [58]. Because of our findings of ApoD localization on the plasma membrane, we wanted to know if ApoD is being endocytosed via a Basigin-dependent mechanism.

1321N1 cells express large amounts of Basigin in the membrane both in control (Fig. 10A) and PQ-induced oxidative stress (Fig. 10B). Basigin is evenly expressed on the plasma membrane; a labeling pattern very different from that of ApoD (Fig. 10C,D), but similar to other membrane proteins such as Caveolin (Fig. 10E). Due to the homogeneous plasma membrane distribution of Basigin, we detected membrane co-localization of Basigin and ApoD. However, we did not observe co-localization in the intracellular vesicular compartments, suggesting that Basigin and ApoD do not follow the same endocytic process.
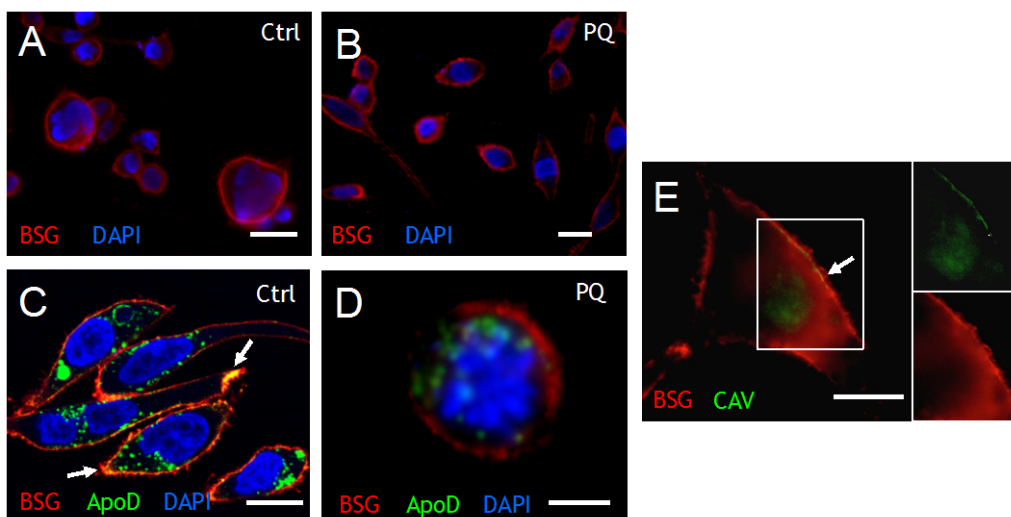

Figure 10. Basigin shows a homogeneous distribution on 1321N1 astroglial cell membranes, and does not co-localize with ApoD in intracellular vesicular compartments. A-B. Representative fluorescence microscopy images of non-permeabilized 1321N1 astroglial cells labelled with anti-Basigin (BSG) antibody (red) in control (A) and 500 μM PQ conditions (B).

Basigin shows a uniform cell-surface pattern. No changes in Basigin localization are observed under PQ-induced oxidative stress. **C-D**. *Permeabilized 1321N1 cells were labeled with Basigin (red), ApoD (green) and DAPI (blue) in control (C) and 500 μM PQ conditions (D). Representative sections of confocal microscopy z-stacks are shown. Yellow pixels mark co-localization between Basigin and ApoD (arrowheads). Only ApoD is internalized upon oxidative stress.* **E**. *Representative fluorescence microscopy image of Basigin and Caveolin distribution in astroglial 1321N1 cells. Both proteins co-localize at the cell surface. Calibration bars: 15 μm.*

A co-localization of Basigin and ApoD is not observed in HEK293T cells, which do not express ApoD endogenously, if we add purified hApoD for two hours (Fig. 11). ApoD is able to enter the cell and reach cellular organelles. However, Basigin remains on the membrane. All this suggests that although Basigin could be interacting with ApoD in the plasma membrane, its function could be spared to target ApoD endocytosis.
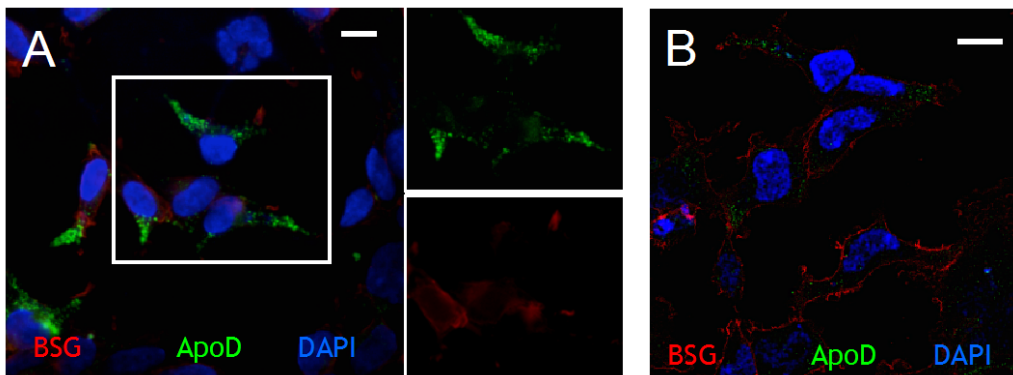
Figure 11. Exogenous hApoD does not co-localize with Basigin in HEK293T cells vesicular compartments. A-B. *Representative fluorescence microscopy image (A) and confocal sections (B) of HEK293T cells labelled with hApoD (green) and BSG (red) after exposure to 10 nM purified hApoD (2 h pulse). The insets in A show hApoD and BSG labelling separately. Calibration bars: 15 μm.*

To determine whether ApoD entry is regulated by Basigin in glial cells, we studied the localization pattern of both proteins in U87 human glioblastoma cell line, where a Basigin-KO mutant has recently been reported [131]. Both wild type and Basigin-KO

glioblastoma cells are able to internalize ApoD in control (Fig. 12A,B) and after PQ-treatment (Fig. 12C,D).
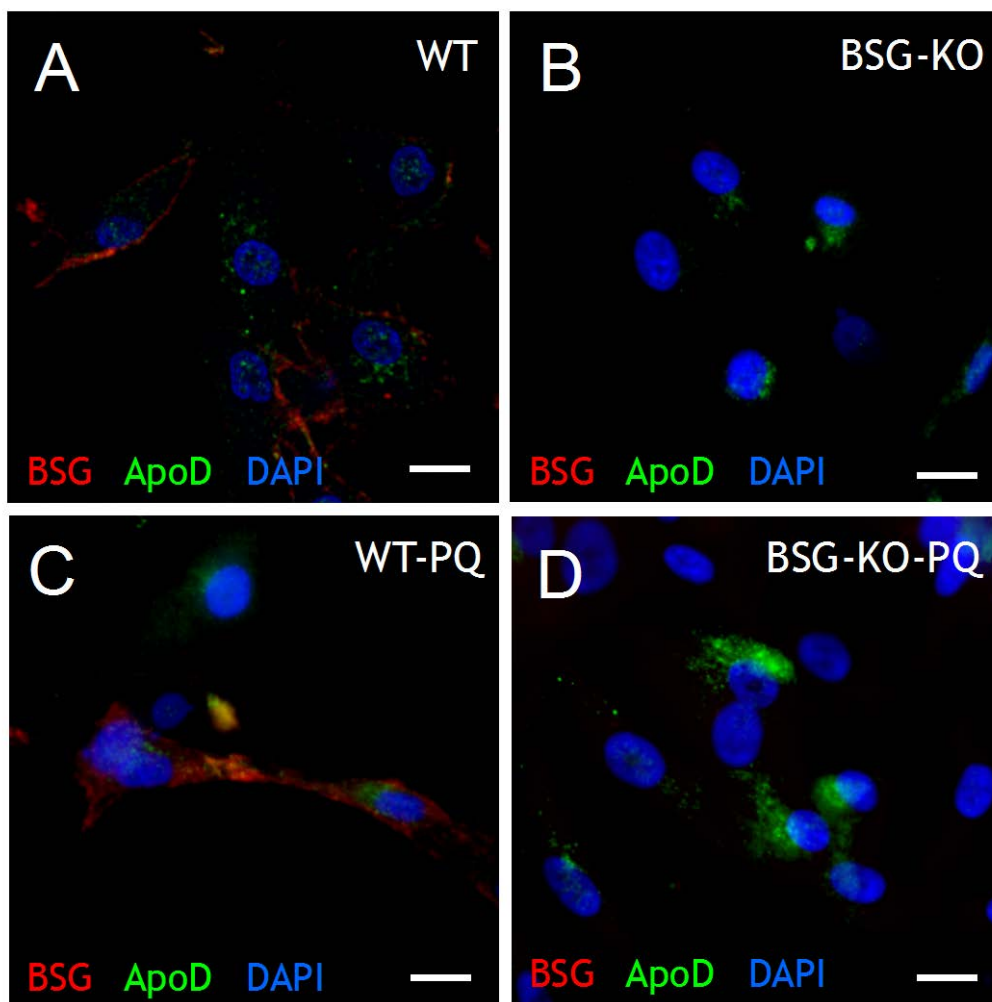
Figure 12. Basigin is not necessary for ApoD internalization in U87 human glioblastoma cells. A-D. Representative fluorescence microscopy images of WT or Basigin-KO U87 cells in control conditions (A-B) or after 500 μM PQ treatment (C-D) labelled with Basigin (red), ApoD (green) and DAPI (blue). Internalized ApoD does not co-localize with Basigin in WT cells. Internalization, enhanced upon oxidative stress, also occurs in the absence of Basigin. Calibration bars: 15 μm.

1.3 Astroglial ApoD traffics through clathrin- and caveolin-dependent endocytic pathways, and concentrates prominently in the late endosomal-lysosomal compartment (LELC).

We studied ApoD subcellular localization by detecting the native protein in astroglial cells (1321N1), A set of nine different markers for intracellular organelles were used to evaluate co-localization with ApoD in control, low serum (LS) and treatment with the oxidative stress-inducing agent paraquat (PQ) at 2 and 24 hours after stimulus.

Figure 13 and 14 summarize the results of our image analysis from confocal z-stacks of at least 20 cells per condition, selected randomly from two independent experiments with triplicate wells (see *Methods*). Following a principal component analysis (PCA), we selected the ICQ index [136] referenced to ApoD signal (ApoD ICQ) and the % Pixel Overlap referenced to ApoD signal (ApoD Overlap) to quantify ApoD protein targeted to each organelle (Fig. 13) (see *Methods*). We use a 2xICQ threshold of 0.1 for a co-localization not to be considered due to chance. Since most variables covariate between control and LS, only PQ referred to the control condition is shown for simplicity in most figures.
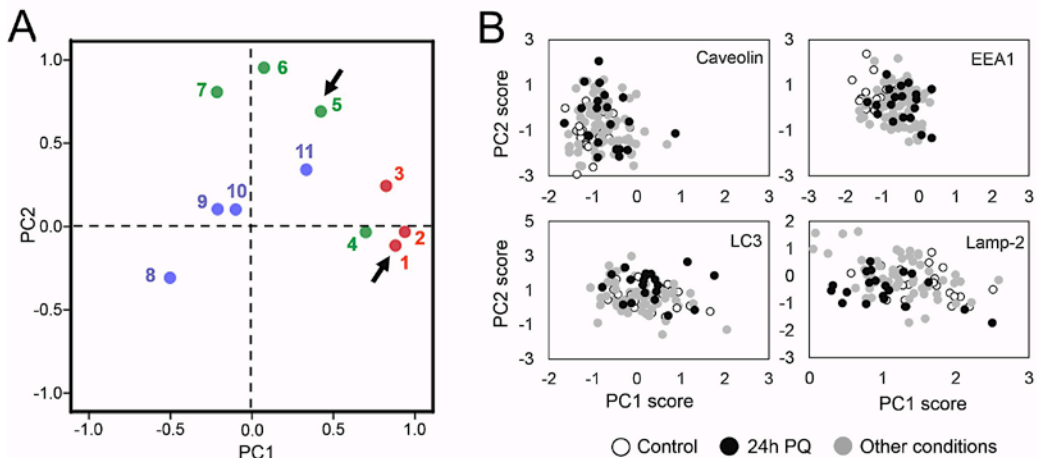

Figure 13. A multivariate analysis of the fluorescent signals of ApoD and organelle markers guide the selection of the most explicative variables. A. Principal component analysis (PCA) on 11 quantitative variables obtained from confocal z-stacks (see Methods). The variables

related to the ICQ are represented in red, in green those related to signals overlap and in blue those related to the number and volume of objects. The position of a variable relative to axes (dashed lines) indicates its contribution to the two most explicative components. ICQ variables (1-3, red) show a strong weight on the first component, whereas overlap variables (4-7, green) contribute mainly to the second one. None of the object-related variables (8-11, blue) show a big impact on these components, but ApoD object variables (8 and 11) are more informative than the marker ones (9 and 10). Arrows point to the co-localization variables related to ApoD signal. **B.** *Scatter plot of the image analysis datasets against the first two principal components shown in panel A. The homogeneous distribution of Caveolin and LC3 data show the lack of differences between conditions (see Methods). A significant segregation of EEA1 and Lamp-2 datasets appear between control and PQ conditions (Two-way ANOVA, Holm-Sidak post-hoc method, $p < 0.05$).*

ApoD concentrates significantly in Clathrin, EEA1, Lamp-2 and LC3-positive organelles, with particular prominence in the late endosome-lysosome compartment (LELC) labeled by Lamp-2 (Fig. 14A-G). Borderline average values of 2xICQ are detected for ApoD co-localization with Caveolin-1 (Fig. 14G), though some cells in the sample studied show clear co-localization over the threshold (Fig. 14B). A significant PQ-dependent enrichment is observed in ApoD co-localization with Clathrin, Lamp-2 and LC3 at 24 h of treatment (asterisks in Fig. 14G and Fig. 15). At shorter times (2 h) no PQ-dependent enrichment of ApoD is observed in the lysosomal or autophagosomal compartments of 1321N1 cells, while a prominent co-localization is seen for ApoD-Clathrin (asterisk in Fig. 14H).
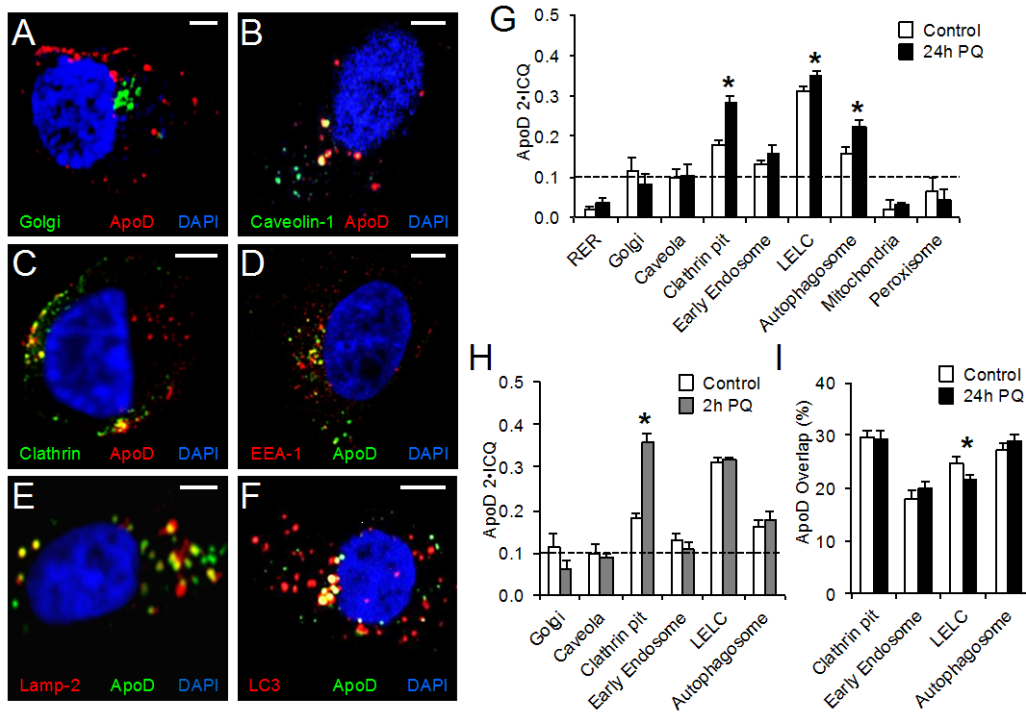
Figure 14. Astroglial ApoD traffics through Clathrin- and Caveolin-dependent endocytic pathways, concentrating prominently in the late endosomal-lysosomal compartment upon stress. A-F. *Co-localization of ApoD with Golgi, caveola (Caveolin 1), Clathrin-coated pits and vesicles, early endosome compartment (EEA-1), late endosome-lysosome compartment (LELC, marked with Lamp-2), and autophagosomes (LC3) in 1321N1 cells. Representative sections of confocal microscopy z-stacks are shown. All markers were detected by immunocytochemistry, except for the Golgi apparatus, where cells are transfected with an organelle-directed GFP construct using the Galactosyltransferase II signal sequence (see Methods). Co-localization appears in yellow.* **G-H.** *Average co-localization index referenced to ApoD signal (ApoD 2xICQ) for different 1321N1 organelles in control and after 24 h PQ treatment (G), or after 2 h PQ treatment (H). The dotted line represents the co-localization threshold (2xICQ<0.1 is considered due to chance).* **I.** *Spatial co-localization (Overlap referenced to ApoD signal) for the organelles showing ICQ-based index above threshold in G. Error bars in G-I represent SEM (n=20 cells/marker from at least two independent experiments). Asterisks show statistical significance (p<0.05) assessed by Student's t-Test between control and PQ conditions. Calibration bars in A-F: 5 μm.*

On the contrary, ApoD is not detected in mitochondria or peroxisomes, two organelles involved in oxidative stress generation and management (Fig. 14G and Fig.

15). To further analyze the spatial domain of ApoD overlap with organelle markers, we calculated a percent pixel overlap (referenced to the ApoD signal) as a parameter independent of the fluorescence intensity taken into account in ICQ (Fig. 14I). The representation of Clathrin pits, early endosomes, LELC and autophagosomes within the ApoD spatial domain is quite high (18-30%), indicating that these organelles are common residence sites for ApoD. No enrichment in spatial overlap is detected upon PQ treatment, suggesting that the elevated ApoD 2xICQ values reported above (Fig. 14G-H) represent a stress- and time-dependent increase in ApoD concentration in those stable spatial domains.
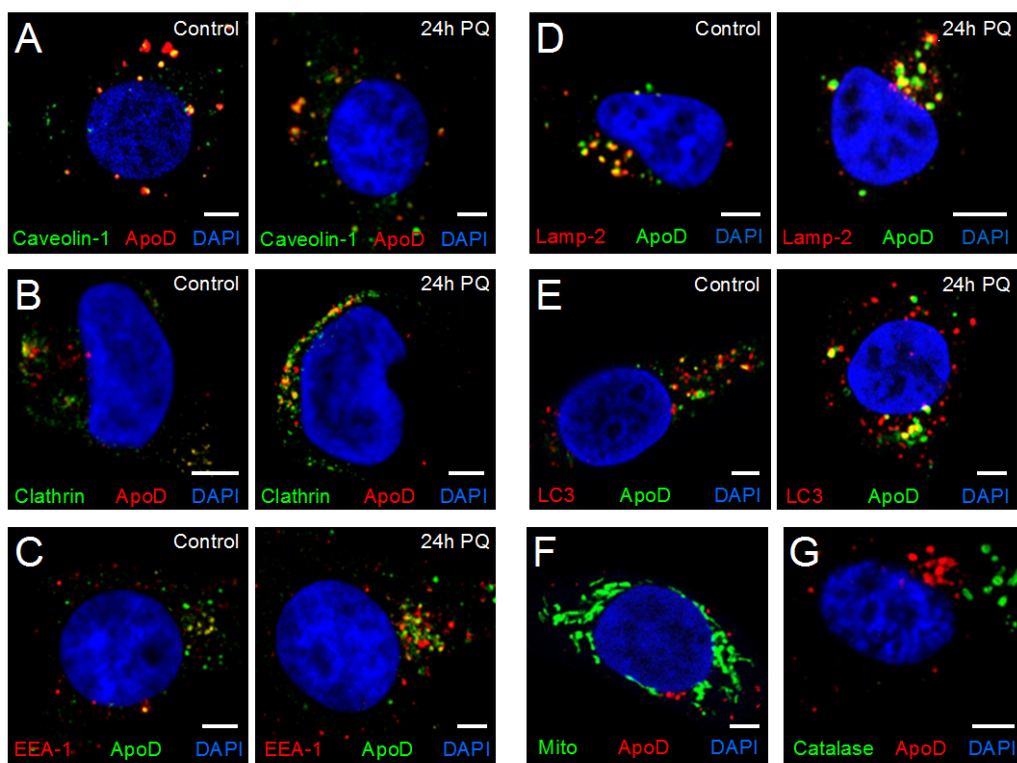
Figure 15. ApoD is specifically enriched in a subset of organelles upon stress. A-E. Co-localization of ApoD in control and 24 h PQ conditions in 1321N1 cells. Co-localization with caveola (Caveolin 1) (A), Clathrin-coated pits and vesicles (B), early endosome compartment (EEA-1) (C), late endosome-lysosome compartment (Lamp-2) (D), and autophagosomes or autophagolysosomes (LC3) (E). Representative sections of confocal microscopy z-stacks are shown. *F-G.* No co-localization was detected for ApoD with mitochondria (F) or peroxisomes

(Catalase) (G). All markers were detected by immunocytochemistry except for the mitochondria, where cells were transfected with an organelle-directed GFP construct (using COX VIII signal sequence, see Methods). Co-localization appears in yellow. Calibration bars: 5 μm.

1.4 ApoD is transiently enriched in the LELC upon oxidative stress, and is subsequently transported to autophagosomes.

Given the prominent co-localization of ApoD with the LELC marker Lamp-2 in 1321N1 cells, we performed a more detailed time course analysis of their spatial overlap. PQ triggers specifically a significant and transient increase in pixel overlap (Fig. 16A), which is accompanied by a change in the distribution of the ApoD signal (Fig. 16B): an initial phase of large and less numerous ApoD objects is followed by a late phase with more objects of small average size. This analysis suggests a PQ-dependent early enrichment of ApoD in LELC that might coincide with organelle fusion, probably autophagolysosomes, followed by ApoD traffic to smaller vesicles.

The early distribution of ApoD signal in permeabilized cells upon PQ treatment (Fig. 14H) suggests organelle fusion, and ApoD is a common resident in LC3-positive organelles of 1321N1 cells (Fig. 14F). Therefore, we studied ApoD trafficking in the autophagy process. We show that ApoD entry in autophagolysosomes is dependent on a proper lysosome-autophagosome fusion since chloroquine (CQ), known to alkalinize lysosomal pH and prevent its fusion [146], completely abolished co-localization of ApoD with LC3 (Fig. 16C). We then quantified the co-localization of ApoD with Lamp-2 or LC3 (2xICQ index referenced to ApoD signal; Fig. 16D). The presence of ApoD in LELC is relatively stable, while co-localization with LC3 drops below random levels both, when lysosome-phagosome fusion is impaired by CQ or when autophagy initiation is blocked at an early step using 3-methyladenine (3-MA). Likewise, a significant increase in ApoD-LC3 co-localization is observed when autophagy is stimulated by the mTOR inhibitor Rapamycin (Rap).
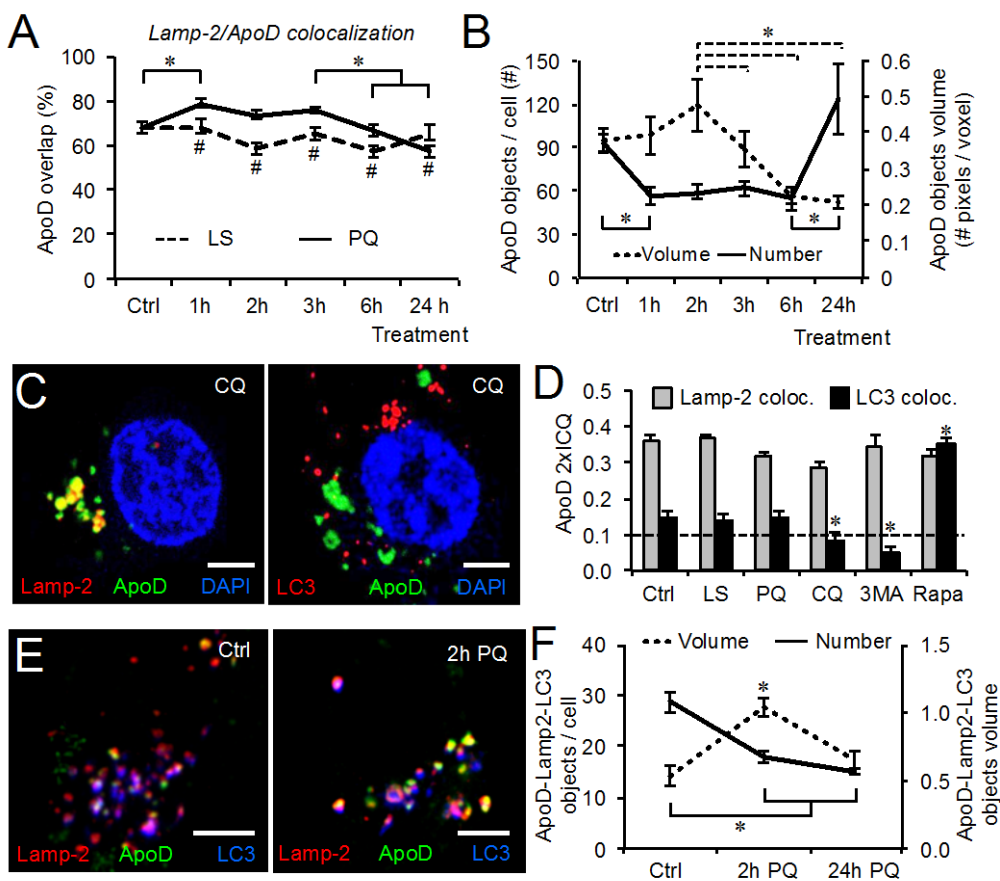
Figure 16. Lysosomal location of ApoD is followed by entrance in autophagolysosomes. A. *Spatial co-localization of ApoD with Lamp-2 (Overlap referenced to ApoD signal) in 1321N1 cells in control and PQ treatment over time.* ***B.*** *Number and volume of ApoD-positive objects along PQ treatment.* ***C.*** *Representative confocal sections of 1321N1 cells labeled with ApoD and either Lamp-2 or LC3 after 1 h of chloroquine (CQ) treatment, demonstrating that ApoD entrance in autophagolysosomes is dependent on lysosome-phagosome fusion.* ***D.*** *Co-localization index referenced to ApoD signal for LELC and autophagolysosomes in control and experimental conditions: 2 h low serum (LS); 2 h PQ; 1 h chloroquine (CQ); 1 h 3-methyladenine (3-MA) and 1 h Rapamycin (Rapa).* ***E.*** *Representative confocal sections showing triple co-localization of ApoD, Lamp-2 and LC3 in control and 2 h PQ treatment.* ***F.*** *Number and volume of ApoD/Lamp-2/LC3-positive objects in control and after 2 or 24 h PQ treatment. Error bars in all graphs represent SEM (n=20 cells/marker from at least two independent experiments). Object volume was measured by number of pixels/voxel in B and F. Statistical differences were assessed by ANOVA on Ranks (p<0.001) with Tukey post-hoc method (p<0.05,*

denoted by asterisks within variables, and by number sing between variables). Calibration bars in C, E: 5 μm.

An object-based analysis of ApoD-Lamp2-LC3 triple co-localization in 1321N1 cells exposed to PQ (Fig. 16E-F), shows a transient increase in the volume of objects labeled by the three markers (ApoD-positive autophagolysosomes) and a decrease in their number. This suggests that a basal level of autophagic activity exists in these cells, and that after an initial phase of fusions of autophagolysosomes upon PQ treatment, autophagy is resolved with a net decrease of objects with the markers. These data, together with the increased ApoD-LC3 co-localization after 24 h PQ (Fig. 14G) suggest that ApoD is enriched in autophagolysosomes upon oxidative challenge.

The subcellular localization of ApoD in 1321N1 cells in control and PQ conditions was further confirmed by morphological criteria of immunoelectron microscopy (Fig. 17). In control conditions ApoD was mostly detected in early endosomes, small and located close to the plasma membrane (Fig. 17A), as well as in lysosomes, electron-dense vesicles close to the nucleus (Fig. 17B). Clear differences are observed upon PQ treatment in the representation of labeled subcellular localizations. After 2 h of PQ treatment ApoD signal was observed on the plasma membrane (Fig. 17C), being secreted or endocytosed in Caveolae (Fig. 17D) or Clathrin-coated pits (Fig. 17E), in larger late endosomes (Fig. 17F), in electron-dense lysosomes (Fig. 17G), in secondary lysosomes (Fig. 17H-I), and in autophagolysosomes (Fig. 17J). In most cases, ApoD signal is observed associated to membranes. Interestingly, lysosomes under oxidative stress show clear enrichment of membrane-associated ApoD (Fig. 17G) compared to control conditions (Fig. 17B).
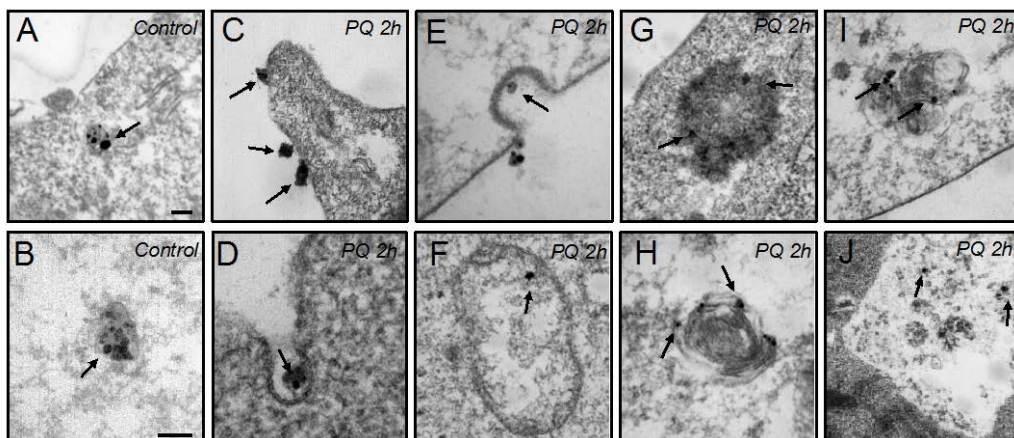
Figure 17. Immunoelectron microscopy micrographs of the subcellular localization of ApoD in 1321N1 cells in control and oxidative stress conditions. *ApoD labeling is shown by means of silver-enhanced gold particles, some of them denoted by arrows. **A.** Localization of ApoD in early endosomes, near the plasma membrane, in control conditions. **B.** In control cells, ApoD locates at the membrane of small perinuclear lysosomes. **C.** ApoD is frequently found associated with the plasma membrane in PQ treated cells. **D.** ApoD is secreted or endocytosed in Caveolae-coated pits upon oxidative stress. **E.** ApoD is internalized through Clathrin-coated pits, identified by the characteristic inner plasma membrane coating at this particular location. **F.** In treated cells, ApoD is also found in large late endosomes. **G.** Under PQ conditions, ApoD is recruited to large and electron-dense late endosomal-lysosomal compartment. **H-I.** ApoD is also found in larger and mature secondary lysosomes, which contain particles undergoing digestion in the treated cells. **J.** ApoD was also located in autophagolysosomes, identified by their double membrane and a heterogeneous content with partially digested parts of cellular organelles. Calibration bars: 100 nm.*

1.5 The LELC is a "functional niche" for ApoD.

Since the LELC and autophagolysosomal compartments participate in protein degradation, we tested whether the ApoD passage through them simply reflects its degradation pathway. We used cells not expressing ApoD (HEK293T) subjected to a 2 h pulse-chase experiments with purified human ApoD. After a 2 h period of ApoD exposure, ApoD labeling was evaluated in cells for up to 48 h. The intracellular content of ApoD was very stable along the experimental period when we used native human ApoD (Fig. 18A). However, a bacterially produced non-glycosylated human ApoD is

rapidly endocytosed and quickly degraded (Fig. 18B). Co-localization with Lamp-2 (Fig. 18C-D) shows that bacterial recombinant ApoD reaches the LELC, but the signal disappears with a fast time course. Using immunoblot, we have estimated that only 30% of endocytosed native human ApoD is lost during a division cycle in HEK293T cells (Fig. 18E-F), and a fraction of that loss corresponds to ApoD secretion to the culture medium (Fig. 8B).
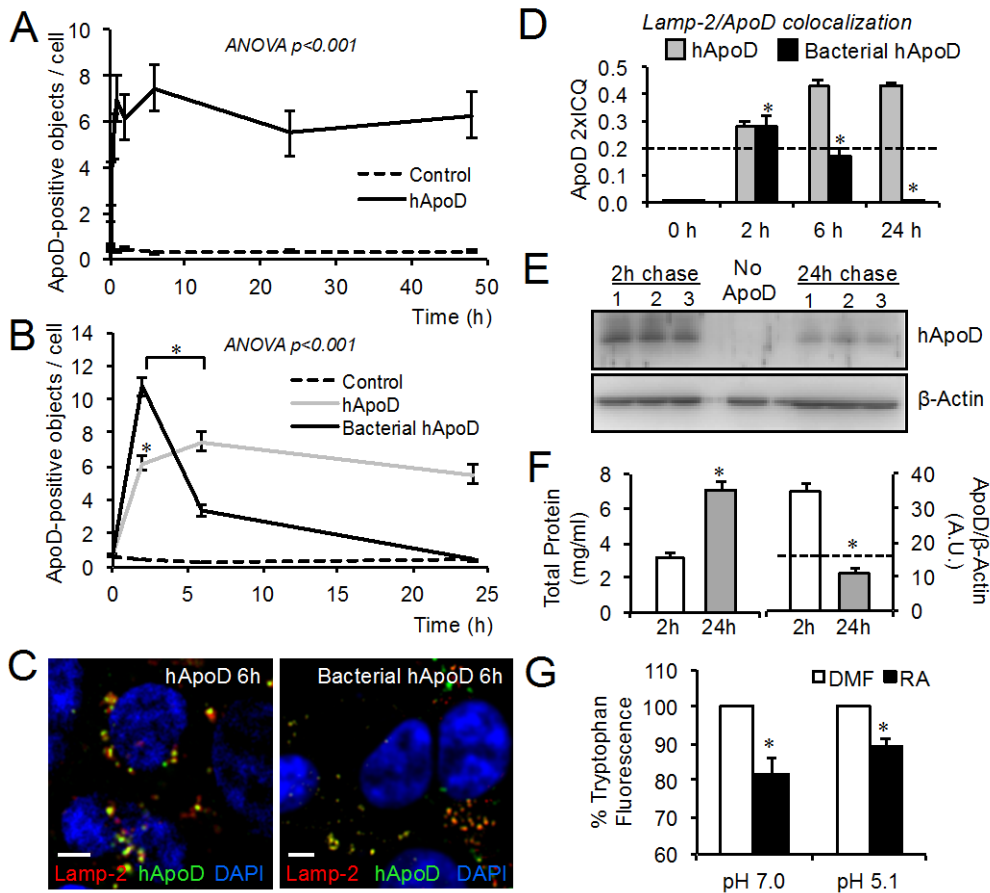
Figure 18. The stability of ApoD in LELC is dependent on its glycosylation state, and the Lipocalin fold maintains ApoD lipid binding functionality in acidic pH. A.** Number of ApoD-positive objects in HEK293T cells after exposure to 10 nM native human ApoD protein (2 h pulse/48 h chase).* ***B. *A 2 h pulse/24 h chase experiment is performed with bacterially-expressed ApoD protein. Control in A and B are HEK293T cells not exposed to ApoD.* ***C.*** *Co-localization of ApoD with Lamp-2 (6 h chase) after exposure to either native human ApoD or bacterially-expressed human ApoD for 2 h. Representative confocal sections are shown.* ***D.*** *Lamp-2 co-*

*localization index referenced to ApoD signal (ApoD 2xICQ) in HEK293T in a 2 h pulse/24 h chase experiment with native or bacterially-expressed ApoD. **E.** Immunoblot analysis of ApoD loss rate in HEK293T subject to 2 h pulse/24 h chase with native human ApoD. Equal amounts of total protein (40 µg) are loaded from three independent cultures. A control culture with no ApoD addition is shown in the center lane. **F.** Total protein concentration duplicates during the experiment due to cell division (left graph). The dashed line marks (right graph) the concentration value expected for ApoD following dilution by cell division. **G.** Tryptophan fluorescence quenching analysis of retinoic acid (RA) binding to native human ApoD at neutral and acidic pH (pH value selected from peak of lysosomal-pH distribution upon 2 h PQ treatment; see Fig. 14E). Dimethylformamide (DMF) was used as carrier. Error bars represent SEM in all figures. A-D: n=20 cells from at least two independent experiments. E-G: n=3-5 independent experiments analyzed; asterisks represent significant differences (p<0.01) assessed by ANOVA with Holm-Sidak post-hoc method. Calibration bars in C: 5 µm.*

These experiments demonstrate a very stable presence of native ApoD in the intracellular compartments analyzed above, and particularly in LELC, which suggests a functional role there. It is well known that proteins with essential functions within lysosomes bear carbohydrate shields against proteolysis [147]. In addition to the stable Lipocalin folding, ApoD N-linked glycosylation [19] might be responsible for such biochemical stability in protease-rich environments.

To further assay whether the Lipocalin folding can be stable in the acidic lysosomal lumen, we performed ligand binding assays at pH 7.0 and 5.1 (Fig. 18G; pH chosen in light of the pH distribution of ApoD-positive lysosomes under stress conditions, see below). Binding to retinoic acid, a generic hydrophobic ligand known to bind all human Lipocalins tested so far [17], indicates that ApoD ligand binding is functional under acidic conditions.

CHAPTER 2:   **ApoD controls lysosomal functional integrity and stabilizes their pH.**

2.1 ApoD identifies two pH domains in the astroglial lysosomal compartment with differential responses to oxidative stress.

2.2. Oxidative stress produces an increase of ApoD-positive lysosomes near the plasma membrane.

2.3 ApoD is targeted to the lysosomal compartment in an oxidative stress-dependent manner, both in differentiated neurons and primary astrocytes.

2.4 ApoD has an active role in the oxidation-sensitive lysosomal subdomain of cells, including neurons and astrocytes.

2.5 ApoD expression and targeting to lysosomes prevent lysosomal permeabilization.

Environmental insults such as oxidative stress (OS) can damage cell membranes. Lysosomes are particularly sensitive to membrane permeabilization since their function depends on intraluminal acidic pH and require stable membrane-dependent proton gradients. Cell types in the defense frontline, such as astrocytes, secrete ApoD to help neurons cope with the challenge.

In this chapter, we demonstrate ApoD role in lysosomal pH homeostasis upon paraquat-induced OS. By combining single-lysosome *in vivo* pH measures with immunodetection of ApoD, we demonstrate that ApoD is targeted to a subset of vulnerable lysosomes in a stress-dependent manner, it is functionally stable in this acidic environment, and its presence is sufficient and necessary for these lysosomes to recover from oxidation-induced lysosomal alkalinization, both in astrocytes and neurons.

2.1 ApoD identifies two pH domains in the astroglial lysosomal compartment with differential responses to oxidative stress.

An acidic pH is a defining functional property of lysosomes that allow their protease and lipase activities to be tightly controlled within the cell in addition to influence lysosomal fusions and trafficking. We set to study the functional relationships of ApoD to lysosomal pH by using the membrane permeable LysoSensor Yellow/Blue DND-160, a ratiometric dye specifically targeted to all lysosomes, and not only those reaching the LELC through the endocytic pathway [148, 149]. We used either excitation analysis in cell populations, suitable for pH 4.0-6.0, or emission

81

spectral analysis of single lysosomes in confocal microscopy optical sections combined with ApoD immunodetection (see *Methods*).

We first analyzed the effects of the treatments used in our experimental paradigm on the average lysosomal pH in 1321N1 cell populations (Fig. 19A). Chloroquine (CQ) was used as positive control. Two hours of PQ treatment resulted in significant lysosomal alkalinization (with an average increase of 0.5 pH units), in agreement with the reported sensitivity of lysosomal membranes to oxidative stress [117] resulting in proton leakage that counteracts pH gradient generation mechanisms.

When pH was measured at the single organelle level combined with ApoD labeling, we discover a striking difference in the frequency distributions of pH values (Fig. 19B). Lysosomes without ApoD show a narrow pH distribution with a frequency maximum at pH 4.4, while ApoD-positive lysosomes show a broaden distribution (range: 4.4-5.5) and a mode at pH 4.7 still in the range of lysosomal pH. This difference observed in control conditions is maintained when lowering serum in the culture medium. When we apply PQ, ApoD-negative lysosomes suffer a mild alkalinization (average peak shifts 0.2 pH units; Fig. 19C) that is persistent after 24 h of treatment. However, when the ApoD-positive lysosome pool is analyzed (Fig. 19D), a larger pH increase is observed (average of 0.5 pH units). This alkalinization is transitory, since lysosomal pH distribution returns after 24 h of PQ treatment to more acidic values, within the range of ApoD-positive lysosomes in control conditions. These data support the existence of subsets of lysosomes differing not only in their pH and ApoD content, but also in their sensitivity and response to an oxidative insult.

Our results show that ApoD is present in a subset of lysosomes specifically sensitive to oxidative stress that undergo a large but reversible alkalinization in response to PQ. Does the spatial distribution of ApoD-positive lysosomes influence PQ sensitivity?
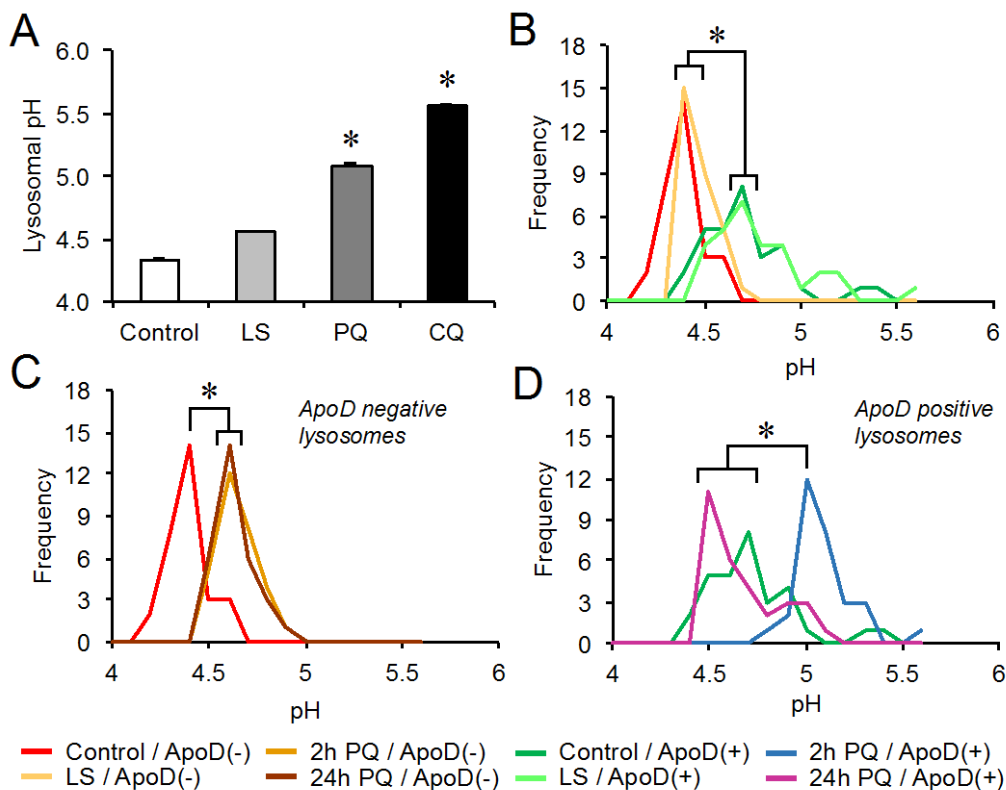
Figure 19. Single lysosome pH measurements combined with ApoD labeling identify two domains in the astroglial lysosomal compartment with differential responses to oxidative stress. A. *LysoSensor ratiometric excitation analysis of lysosomal pH in 1321N1 cell populations under LS (2 h), PQ (2 h), or CQ (1 h) conditions (n=9 cultures/condition). Oxidative stress generated by PQ alkalinizes the lysosomal compartment. CQ was used as positive control for alkalinization.* **B-D.** *Frequency distribution of lysosomal pH measured by confocal emission spectra analysis in single lysosomes of 1321N1 cells. Immunolocalization of ApoD allows for the detection of ApoD-positive and negative lysosomes (n=30 lysosomes/category). ApoD-positive and negative lysosomes in control and LS conditions are compared in B. ApoD-positive lysosomes distribution peak at pH 4.7 in both conditions, while that of ApoD-negative lysosomes is 4.4. The response of ApoD-negative lysosomes to PQ is shown in C. A small alkalinization (0.2 pH units) is established by 2 h and maintained after 24 h of PQ treatment. The response of ApoD-positive lysosomes to PQ is shown in D. ApoD is present in a subset of lysosomes specifically sensitive to oxidative stress that undergo a large (0.5 pH units) but reversible alkalinization in response to PQ. Differences were assessed by ANOVA on Ranks with Tukey post-hoc method (p<0.05, denoted by asterisks).*

2.2. Oxidative stress produces an increase of ApoD positive lysosomes near the plasma membrane.

Lysosomes have many diverse functions: degradation, recycling, secretion,… [150] that rely not only in the pH of a lysosome at a given moment, but also on its position in the cell cytoplasm. During lysosomal exocytosis lysosomes relocate from their perinuclear localization to the close vicinity of the plasma membrane [151], they fuse with each other and with the plasma membrane. This requires an increase in intracellular concentration of calcium [152]. Chii-Shiarng Chen [121] have reported that lysosomes closer to nucleus show lower pH. Using LysoSensor Yellow / Blue DND-160, we analyzed the relationships of ApoD to lysosomal pHand their location within the intracellular space. In Figure 19 we have reported that oxidative stress triggered by PQ induces a transient alkalinization in ApoD-positive lysosomes.

An analysis of the 1321N1 single lysosome data (Fig. 20A) shows a low proportion of ApoD-positive lysosomes in control conditions, and a significant early increase upon PQ treatment that is maintained after 24 h (overriding the proportion of ApoD-negative lysosomes).

We used emission spectral analysis of single lysosomes in confocal microscopy with combined ApoD immunodetection in three cell zones: the perinuclear zone, an intermediate zone, and an area close to the plasma membrane. To analyze the relationship between the presence of ApoD, pH and the zone where lysosomes are distributed, we generated an enrichment variable for each zone (Fig. 20B-C). This variable represents the difference between ApoD positive lysosomes and ApoD lysosomes of each cellular region. If a given zone has many lysosomes with ApoD, the enrichment variable will be positive, whereas if the zone shows ApoD–negative lysosomes, the enrichment variable will be negative.

Consistent with other published results, the lysosomal pH decreases as we move away from the nucleus (Fig. 20B). Analyzing pH and the ApoD enrichment of lysosomes of each region, we observed that the perinuclear zone is the least enriched region in ApoD. We observe the same alkalinization of lysosomal pH in the different regions analyzed with PQ-treatment, which indicates that PQ has homogeneously

affect the cell. However, we observed an enrichment in ApoD close to the plasma membrane. Peripheral lysosomes go from being "impoverished in ApoD" to being enriched with PQ treatment. This suggests that lysosomes with ApoD are moving to the periphery, or the periphery is attraying the ApoDentry for being the most sensitive.
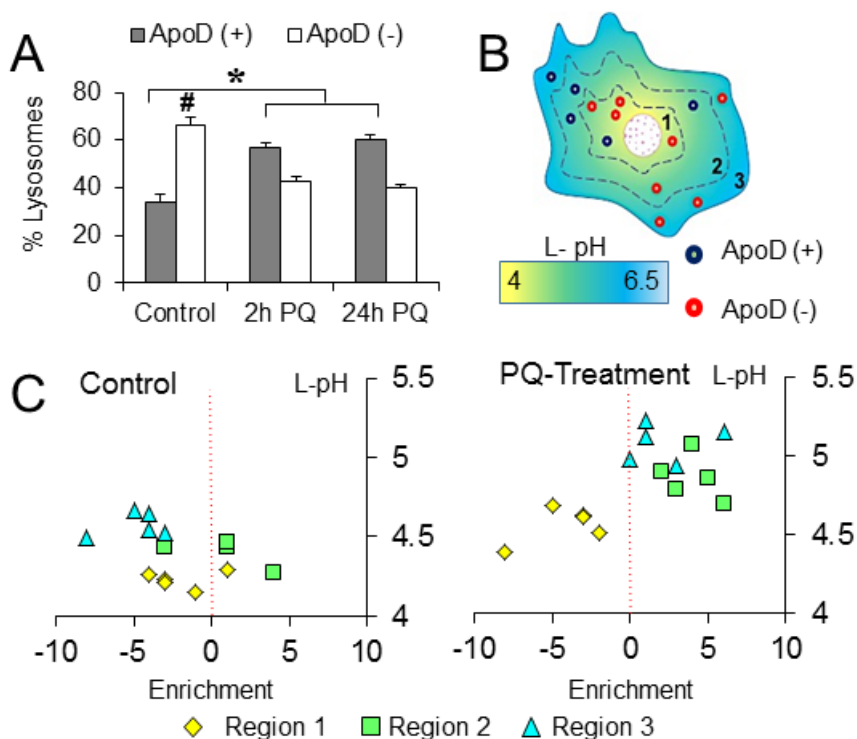
Figure 20. Lysosomes near the plasma membrane are enriched in ApoD in response to oxidative stress in 1321N1 astroglia. A. Lysosome quantification using LysoSensor combined with ApoD immunolabeling in 1321N1 cells. The proportion of ApoD-positive and negative lysosomes are shown (n=30 cells/condition). PQ triggers a significant enrichment in ApoD-positive lysosomes and depletion of ApoD-negative lysosomes. B. Schematic representation of the lysosomes in different cell regions (1-perinuclear, 2-intermediate, 3-near the membrane). ApoD-positive lysosomes (blue) and ApoD-negative lysosomes (red) are shown. Lysosomal pH is represented with a yellow-blue color gradient C.Distribution of lysosomal pH (L-pH; measured with LysoSensor ratiometric excitation analysis) in the different cell regions in control conditions or after 2 h of PQ treatment as a function of ApoD enrichment. (Enrichment= ApoD positive-ApoD negative lysosomes) (n=5 cells/condition; n > 20 lysosomes/cell). Upon oxidative stress ApoD-positive and more alkaline lysosomes are found close to the plasma membrane.

Our results show an increase in the amount of ApoD present in a subset of lysosomes sensitive to oxidative stress near the plasma membrane. To know if ApoD is responsible for these changes or if it is located in lysosomes passively subjected to to the PQ-triggered pH shifts, we need to make exogenous additions of ApoD to cell cultures.

In order to explain a cause (PQ treatment) -effect relationship (Targetting ApoD to vulnerable lysosomes), it is convenient to move to a situation in which we control the factors that make ApoD enter lysosomes. For that, in the next section we will treat two strategies: 1) add exogenous ApoD to neurons, which do not express ApoD, and 2) observe the behavior of ApoD in primary astrocytes, where in a normal situation there is no ApoD in lysosomes.

2.3 ApoD is targeted to the lysosomal compartment in an oxidative stress-dependent manner, both in differentiated neurons and primary astrocytes.

A Lamp-2/ApoD co-localization analysis in differentiated SH-SY5Y neurons after a two-hour pulse of exogenous human ApoD (Fig. 19A-B) shows that, in contrast with the observed rapid entrance into the LELC compartment in HEK293T cells (Fig. 18), differentiated neurons show no co-localization in control conditions 2 h after ApoD addition (Fig. 21A-B). Co-localization is evident later on, after a 24 h chase (Fig. 21B). In contrast, a significant co-localization is observed at 2 h in the presence of PQ and keeps increasing during the 24 h post-ApoD supplementation period (Fig. 21B). Thus, ApoD entry into lysosomes in neurons is dependent on stress conditions, being slow in the absence of stress, but very quick in its presence.

A similar phenomenon is observed with native murine ApoD in primary astrocytes (Fig. 21C), though with a remarkable feature: In control condition WT astrocytes show a clear predominant plasma membrane localization of ApoD and no co-localization with Lamp-2. ApoD entrance into the LELC is PQ-dependent and has a fast time course, with a substantial co-localization at 2 h.

We can conclude that the accelerated targeting of ApoD to the lysosomal compartment of neurons and primary astrocytes under stress conditions is a regulated process.
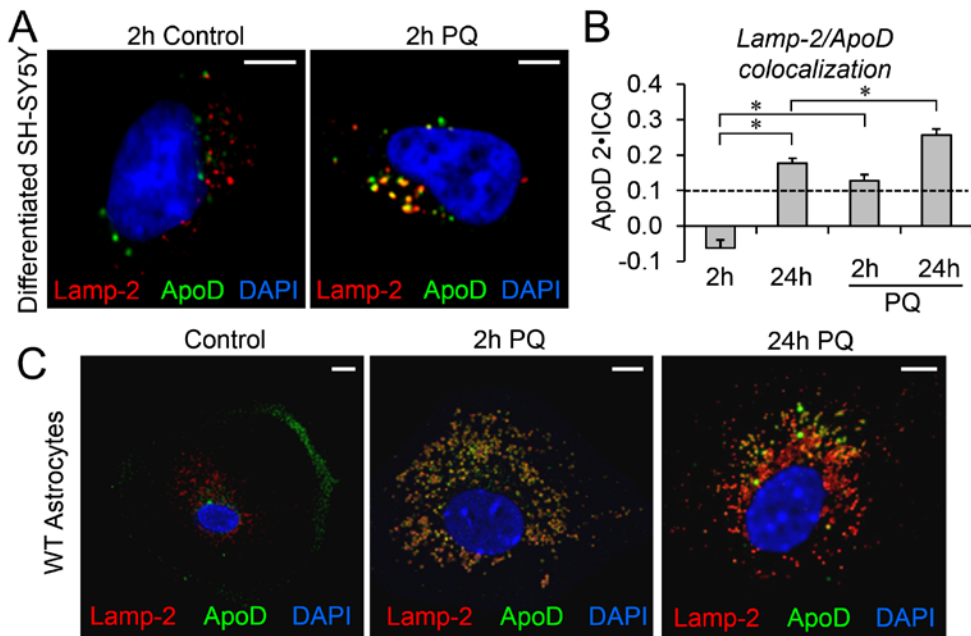
Figure 21. ApoD is targeted to the lysosomal compartment in an oxidative stress-dependent manner, both in differentiated neurons and primary astrocytes. A. Representative confocal microscopy images of ApoD and Lamp-2 in differentiated SH-SY5Y neurons after 2 h exposure to hApoD with or without simultaneous PQ treatment. B. Average co-localization index referenced to ApoD signal (ApoD 2xICQ) in neurons treated with hApoD in control and PQ conditions. Significant co-localization is observed in control conditions only 24 h post-ApoD exposure. Rapid entry into lysosomes is observed upon PQ treatment at 2 h. The dotted line represents the co-localization threshold. Statistical differences (asterisks) were assessed by two-way ANOVA, Holm-Sidak post-hoc method (p<0.01). C. Representative fluorescence microscopy images of ApoD and Lamp-2 in primary WT murine astrocytes in control and PQ conditions. ApoD distribution changes dramatically from membrane labeling (concentrated in lamellae) to intracellular organelles showing a time-dependent LELC co-localization. Calibration bars in A,C: 5 μm.

2.4 ApoD has an active role in the oxidation-sensitive lysosomal subdomain of neurons and astrocytes.

Is there a causal relationship between ApoD presence and lysosomal pH? To test this we added exogenous purified human ApoD to non-expressing HEK293T cells, either simultaneous to PQ exposure (2 h treatment) or sequentially, by first provoking lysosomal alkalinization with PQ (2 h) and then adding exogenous ApoD (Fig. 22A). We have already shown that by 2 h, ApoD has entered the LELC in HEK293T cells (Fig. 18D). The addition of ApoD prevents the PQ-triggered alkalinization and is able to reverse an already established effect of PQ (asterisks Fig. 22B).

We also added purified ApoD to differentiated SH-SY5Y neurons that do not express the Lipocalin (Fig. 15C). Here a longer simultaneous ApoD-PQ treatment was applied due to the dynamics of ApoD entry into neuronal LELC (Fig. 21). Again, ApoD is able to prevent (particularly prominently in the long 24 h treatment), as well as to revert, the alkalinizing effects of PQ (asterisks in Fig. 19C).

Aside of modifying ApoD presence by exogenous addition, we cultured murine primary astrocytes from wild type (WT) or knock-out (ApoD-KO) mice (Fig. 22D). Using this model, we demonstrate that: 1) The PQ-dependent alkalinization and re-acidification of 1321N1 lysosomes is also present in WT primary astrocytes. 2) ApoD-KO lysosomes do increase their pH upon oxidative stress, therefore indicating that the alkalinization itself is not related to ApoD presence. 3) No re-acidification is achieved in the absence of ApoD.

Summarizing, our data show that ApoD is present in a particular subset of PQ-sensitive lysosomes, which inevitably alkalinize in the presence of oxidative stress, an effect known to be due to lysosomal membrane damage [117, 153]. We also show that ApoD is responsible for the pH recovery of PQ-challenged lysosomes. These data support the hypothesis that lysosomal membrane recovery is compromised in the absence of ApoD, and that this Lipocalin, with its structure and lipid binding properties preserved, contributes to the repair of damaged lysosomal membranes in astrocytes and neurons.
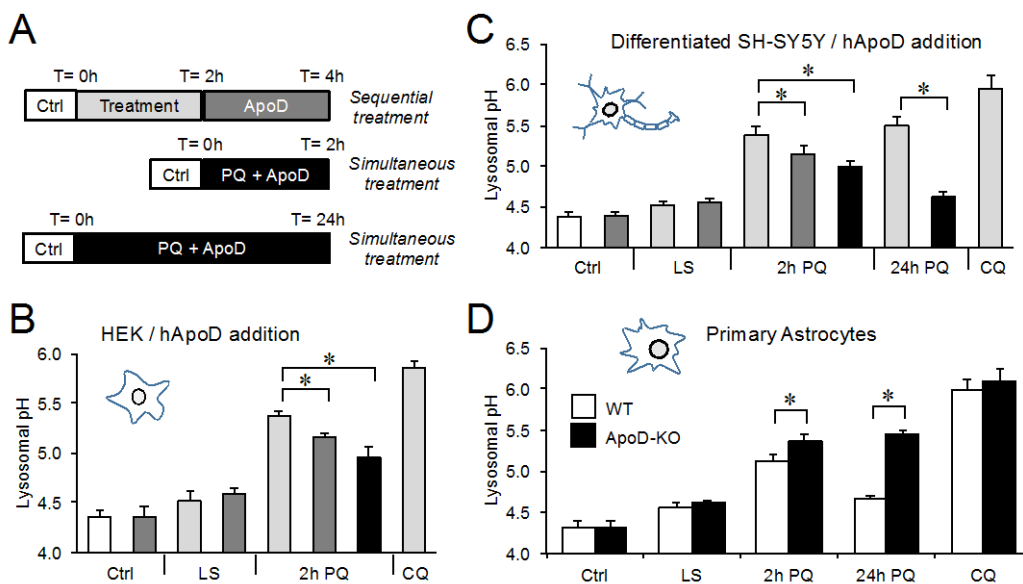
Figure 22. ApoD prevents and reverts oxidation-dependent alkalinization of lysosomes in cell lines, differentiated neurons and primary astrocytes. A. *Graphic representation of cell treatment protocols used to analyze lysosomal pH changes.* **B**. *HEK293T cells (not expressing ApoD) are treated with exogenous ApoD and PQ (short simultaneous or sequential applications). ApoD is able to prevent (black bar) and to revert (dark grey bars) the PQ-induced lysosomal alkalinization.* **C.** *In differentiated SH-SY5Y neurons (also without ApoD expression), we used short (2 h) interval protocols, as in HEK293T cells, and a long (24 h) simultaneous ApoD-PQ treatment. ApoD is able to modify neuronal lysosomal pH (dark grey bars) and to re-acidify oxidized lysosomes (black bars). This protective effect is durable over the time period studied, and reversion is complete by 24 h.* **D.** *Primary WT and ApoD-KO astrocytes (without exogenous ApoD addition) show PQ-dependent lysosome alkalinization, but only WT astrocytes are able to return to the basal pH level. The control CQ treatment in B-D results in lysosomal pH values at the edge of the LysoSensor probe dynamic range. Differences in B-D were assessed by ANOVA on Ranks with Tukey post-hoc method (p<0.05, denoted by asterisks).*

To further explore the consequences of this process we measured the levels of 4HNE (Fig. 23A-C), a lipid peroxidation-derived adduct, as a proxy for oxidative stress in each experimental condition. Interestingly, primary WT astrocytes have very low 4HNE levels in control conditions; they increase their oxidation levels by 2 h of PQ treatment, but return to basal levels by 24 h (Fig. 23A,C). By contrast, ApoD-KO

astrocytes show a significant basal level of oxidative stress and fail to recover from the insult (Fig. 23B,C), further demonstrating the reported protective role of ApoD upon oxidative stress [60]. Starting with a higher oxidation state, the level achieved by 2 h PQ in ApoD-KO astrocytes matches WT levels, indicating that cells have reached a 4HNE maximum. Therefore, ApoD entrance into lysosomes of WT astrocytes occurs at the peak of oxidative stress.

If ApoD targeting to lysosomes is regulated by oxidative stress, we wondered why there is a significant co-localization of ApoD with Lamp2 in 1321N1 astrocytoma cells under control conditions (Figs. 13-16). Figure 23C demonstrates that 1321N1 cells have a high basal oxidative stress, coherent with the high metabolic rate of cancer cells. Thus, ApoD is targeted to lysosomes under these conditions. The levels of 4HNE further increase in response to PQ treatment, and are followed by a substantial clearance of 4HNE adducts. This rebound effect is consistent with the pH recovery effect observed in our single-lysosome study (Fig. 19D), and suggests that oxidative-challenged cells transiently activate protective mechanisms (ApoD among them) that clear lipid peroxidation products. Thus, a mechanism controlling lysosomal targeting of ApoD also occurs in the astrocytoma cell line 1321N1. The efficient clearance of oxidized products might be the result of a very efficient lysosomal function, contributed by the ApoD-dependent re-acidification after PQ insult.

An active role of ApoD in oxidized lysosomes was further demonstrated by measuring lipofuscin, a reported readout of lysosomal pH dysfunction that results in cellular accumulation of damaged oxidized macromolecules [154]. A spectral analysis of confocal microscopy images of WT and ApoD-KO primary astrocytes (Fig. 23E,F) shows that the absence of ApoD generates a significant increase in lipofuscin signal in astrocytes under control conditions, which agrees with the high lipid peroxidation levels reported in Figure 23A-B.
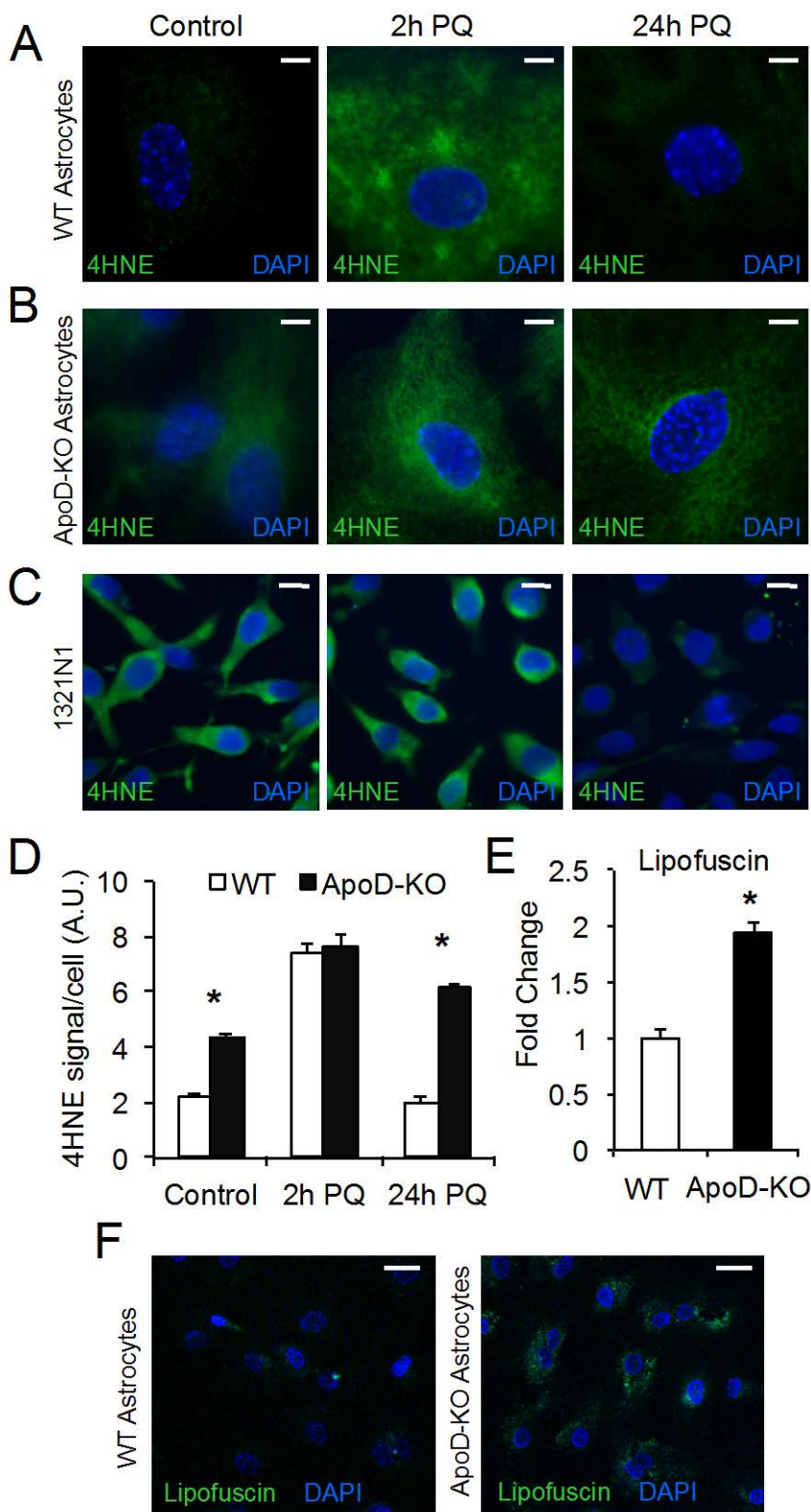
Figure 23. ApoD expression and targeting to lysosomes prevent cell lipid peroxidation and lysosomal accumulation of oxidized cargo. A-B. Immunodetection of 4HNE adducts by fluorescence microscopy in primary WT (A) or ApoD-KO (B) astrocytes in control and PQ conditions. C. Representative fluorescence microscopy images of 4HNE labeling in 1321N1 cells in control and PQ conditions. Basal oxidative stress level is high, compared to primary astrocytes. Long-term response to PQ results in clearance of 4HNE adducts at 24 h. D. Plot representing 4HNE raw intensity/cell (n>400 cells/genotype/condition) in primary astrocytes. WT astrocytes have very low basal 4HNE levels and recover completely after 24 h of PQ treatment. Without ApoD, basal lipid peroxidation is significantly high and astrocytes are unable to counteract PQ long-term effects. E. Plot representing the fold change in lipofuscin signal measured by confocal spectral analysis in ApoD-KO astrocytes compared to WT cells (n>1500 astrocytes/genotype). F. Representative fluorescence microscopy images of lipofuscin signal in WT and ApoD-KO astrocytes under control conditions. Statistical differences in C and E were assessed by two-way ANOVA (p<0.001), and Holm-Sidak post-hoc method (p<0.001). Differences in G were assessed by Student's t-Test. Calibration bars: 10 µm (A,B,C) 20 µm (F).

2.5 ApoD expression and targeting to lysosomes prevent lysosomal permeabilization.

If the mechanism by which ApoD controls lysosomal pH is due to lysosomal membrane stabilization, two predictions can be made for lysosomal behavior in the absence of ApoD: 1) Lysosomal proteases would decrease their activity, and 2) Cytoplasmic proteins would aberrantly enter lysosomes. A Cathepsin B activity assay (Fig. 24A-C) demonstrates the first prediction. In WT astrocytes (Fig. 24A,C), PQ-triggered oxidation reduces Cathepsin B activity, but a clear recovery takes place upon prolonged PQ exposure in parallel with lipid peroxide clearance (Fig. 23A,C). In the absence of ApoD (Fig. 24B,C), Cathepsin B activity is significantly reduced in basal conditions, further deteriorated upon PQ treatment, and no recovery is obtained after 24 h treatment.
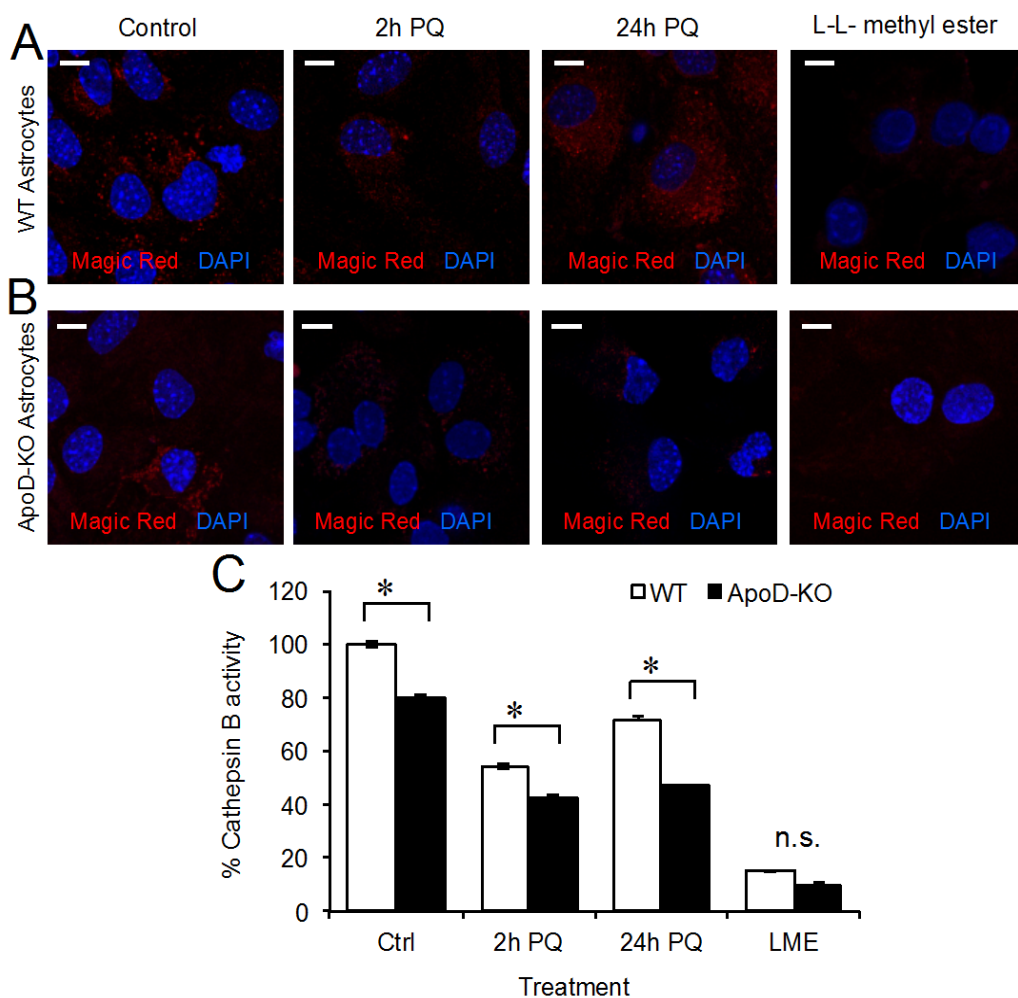
Figure 24. ApoD prevents the decrease of lysosomal activity upon oxidative stress. A-B. Cathepsin B activity monitored by Magic Red assay. The punctate fluorescent signal is proportional to its proteolytic activity, taking place in lysosomes. WT (A) and ApoD-KO (B) primary astrocytes are compared. L-leucyl-L-leucine methyl ester (LLME) is used as positive control for lysosomal membrane rupture. C. Cathepsin B activity is plotted normalized to values obtained in control WT astrocytes. PQ provokes a reduction of Cathepsin B activity that is recovered after 24 h treatment in WT astrocytes. Lack of ApoD results in reduced basal activity and unrecoverable activity loss after PQ insult. Average ± SEM of three independent experiments are shown. Statistical differences in C were assessed by two-way ANOVA (p<0.001), and Holm-Sidak post-hoc method (p<0.001). Calibration bars: 10 μm.

Galectin-3 immunocytochemistry (Fig. 25) demonstrates the second prediction. This lectin shows a diffuse cytoplasmic location in control WT astrocytes cultures, but

translocates to leaky lysosomes undergoing oxidative stress-dependent membrane permeabilization upon PQ insult, giving a punctate labeling pattern [155]. Astrocytes lacking ApoD show evident Galectin-3 puncta in control conditions (arrows in Fig. 25), and the effect is further increased upon 2 h PQ.
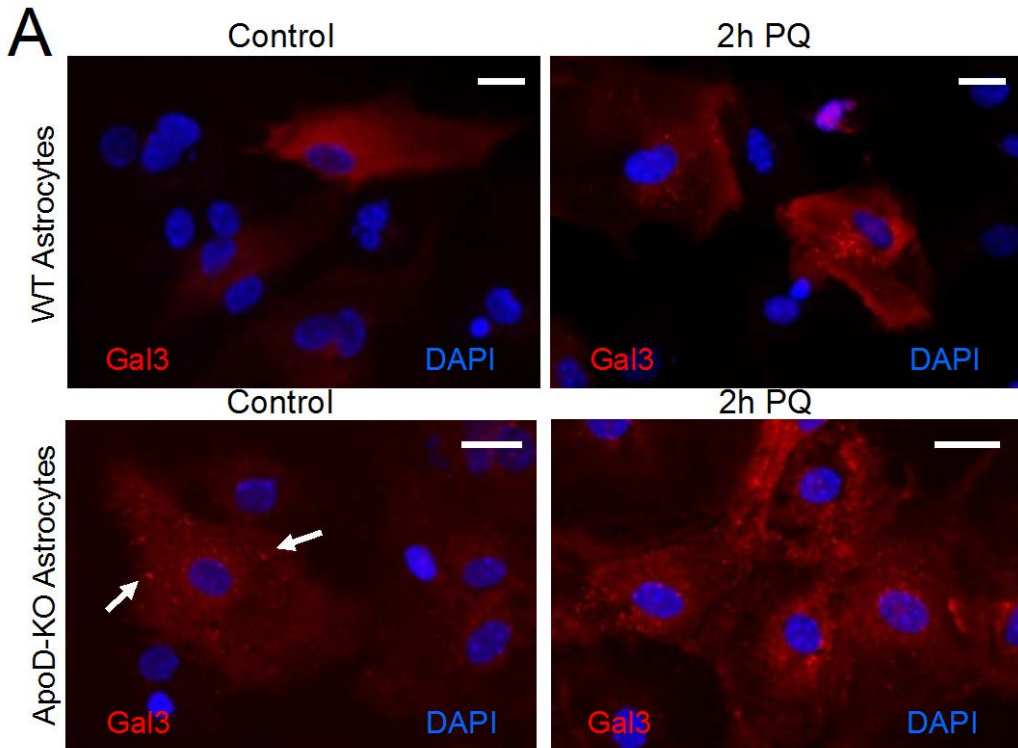
Figure 25. ApoD prevents lysosomal membrane permeabilization upon oxidative stress. A Representative fluorescence microscopy images of Galectin-3 signal in WT and ApoD-KO astrocytes under control and 2 h of PQ treatment. A switch from cytoplasmic to vesicular (lysosomal) Galectin-3 labeling occurs under oxidative stress conditions in WT astrocytes. The lysosomal labeling of Galectin-3 is evident for ApoD-KO primary astrocytes in control conditions (arrows), and increases under PQ treatment. Calibration bars: 20 μm.

In summary, entrance of ApoD into the LELC, and particularly into lysosomes, is actively promoted in pro-oxidative conditions in neurons and astrocytes. Our data demonstrate that ApoD, contributing to lysosomal pH recovery upon oxidative stress, is recruited to a vulnerable subset of lysosomes of the intermediate and external regions, where it helps to keep lipid peroxides levels under control and to safeguard

lysosomal functional integrity by avoiding lysosomal membrane permeabilization. Meanwhile, perinuclear lysosomes are depleted of ApoD.

We have shown that ApoD affects the differential response of a subset of lysosomes to oxidative stress by actively promoting pH recovery.

CHAPTER 3:   **ApoD-enriched astroglial-derived exosomes mediate neuroprotection upon oxidative stress.**

3.1 Glia-neuron communication *in vitro*.

3.2 Neurons uptake glial-derived EVs enriched in ApoD.

3.3 Isolation and characterization of ApoD in glial EVs: ApoD as a very specific marker of glial exosomes.

3.4 ApoD influences EV biogenesis.

3.5 ApoD-containing exosomes underlie the protective reaction of glial cells against oxidative stress and mediate ApoD-dependent neuroprotection.

Nervous sytem function relies on a complex set of cell types interacting and communicating among them. The discovery of extracellular vesicles (EVs) opens up a new mechanism of signal transmission that is changing our understanding of how glia and neurons communicate. Particularly important in brain illnesses is the potential therapeutic use of EVs, given their demonstrated by pass of the blood-brain barrier [103, 104]. In this regard, EVs purposedly loaded with neuroprotective molecules are a promising therapy for neurodegenerative disorders.

Proteomic analyses identified ApoD in serum and cerebrospinal fluid [156, 157]. Thus, we set up to test the contribution of ApoD in glial-derived EVs to improve neuronal viability and function. Is ApoD secreted through EVs from producing to non-producing nervous system cells to protect them?

3.1 Glia-neuron communication *in vitro*.

Until now, we have described how in the presence of oxidative stress produced by PQ the expression of ApoD and its enrichment in the membrane is increased (Chapter 1, Fig. 9). We have also analyzed the internalization trafficking of ApoD and its entry into the lysosome (Chapter 2). The whole study of the subcellular trafficking of ApoD has led us to study the ApoD output of the cell. Is ApoD secreted through the canonical pathway or is it through other types of cell-cell communication?

Although extensive data support the role of extracellular vesicles as mediators of neuron-glia communication in vivo [93, 94], we tested whether this relationship exist between the astroglial 1321N1 and neuronal SH-SY5Y cell lines, since they have been used to unravel the mechanism of action of ApoD (Chapter 2). We studied the

exchange of vesicular contents between these cells by labelling the membranous compartment of 1321N1 astrocytes with the lipophilic compound DiI, and the endo-lysosomal compartment of SH-SY5Y neurons with Dextran-Alexa 488 (see Methods section). Co-culturing these cells in EV-free media for 48 hours and analyzing the fluorescent markers distribution by confocal microscopy, we found that some of the labelled organelles colocalize with CD81, a marker of late endocytic compartments [158] (Fig. 26A,B). In addition, the colocalization of DiI and Dextran-Alexa 488 in astrocytes and neurons (Fig. 26C,D) suggests an exchange of membranous material among them that could be mediated by extracellular vesicles (EVs). Flow cytometry analysis (Fig. 26E-H) confirms that a significant number of cells show DiI-Dextran co-labelling (Fig. 26H), and the distribution of the co-labelled cells (Arrow in Fig. 26H) suggests that EVs transfer might be occurring mainly in the astrocyte-to-neuron direction.

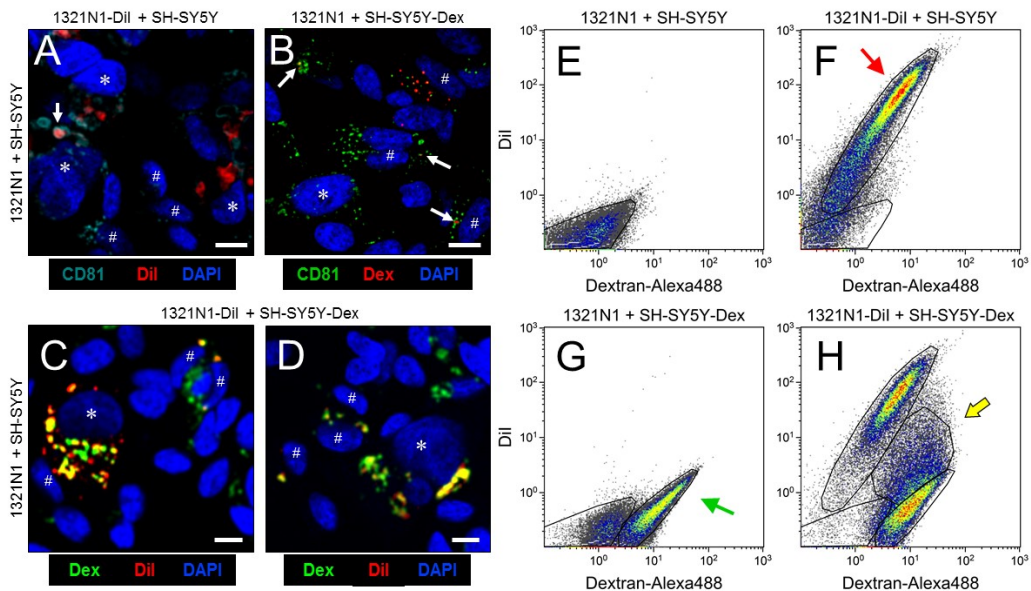*Figure 26. Astrocytes and neurons exchange CD81-positive material. A-D. Representative confocal microscopy images of co-cultures of: 1321N1 astrocytes labelled with DiI with unlabelled SHSY5Y neurons (A), unlabelled 1321N1 with SH-SY5Y labelled with Dextran-Alexa 488 (B), 1321N1 labelled with DiI with SH-SY5Y labelled with Dextran-Alexa 488 (C,D). Immunocytochemistry with the EV marker CD81 is shown in A and B. Arrows point to co-*

localizing signals. Asterisks and pound signs mark astrocyte and neuronal nuclei respectively.
E-H. *Flow cytometry analyses plotting the DiI and Dextran-Alexa 488 signals in the different co-culture conditions. The red arrow in F indicates the DiI-1321N1 population, and the green arrow in G points to the Dextran-Alexa 488-SHSY5Y population. The double labelled cell population is shown in H with a yellow arrow. Calibration bars: 10 μm*

However, the results above can be explained by either a cell-cell direct contact or by the endocytosis of cellular debris generated in the co-cultures such as apoptotic bodies. To test this hypothesis we used a Transwell assay, where we cultured, in EV-free media, DiI-labelled 1321N1 astrocytes as donor cells on the Transwell insert, and SH-SY5Y neurons as the target cells, cultured on the lower compartment. After 48 hours of incubation, a DiI positive population of SH-SY5Y recipient cells (25.10%) is detected by flow cytometry (Fig. 27A-C). These experiments suggest that SH-SY5Y neurons receive and internalize DiI-labelled vesicles secreted by 1321N1 astrocytes.

3.2. Neurons uptake glial-derived EVs enriched in ApoD.

Given that SH-SY5Y neurons do not express ApoD [159], the Transwell co-culture experiments can readily inform us on whether glia-derived vesicles uptaked by them contain astrocyte-derived ApoD. Immunocytochemistry of Transwell co-cultured neurons show significant co-localization of ApoD with EV markers CD63 (Fig. 27D, G) and CD81 (Fig. 27E, G), as well as with the astrocyte-originated DiI signal (Fig. 27F, G). CD63 and DC81 can be either endogenous or transferred in astrocyte-derived EVs, however, the subset of CD63 or CD81-positive organelles that are also ApoD-positive, are strong candidates to have an astrocytic origin. Interestinlgy, the high co-localization index (2xICQ>0.6) of CD81 relative to the DiI signal detected in neurons strongly supports a significant uptake of CD81-DiI-labelled EVs, a portion of which (2xICQ>0.2) bring ApoD with them (Fig. 27G). This quantitation co-localization indexes is in agreement with the high incidence of triple colocalization of ApoD-CD81-DiI (Fig. 27F).
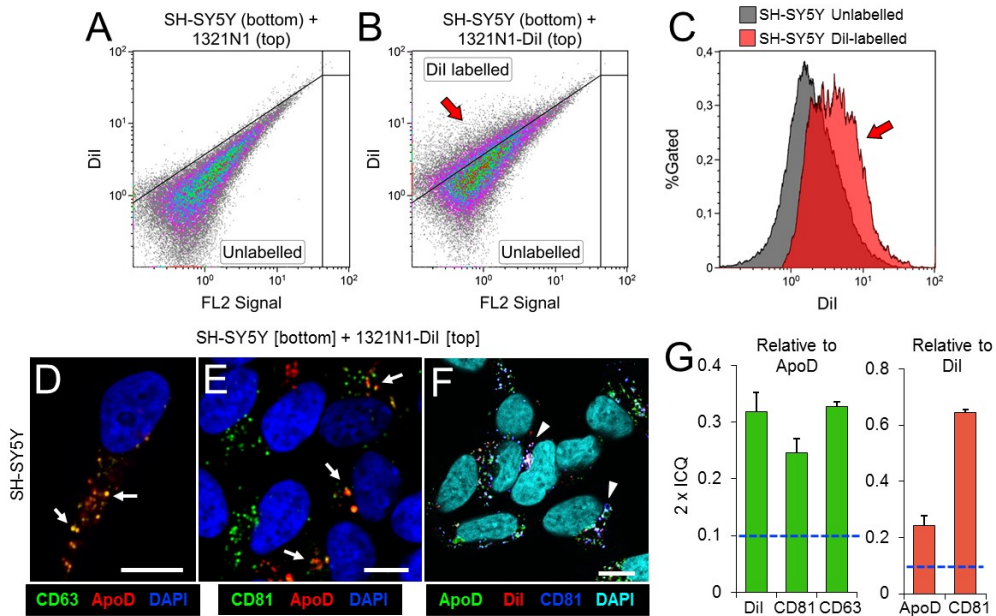
Figure 27. . Astrocyte-to-neuron communication is mediated by EVs that carry ApoD into neurons. A-C. Flow cytometry analyses of SH-SY5Y cells cultured in Transwell with 1321N1 cells, either unlabelled (A) or labelled with DiI (B, C). Dot plots show a population of DiI-positive SH-SY5Y neurons (arrow in B) when cultured with labelled 1321N1 astrocytes. The histogram in C displays the fluorescence increase in DiI-positive neurons (arrow), with median fluorescence increasing from 1.9 to 4.0 (a.u.). D-F. Representative confocal images of unlabelled SH-SY5Y target cells cultured on the lower compartment of a Transwell assay while DiI-labelled 1321N1 donor cells were cultured on the insert. Immunofluorescence with ApoD, CD81 and CD63, and DiI signal are shown with different LUTs to properly display the colocalization of EV markers with ApoD (arrows in D, E) or with DiI (arrowheads in F point to triple co-localization DiI-CD81-ApoD). Calibration bars: 5 μm. G. Average colocalization index (2xICQ) referenced either to ApoD signal (green bars) or to DiI signal (red bars) in SH-SY5Y neurons co-cultured in Transwell with DiI-labelled 1321N1 astrocytes. The dotted lines represent the colocalization threshold. Error bars represent SEM (n = 20 cells/marker from at least two independent experiments).

These results strongly suggest that ApoD is present in EVs that travel from glial cells to neurons. To further contrast this hypothesis, we purified EVs from the culture medium of primary astrocytes, which express ApoD (see Methods), and demonstrated by Western blotting (Fig. 28) the presence of ApoD in both the cell homogenate and

the EV-enriched fraction, where EVs presence is corroborated by the CD81-positive signal. Taking into account the starting material for the cell homogenate and the EV-enriched preparation, we estimate that 0.6% of ApoD protein in an astroglial cell is targeted to EVs.
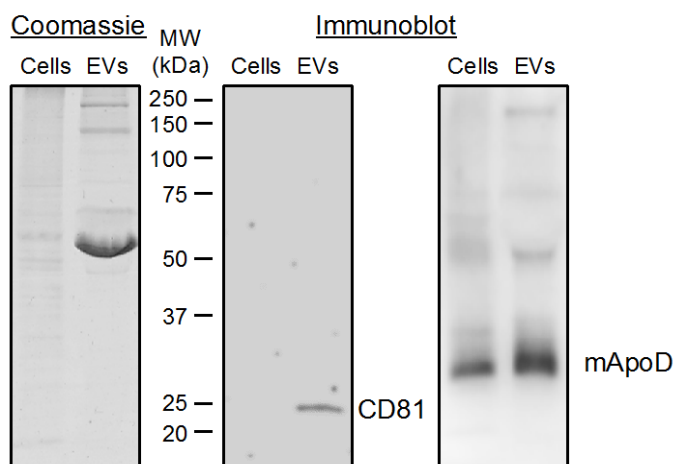
Figure 28. . Astrocytes produce ApoD-positive EVs. *Immunoblot analysis of ApoD and CD81 in cell lysates and EV preparations from WT primary astrocytes. The EV extract loaded in the second lane was originated from 240 times more cells than the homogenate loaded in the first lane. Intracallular CD81 is not detectable in the cell extract.*

3.3. Isolation and characterization of ApoD in glial EVs: ApoD as a very specific marker of glial exosomes.

1321N1 astroglia express the EV marker CD81 (Fig. 26A) which co-localizes with DiI-labelled membranous organelles that can be transferred to neurons (Fig. 27). Also, multivesicular bodies (MVB) can be detected in the cytoplasm of 1321N1 astrocytes by EM (Fig. 29A). Our analysis of intracellular trafficking of ApoD (Chapter 1) revealed its presence in the extracellular side of the plasma membrane, and its trafficking through the endo-lysosomal and autophagosome compartments. Here, we show by means of immunofluorescence and immunoelectron microscopy that ApoD can also be found both in Lamp-2 positive MVBs (Fig. 29B), and in putative extracellular vesicles (arrowhead in Fig. 29C), whose size is in the range of exosomes.
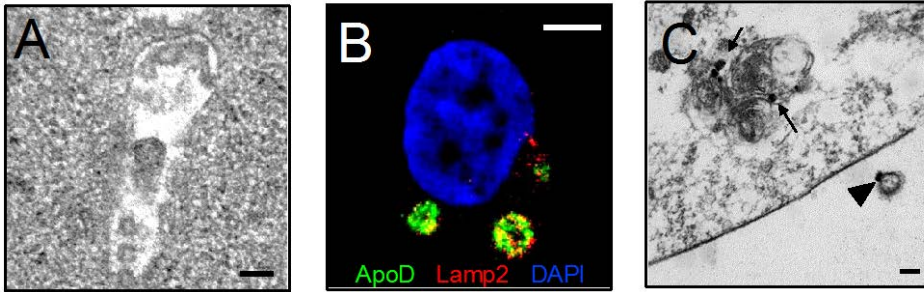
Figure 29. ApoD is a strong marker of astrocyte-derived exosomes. A. *Electron microscopy image of a multivesicular body (MVB) in the cytoplasm of a 1321N1 astrocyte.* ***B.*** *Representative image of a 1321N1 astrocyte showing the colocalization of ApoD and Lamp2 in putative MVBs.* ***C.*** *Immunoelectron microscopy image showing ApoD in a mature lysosome of a 1321N1 cell (arrows), and on the external surface of a putative exosome (arrowhead). Calibration bars: A,C: 100 nm; B: 5 µm.*

Given the locations of ApoD, could it be carried in membrane budding microvesicles (MVs) or in MVB-derived exosomes? When control culture medium (before EVs production) and 1321N1-conditioned medium collected after 72 h are subjected to NTA (Fig. 30A), we found that 1321N1 cells secrete several EV populations, with a group showing a particle size compatible with exosomes (arrow in Fig. 30A). Following sucrose gradient fractionation of the 1321N1 EV preparations we uncover that fractions with densities of 1.176 g/ml and 1.232 g/ml present positive immunoblot signals for ApoD and the exosome marker CD81 (Fig. 30B). Curiosly these exosomes show the presence of both monomeric and dimeric forms of ApoD (see Discussion section). Our results demonstrate that ApoD is specifically enriched in exosomal fractions of 1321N1 astroglial EVs.
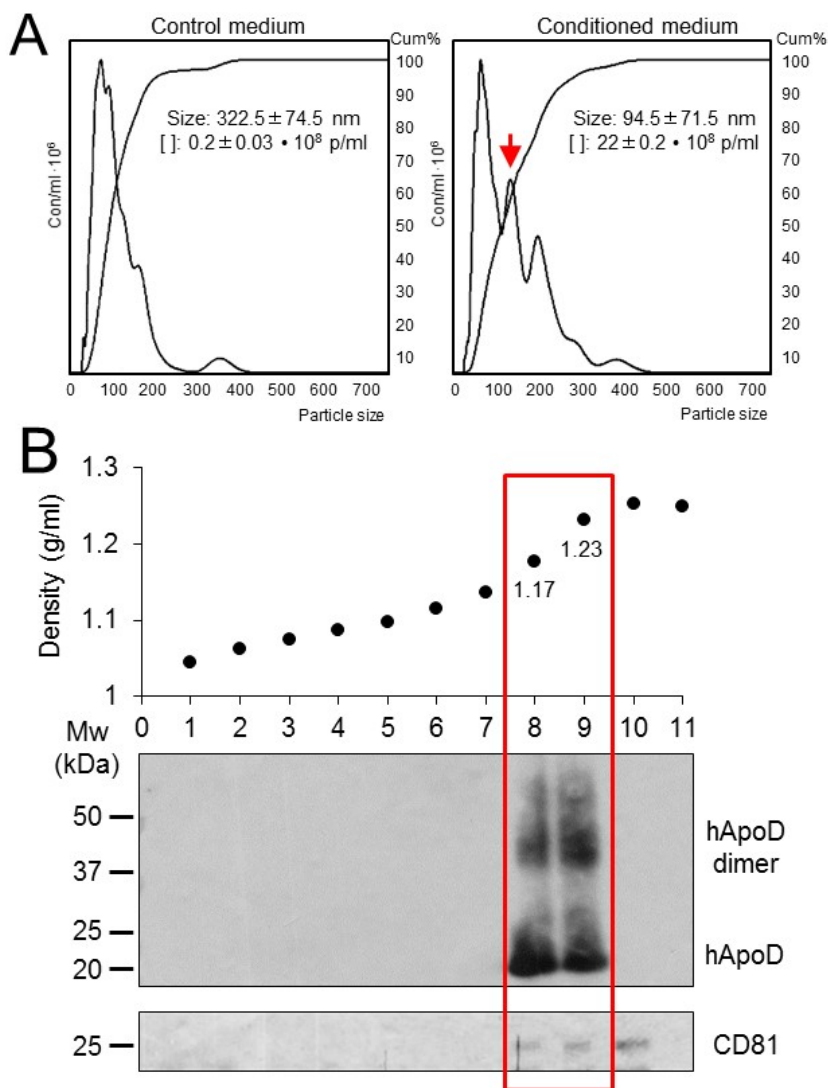
Figure 30. ApoD is a very specific marker of astrocyte-derived exosomes A. *Nanoparticle tracking analysis (NTA) of control culture medium or astrocyte-conditioned medium (n = 2 independent samples), showing that 1321N1 astrocytes secrete several EV populations with a group showing particle size compatible with exosomes (red arrow).* **B.** *Fractionation of EV preparation from 1321N1 astrocytes by sucrose gradient. Plot shows the fraction density along with the immunoblot analysis of each fraction with ApoD and CD81 antibodies. Fractions 8 and 9 are the only ones positive for ApoD, while the exosome marker CD81 appears in fractions 8-10.*

3.4. ApoD influences EV biogenesis.

Because of the role of ApoD in the stability and protection of lysosomal membranes upon oxidative stress, and in the maintenance of lipid peroxidation levels in the cell (Chapter 2, Fig. 23), we explored whether ApoD is just a cargo within exosomes, or it is also involved in the biogenesis and homeostasis of EVs. We therefore studied EVs of astrocyte primary cultures from WT and ApoD-KO mice, by labelling cells with DiI (Fig. 31A) and analyzing the culture medium after 72 h. A fluorimetry analysis of DiI fluorescence in the medium (as read-out of EV production by astrocytes), shows a slight but significant decrease in EV production in the case of ApoD-KO astrocytes comparing to WT (Fig. 31B).

To futher demonstrate the question above, we isolated EVs from WT and ApoD-KO astrocyte culture medium. After confirmimg by electron microscopy the presence of EVs in both preparations (Fig. 31C), we detected ApoD by immunoblot only in the cargo of WT EVs (Fig. 31D), as expected. NTA experiments revealed that WT and ApoD-KO mouse astrocytes generate EVs of similar size, but in agreement with the DiI quantification reported above, the particle concentration is significantly lower in the absence of ApoD (Fig. 31E).

Figure 31. ApoD influences exosome biogenesis. A. Representative confocal images of WT and ApoD-KO primary astrocytes lab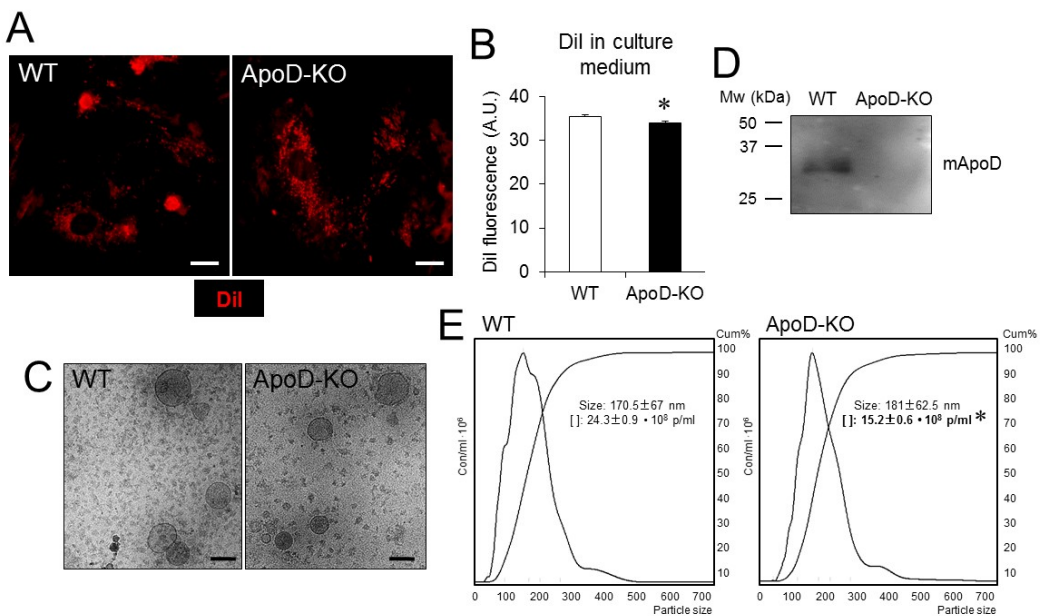elled with DiI (n = 14 samples from two independent experiments). B. Estimation of exosome production from WT and ApoD-KO primary astrocytes by quantifying DiI fluorescence in the culture medium after removal of cell debries by low speed centrifugation. Asterisk point to significant differences (p<0.05) in ApoD-KO medium fluorescence level concentration, assessed by Student t-test. C. Immunoelectron microscopy images of WT and ApoD-KO EVs. Calibration bars: A: 10 µm; C: 100 nm. D. Immunoblot analysis of ApoD in WT and ApoD-KO primary astrocytes EV preparations, confirming the presence of ApoD in WT EVs. E. Nanoparticle tracking analysis of WT and ApoD-KO EVs (n = 2 independent samples). Asterisk point to significant differences (p<0.05) in ApoD-KO particle concentration, assessed by ANOVA with Holm-Sidak post-hoc method. No difference in size is detected.

3.5. ApoD-containing exosomes underlie the protective reaction of glial cells against oxidative stress and mediate ApoD-dependent neuroprotection

A fair amount of data account for the neuroprotective effects of ApoD in astrocytes [60] (Chapter 2, Fig. 23). We therefore tested the effect of astrocyte-derived conditioned media on primary astrocytes of WT and ApoD-KO mice exposed to the ROS generator Paraquat (PQ; 500 µM) for two hours. Figure 31 shows that the viability of PQ-challenged astrocytes significantly improves when they were cultured with astrocyte-derived conditioned media (collected over a 72 h period), regardless of cell genotype or origin of the media (Fig. 32, gray and black bars). For WT astrocytes, the same protection effect is attained with media conditioned by WT or by ApoD-KO cells, an effect that can be explained by the accumulation of various protective factors overtime. However, the more vulnerable ApoD-KO astrocytes are significantly better protected when exosed to ApoD-WT conditioned media (black bar) than when media was conditioned by ApoD-KO astrocytes (gray bar). These results suggest that ApoD, produced by WT astrocytes, and present in the extracellular medium, is significantly contributing to protect astrocytes from OS in an autocrine manner.
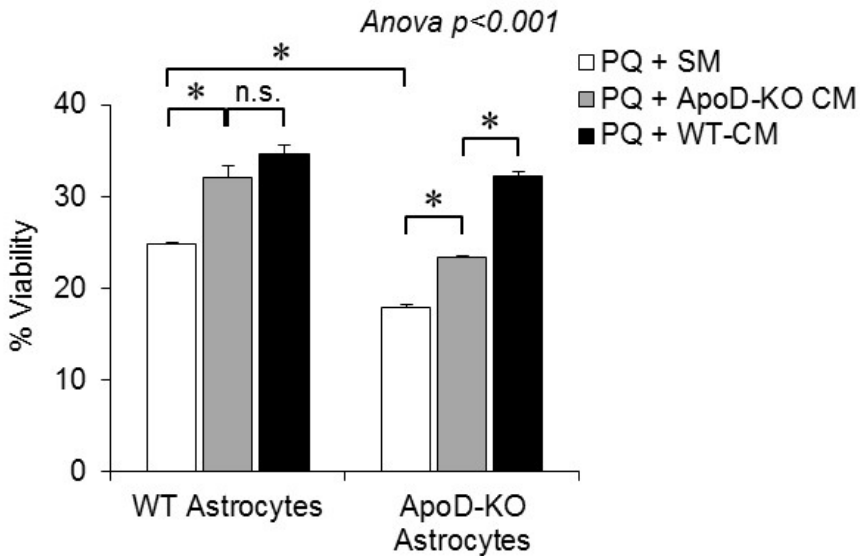
Figure 32. Extracellular ApoD mediates autocrine protection of astroctyes. *Percent viability estimated by the MTT-assay of WT and ApoD-KO astrocytes cultured in standard medium (SM) and astrocyte-conditioned medium (CM), either derived from ApoD-KO astrocytes (grey bars) or from WT astrocytes (black bars), upon an oxidative stress challenge with paraquat (PQ 500 μM, 2 hours). Error bars represent SEM (n = 3 independent experiments). Asterisks point to significant differences (p<0.01) assessed by ANOVA with Holm-Sidak post-hoc method (n.s.: non-significant differences). Only most relevant comparisons are pointed.*

Since now we know that astrocytes produce ApoD-positive exosomes, we wonder how much those EVs contribute to the protection of neurons by ApoD-expressing astrocytes.

In order to assess this hypothesis, we cultured SH-SY5Y neurons with standard media (SM), with 1321N1-conditioned media (CM), with the EV fraction (EVs) obtained by differential ultracentrifugation from the CM, and, finally, with the EV-depleted supernatant (Sup) of the CM. Two types of experiments were carried out in these conditions: an immunocytochemistry ananalysis of ApoD uptake by neurons, and a viability assessment upon PQ challenge.

Double immunofluorescence analysis on cultured SH-SY5Y with CD63 and ApoD shows absence of the Lipocalin labelling in SM-cultured neurons (Fig. 30A), as

expected, since they do not express ApoD. The CD63 signal observed here corresponds to the endogenously expressed by neurons. A clear colocalization of ApoD and CD63 is observed in CM-cultured cells (Fig. 30B), which agrees wih our previous reports showing internalization of ApoD in neurons [25] and with the results obtained in Transwell experiments (Fig. 27). The CD63 signal that co-localizes with ApoD can in this case be part of the ApoD-loaded exoxomes produced by 1321N1 astrocytes (Fig. 29E). ApoD labelling and colocalization with CD63 is also observed after addition of the EV fraction of CM (Fig. 32C). In contrast, no ApoD labelling is obtained after exposure to the EV-depleted CM (Fig. 33D). On the one hand, these results confirm that ApoD is present in EVs purified from astrocyte-conditioned media (as demonstrated in Fig. 28, and detected specifically in the exoxomal fractions of those EVs, Fig. 29). They also confirm that ApoD-positive EVs become internalized by SH-SY5Y neurons. The unexpected result is the absence of detectable ApoD endocytosis into neurons when we use the EV-depleted conditioned medium, which strongly indicate that the majority of extracellular ApoD produced by 1321N1 astrocytes is exosome-associated and not in a free soluble form.

We then tested wether exosome-associated ApoD has an effect on neuronal viability upon an oxidative insult. The presence or absence of ApoD in the media or its EVs does not involve a change in viability under control conditions (white bars in Fig. 32E). However, after an OS stimulus (2 mM PQ for 2 h) the PQ triggered decrease in cell viability observed in standard medium (SM) is significantly ameliorated by complete CM or its EV fraction (Fig. 33E). The protective effect is only partial when the EV-depleted media is used (Sup in Fig. 33E). The beneficial effect of exosomes-associated ApoD compares to that obtained with native ApoD purified of human cystic fluid (Fig. 33F). The specificity of this beneficial effect is proven by its reduction when the protein is previously incubated with a rabbit polyclonal serum anti-ApoD.
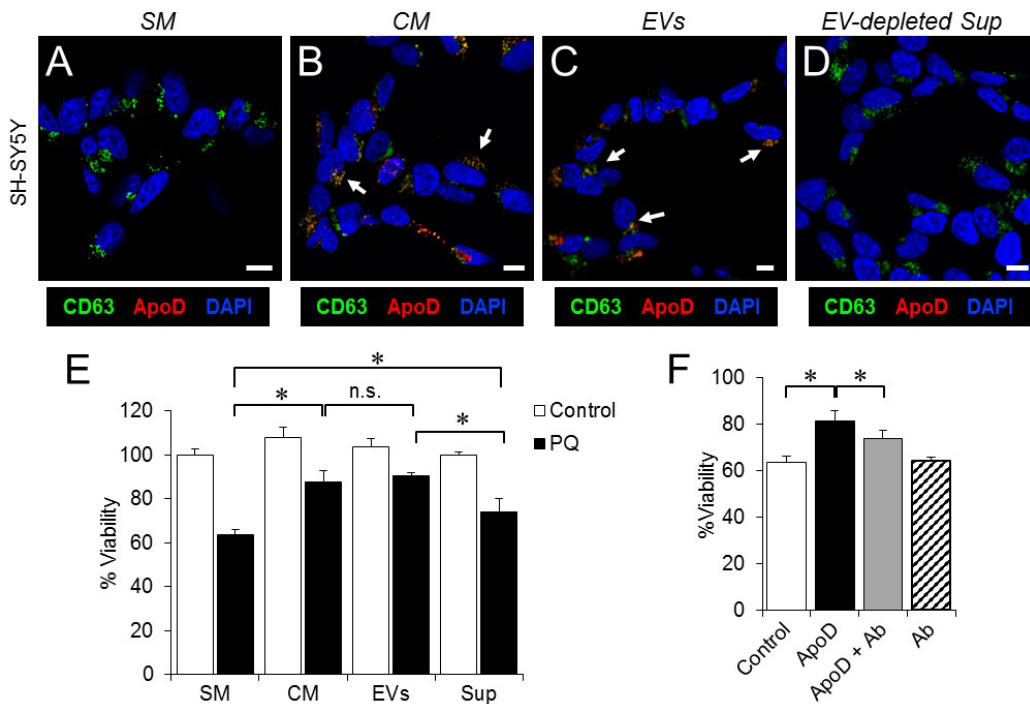
Figure 33. Astrocyte-to-neuron ApoD trafficking and neuroprotective effect are exclusively mediated by EVs. A-D. *Representative confocal images of SH-SY5Y cells cultured with standard medium, SM (A), astrocyte-conditioned medium, CM (B), purified astrocyte EVs (C), or EV-depleted astrocyte-derived supernatant, Sup (D). Arrows point to the colocalization of the exosome marker CD63 and ApoD. Calibration bars: 10 μm.* ***E-F.*** *Cell viability measured by the MTT-assay in SH-SY5Y neurons cultured with the different culture media used in A-D (E) or with purified native ApoD (F) in the absence or presence of an anti-ApoD monoclonal antibody. Error bars represent SEM (n = 3 independent experiments). Asterisks represent significant differences (p<0.01) assessed by ANOVA with Holm-Sidak post-hoc method. Only most relevant comparisons are pointed.*

Our data demonstrate that a considerable fraction (H 0.6%) of the ApoD protein expressed by 1321N1 astrocytes is targeted to EVs, and particularly to the exosome fraction of EVs. We also demonstrate that, surprisingly, it is in this form of cell-cell communication, and not in free soluble form, that ApoD gets internalized by SH-SY5Y neurons, where it is able to protect them from PQ-triggered OS. These results set the stage to study whether in vivo we find such an important contribution of exosomes in the ApoD astrocyte-to-neuron traffic both in physiological and pathological situations.

CHAPTER 4: **In addition to cell survival, ApoD affects biological processes in which optimal lysosomal function is important for glial cells.**

4.1 ApoD modifies the dynamics of myelin phagocytosis by astrocytes.

4.2 Stable presence of ApoD in the lysosome is required to rescue ApoD-KO hypersialylated glycocalyx in astrocytes.

4.3 ApoD is required for the process of myelin glycocalyx removal and adequate subcellular localization of lysosomal and membrane sialidases in Schwann cells.

In this work we have focused on astrocytes and other glial cells, the front line of defense against oxidative stress and one of the nervous system cell types that express ApoD. Since ApoD conditions the pH-dependent functionality of the lysosomal compartment, how does it affect biological processes where a lysosomal optimal function is important for glial cells? In this chapter we will analyze how the presence of ApoD affects the different glial functions such as phagocytosis and elimination and recycling of glycocalyx from the plasma membrane in different glial cells: astrocytes and Schwann cells.

4.1 ApoD modifies the dynamics of myelin phagocytosis by astrocytes.

Recent studies reveal that astrocytes have phagocytic functions [160-162]. They digest the phagocytosed cargo through a process regulated by lysosome pH levels and autophagosome-lysosome fusion [163]. This is a slow process in astrocytes, and is proposed to regulate antigen presentation by these cells through lysosomal fusion to the plasma membrane. We have shown that lysosomal ApoD either enters autophagolysosomes or traffics back to the plasma membrane (Chapter 1, Fig. 9,14), the peripheral lysosomes are enriched in ApoD in OS treatment (Chapter 2, Fig. 20) in possible secretory lysosomes, and that lysosomal pH depends on the presence of ApoD (Chapter 2, Fig. 19-22). Therefore, ApoD might be a candidate regulator for the "digest-or-present" process in astrocytes.

Astrocytes are reported to start degrading phagocytosed cargo in acidic lysosomes at 6 days after exposure to cell debris [163]. We thus exposed primary astrocytes to DiI-labeled myelin for 3 days and monitored DiI signal at 2 and 6 days after myelin removal (Fig. 34 and Fig. 35). We estimated the phagocytosis potential of WT and ApoD-KO astrocytes by measuring the number and size of DiI-labeled myelin particles (see *Methods*). Starting with comparable initial levels of phagocytic activity (Fig. 34A; no differences are observed in the number of myelin particles phagocytosed during the 3 days exposure period), both astrocyte genotypes decrease the number of particles over time. However, this reduction in numbers is accompanied by a significant increase in large myelin particles at 6 days post-myelin exposure in ApoD-KO astrocytes only (Fig. 34B,E,F), indicating that phagocytosis resolution is impaired in the absence of ApoD. These results agree with the high load of phagocytosed material observed in alkaline astrocyte lysosomes [163]. Taking into account that myelin phagocytosis induces ROS production [164], the more alkaline ApoD-KO lysosomes are expected to be less efficient, resulting in delayed myelin degradation. No differences are found at earlier times, suggesting that the absence of ApoD results in a deregulated processing of the already ingested myelin, requiring the maintenance of lysosomal optimal pH and functionality.

On the other hand, recently it has been described that there are structural anomalies caused by the lack of ApoD in myelin altering its biochemical properties [57] and so its processing. To further confirm this, we measured the level of WT and ApoD-KO myelin particles phagocytosed and degradated by WT astrocytes (Fig. 35).
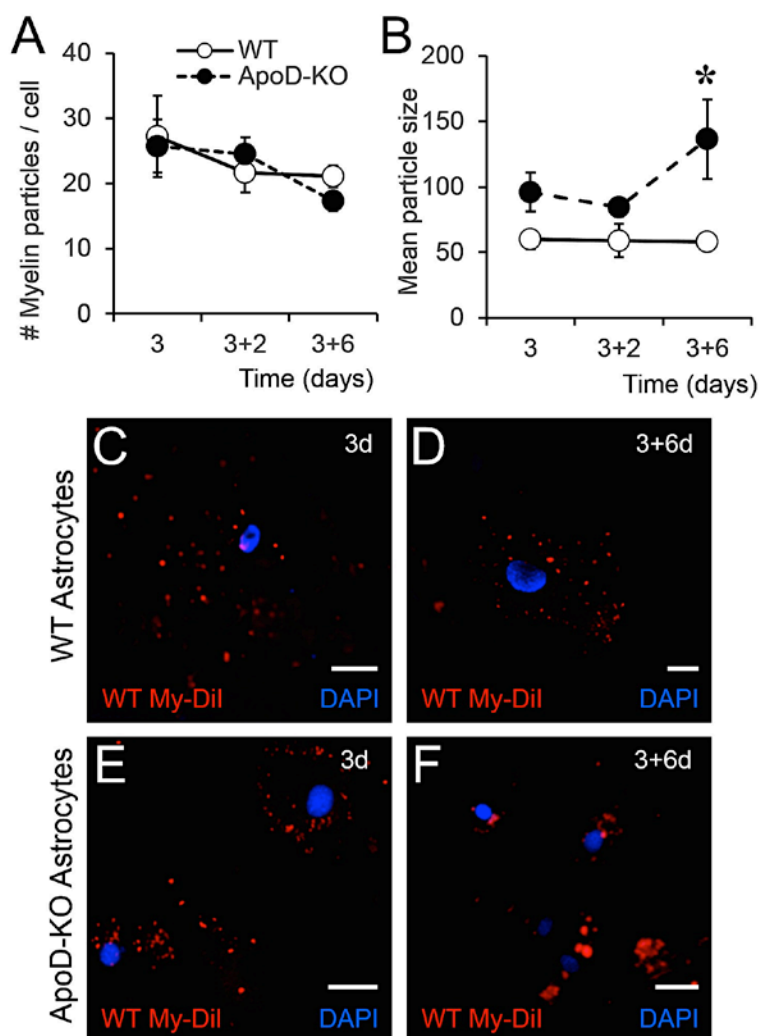
Figure 34. ApoD presence in mouse astrocytes is required for adequate processing of phagocytosed myelin. *WT and ApoD-KO astrocytes were exposed to DiI labeled myelin for 3 days, and DiI signal was evaluated by fluorescence microscopy 2 and 6 days after removal of myelin. Three-way ANOVA was used to evaluate variable interactions, followed by two-way ANOVA to detect the origin of differences.* ***A.*** *Number of DiI-myelin particles phagocytosed by primary WT and ApoD-KO astrocytes (n > 10 cells/genotype from three independent experiments). No differences are found between genotypes, indicating comparable initial levels of phagocytic activity.* ***B.*** *Mean particle size of DiI-positive objects is dependent on time of treatment (p=0.032, three-way ANOVA). The values at 6 days post-myelin removal account for the difference (p<0.001, Holm-Sidak method). Only ApoD-KO astrocytes show a significant increase in large myelin particles.* ***C-F.*** *Representative fluorescence images of DiI-myelin*

signal in primary WT or ApoD-KO astrocytes after myelin exposure (3d; C,E) and 6 days after myelin removal (3+6d; D,F). Calibration bars: 20 μm.

Fig. 35 shows the results of WT astrocytes exposed to WT or ApoD-KO myelin. Initially, comparable levels of phagocytosis of both genotypes were observed. However, the number of particles decreases faster in ApoD-KO DiI labeled myelin over time. These differences in the accumulation of myelin particles at 6 days after myelin removal (Fig. 35A) might be due to an altered myelin degradation rate once myelin has been internalized in each astrocyte. In addition, this reduction in numbers is accompanied by a significant increase in large myelin particles at 6 days post-exposure of WT astrocytes to ApoD-KO myelin only (Fig. 35B, D). The recently described changes in biochemical composition of myelin [57] and this can alter how myelin is processed by the astrocytes.

Figure 35. The lack of ApoD in myelin causes an acceleration in the processing of myelin phagocytosed by mouse astrocytes. WT astrocytes were exposed to WT and Ap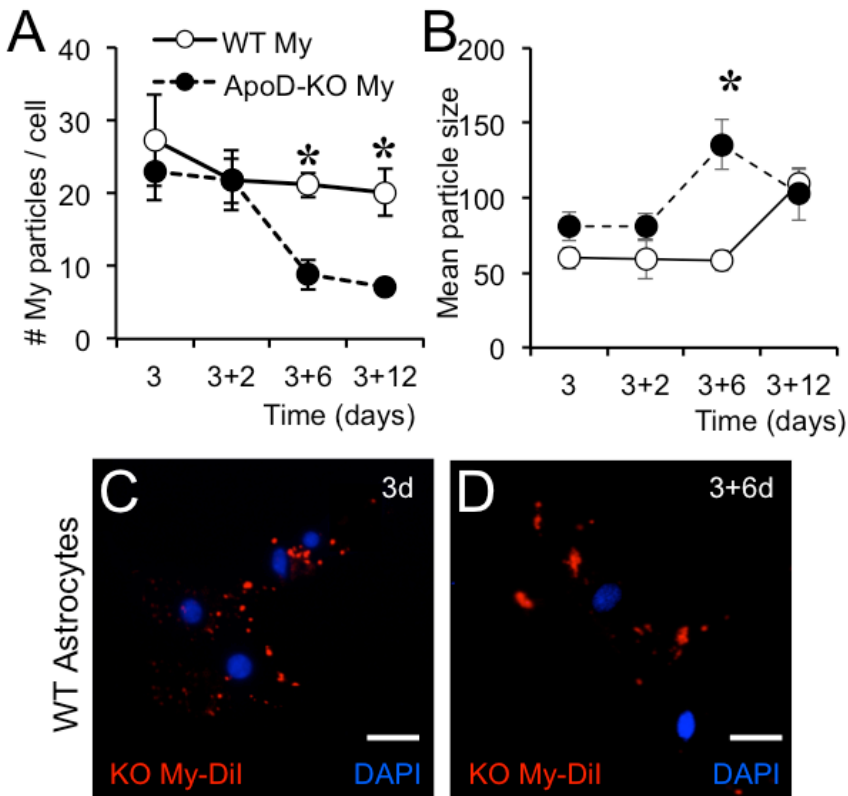oD-KO DiI labeled myelin for 3 days, and DiI signal was evaluated by fluorescence microscopy 2, 6 and 12 days after removal of myelin. Three-way ANOVA was used to evaluate variable interactions, followed by two-way ANOVA to detect the origin of differences. A. Number of WT and ApoD-KO DiI-myelin particles phagocytosed by primary WT astrocytes (n > 10 cells/genotype from three independent experiments). Initially, no differences are found between genotypes, indicating comparable levels of phagocytosis. However, the number of particles decreases faster in ApoD-KO DiI labeled myelin over time B. Mean particle size of DiI-positive objects is dependent on time of treatment (p=0.032, three-way ANOVA). The values at 6 days post-myelin removal account for the difference (p<0.001, Holm-Sidak method). Only WT astrocytes exposed to WT and ApoD-KO DiI labeled myelin show a significant increase in large myelin particles. C-D Representative fluorescence images of ApoD-KO DiI-myelin signal in primary WT astrocytes after myelin exposure (3d; C) and 6 days after myelin removal (3+6d; D). Calibration bars: 20 μm.

4.2 A stable presence of ApoD in lysosomes is required to rescue ApoD-KO hypersialylated glycocalyx in astrocytes.

Another of the important lysosomal functions described so far is the elimination and recycling of glycocalyx from the plasma membrane, a process required for compaction of extracellular myelin leaflets [165]. ApoD-KO results in a specific defect in myelin extracellular leaflet compaction in peripheral and central nervous system, which results in reduced conduction velocity and suboptimal behavioral outputs: motor learning is compromised [57]. In myelinating glia, this process is the limiting factor for extracellular leaflet compaction. To compact the extracellular sides of myelin, an important transition must take place: from membrane sliding, while building the wraps, to membrane adhesion and water exclusion. In this case, can we reverse a defective glucocalyx by supplying ApoD to the cell? To answer this question, we used primary astrocyte cultures to first test whether glycocalyx control is a general biological function of ApoD in glial cells.

ApoD-KO astrocyte membranes have significantly higher sialic acid content, as revealed by *Maackia amurensis* lectin labeling (Fig. 36A,B). PQ-triggered oxidative

stress, which results in partial lysosomal membrane permeabilization and lysosomal alkalinization (Chapter 2), further increases sialic acid content (Fig. 36B), as expected if both processes are causally linked. Treatment of ApoD-KO astrocytes with exogenous human ApoD (hApoD) during a 7-day period (with replacement every 48–72 h) completely rescues the hypersialylated glycocalyx phenotype (Fig. 36A,C). No rescue is obtained after a short 24 h treatment with hApoD (Fig. 36B), as could be expected if ApoD had direct enzymatic activity on the cell glycocalyx.

To test whether the presence and stability of ApoD in lysosomes is required for glycocalyx remodeling, we performed the treatment with recombinant bacterial hApoD. This protein is also endocytosed and targeted to lysosomes, but it is rapidly degraded (Fig. 18), in contrast with the fully glycosylated purified native hApoD. Co-localization with Lamp-2 at the end of the treatment (Fig. 36D) shows that only the native form is maintained in the lysosomal compartment. Bacterial hApoD has minor effects in the cell glycocalyx (Fig. 36C), coherent with its brief and intermittent presence in lysosomes.

In summary, by maintaining lysosomal functional integrity ApoD is necessary and sufficient for glial cells to remodel their glycocalyx. Removal of the negatively charged glycocalyx becomes the limiting factor in such transition. This glycocalix could be remodeled correctly in lysosomes, such as in astrocytes. Does the lack of ApoD result in altered compaction of the extracellular leaflet of myelin? Given the importance of ApoD in maintaining lysosomal stability, this could be the key point of ApoD in myelination.
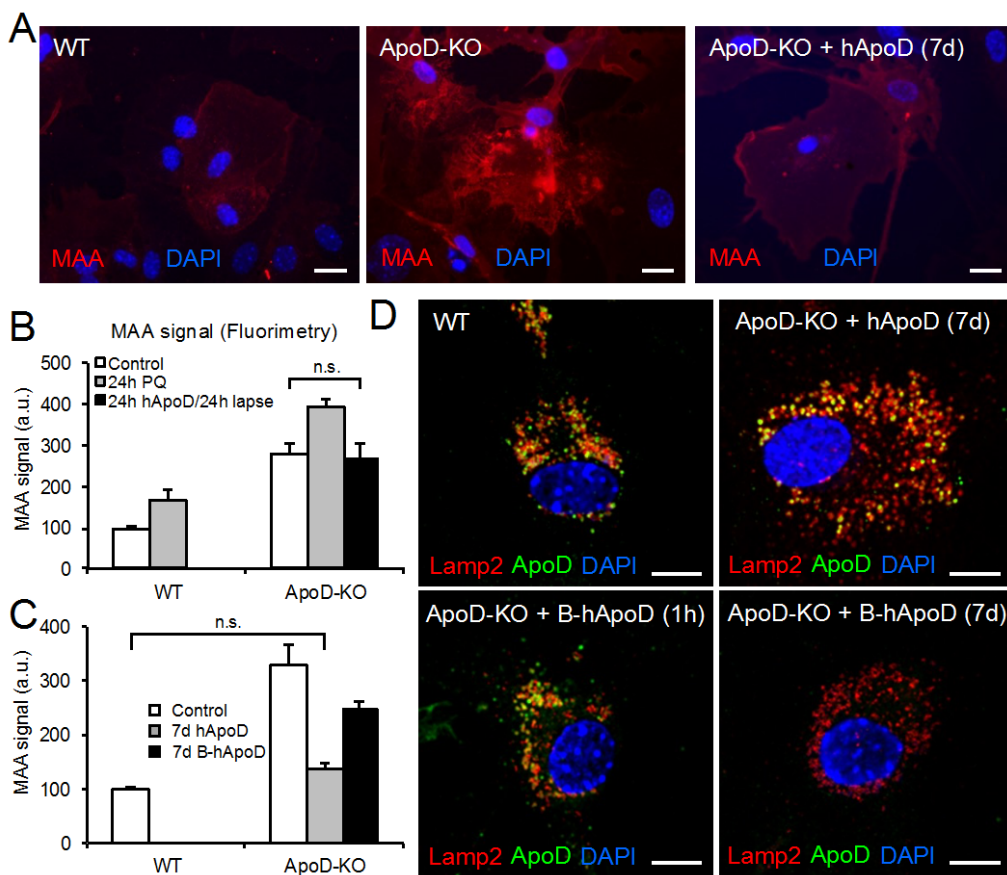
Figure 36. Hypersialylation of ApoD-KO astrocytes membrane is rescued when ApoD is stably present in lysosomes. *Sialic acid content in WT and ApoD-KO astrocyte membranes monitored by Maackia amurensis lectin labeling in the absence of detergents. Representative fluorescence images (A) and fluorescence quantitation in cell populations (B and C) are shown. A. Sialic acid labeling increases significantly in ApoD-KO astrocytes (n > 10 cells/treatment from three independent experiments). Treatment with exogenous hApoD for 7 days (with replacement every 48–72 h) reverts sialic acid content to control levels. B. Oxidative stress increases sialic acid content in both WT and ApoD-KO astrocytes (gray bars). Short term treatment with hApoD followed by a 24 h waiting period does not modify the high levels of sialic acid in ApoD-KO astrocytes. C. Quantitative analysis of hApoD dependent rescue. A complete reversion of the phenotype is achieved after 7-day continuous treatment with fully glycosylated purified hApoD (gray bar), but not with recombinant bacterial hApoD (bhApoD). D. hApoD, but not bhApoD, is present in astrocytes lysosomes at the end of the treatment, though both are internalized early after each addition (1 h post addition is shown).*

Representative confocal microscopy sections within a z-stack are shown. Statistical differences assayed in B and C by ANOVA followed by Tukey post-hoc test. Only pairwise comparisons not significantly different are pointed (n.s.). Calibration bars: 20 μm (a), 10 μm (d).

4.3 ApoD is required for the process of myelin glycocalyx removal and adequate subcellular localization of lysosomal and membrane sialidases in Schwann cells.

Recently it has been described that the structural and functional abnormalities caused by the lack of ApoD in both CNS and PNS myelin predict that basic biochemical properties of myelin sheaths should be altered [57]. The outer surface glycocalyx of myelinating cells is initially abundant and negatively charged, due to sialylated glycolipids and glycoproteins, favoring displacement of myelin sheaths as they wrap axons. However, this hydrophilic cover needs to be extensively removed in order to promote the final adhesion of the two apposed membranes [166, 167]. The most direct cause of the anomalous hydrophilicity and uncompacted outer leaflet in ApoD-KO myelin would be a deficit in glycocalyx removal. To test this prediction, *Maackia amurensis* lectin was used to assay sialic acid content in sciatic nerves. A clear increase is observed in ApoD-KO nerves (Fig. 37).
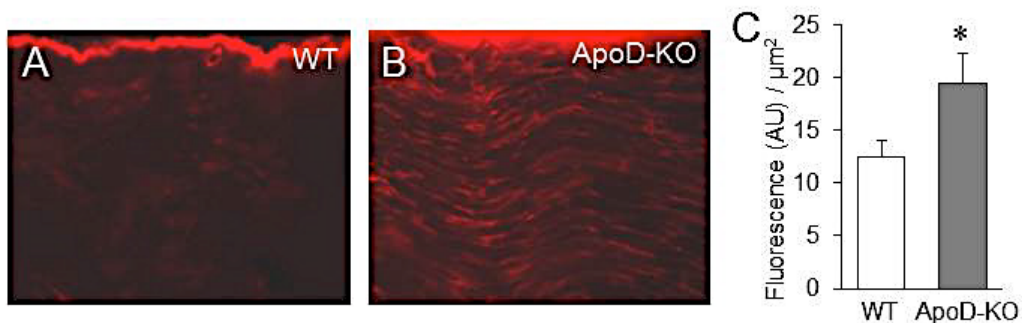
Figure 37. Sialic acid content is altered in the absence of ApoD. A-B. *Representative fluorescence images of sialic acid in WT and ApoD-KO sciatic nerves visualized by Maackia amurensis lectin labelingin cryostat sections.* ***C.*** *Sialic acid content in WT and ApoD-KO sciatic nerves was quantified (n= 6 nerve sections from four mice per genotype). A significant increase is observed in ApoD-KO nerves, while the perineurial labeling is not dependent on genotype. Statistical differences assayed by unpaired Student's t-test. *: p< 0.05.*

These results demonstrate that ApoD is required for proper glycolipid management during myelin membrane compaction. All previous stages of myelination initiation and wrapping of axons are unaltered, but in the last phase of myelin maturation sialic acid moieties are not removed properly from the abundant glycolipids of myelin membranes. The altered final distribution of these important myelin components must be the reflection of disturbances in the process of myelin membrane recycling underlying the composition changes needed to transition from myelin sheaths growing and sliding to build the wraps, to the final phase of membrane apposition, adhesion and compaction of the extracellular leaflet.

To further understand the mechanism of myelin membrane remodeling preceding the final step of extracellular leaflet compaction in the PNS, we analyzed the subcellular localization of sialidases, in charge of removing sialic acid moieties from glycolipids and glycoproteins (reviewed by [168]). Our recent discovery that ApoD traffics from plasma membrane to lysosomes in astrocytes and neurons (Chapter 1) led us to test lysosomal and membrane sialidases. Lysosomal Neu1 has glycoproteins as preferential substrates. Neu3, located at the plasma membrane, acts primarily on glycolipids and its expression is boosted as part of the acute response to nerve injury, contributing to myelin degradation [169].

As in astrocytes, ApoD is present in Schwann cell lysosomes, as evidenced by co-localization with Lamp-2 (Fig. 38A–C). In normal conditions, ApoD scattered and stochastic pattern of expression indicates that Schwann cells turn on ApoD expression when undergoing tasks that do not take place simultaneously along the nerve [56]. Lysosomal Neu1 is co-expressed with ApoD (Fig. 38D,E) in the same subset of Schwann cells and, as expected, also co-localizes with ApoD (Fig. 38F–K).

Plasma membrane Neu3 is also co-expressed with ApoD in Schwann cells (Fig. 38M,N), and it is abundant in myelin membrane, as evidenced in teased nerve preparations (Fig. 38L). Therefore, there must be common signals coordinating the expression of ApoD with both Neu1 and Neu3.
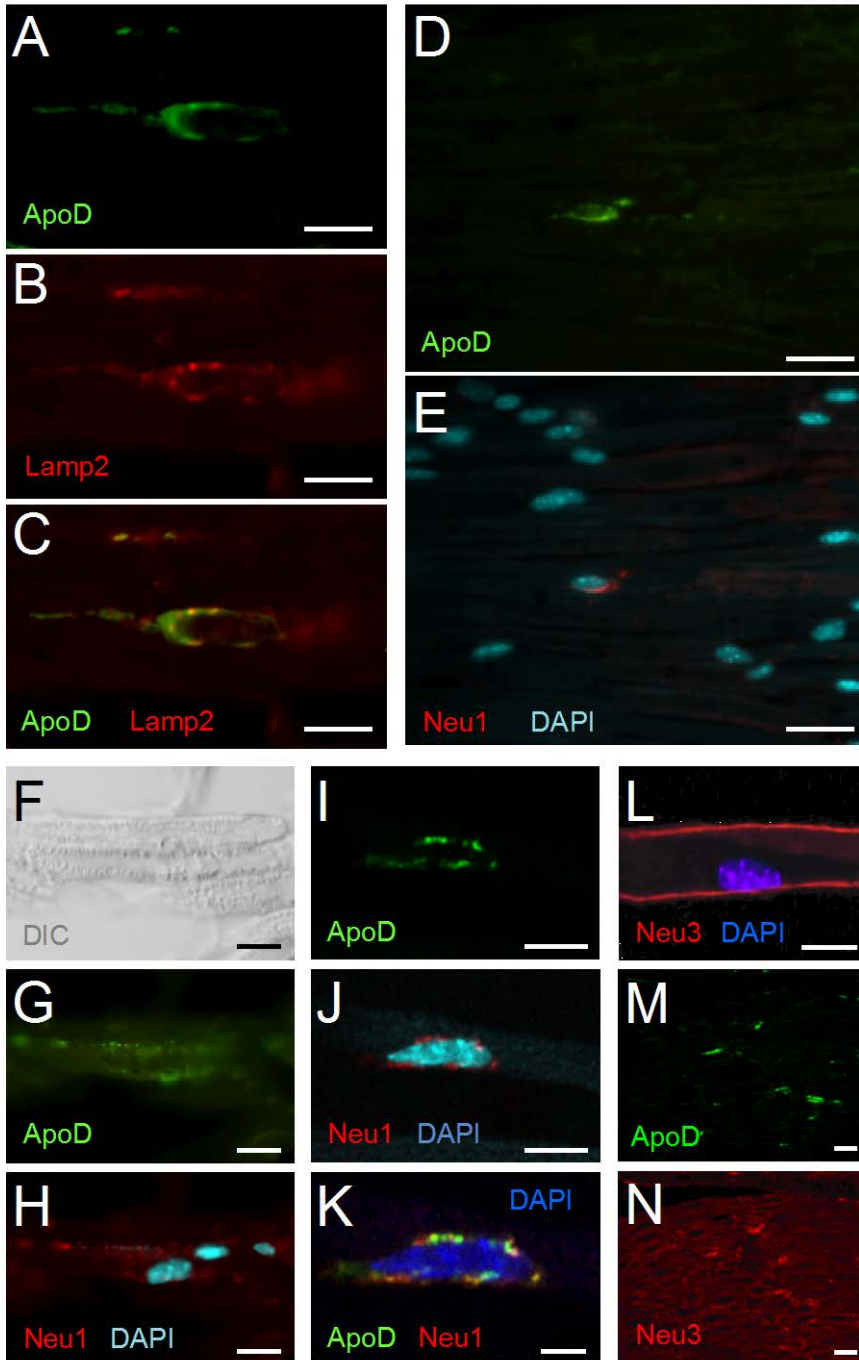
Figure 38. ApoD is located in Schwann cell lysosomes, and its expression is co-regulated with both lysosomal and membrane sialidases. A–C. Co-localization of ApoD with LELC marked with Lamp-2. Representative immunofluorescence images from sagittal paraffin

*sections of wild type adult sciatic nerves. **D–E.** The characteristic pattern of scattered ApoD-positive Schwann cells coincides with the pattern of lysosomal Neu1. **F–K.** Co-localization of ApoD with lysosomal Neu1 shown in paraffin sections (F–H, immunofluorescence) and teased nerves preparations (I–K, confocal imaging). **L:** Membrane Neu3 shows labeling in myelin sheaths (high magnification confocal imaging in teased nerves preparation). **M-N.** ApoD and Neu3 are also co-expressed in subsets of Schwann cells (low magnification confocal images in paraffin sections). Calibration bars: 5 μm (K), 10 μm (A–C, F–L), 20 μm (D and E, M and N).*

In astrocytes, ApoD is targeted to a subset of lysosomes particularly vulnerable to oxidative stress, and the lack of ApoD results in lysosomal partial permeabilization and alkalinization (Chapter 2). Using teased nerve preparations to isolate single fibers, we analyze Neu3 expression pattern (Fig. 38A), the results suggest that either it gets down regulated or its membrane location is reduced in ApoD-KO fibers (Fig. 38B).
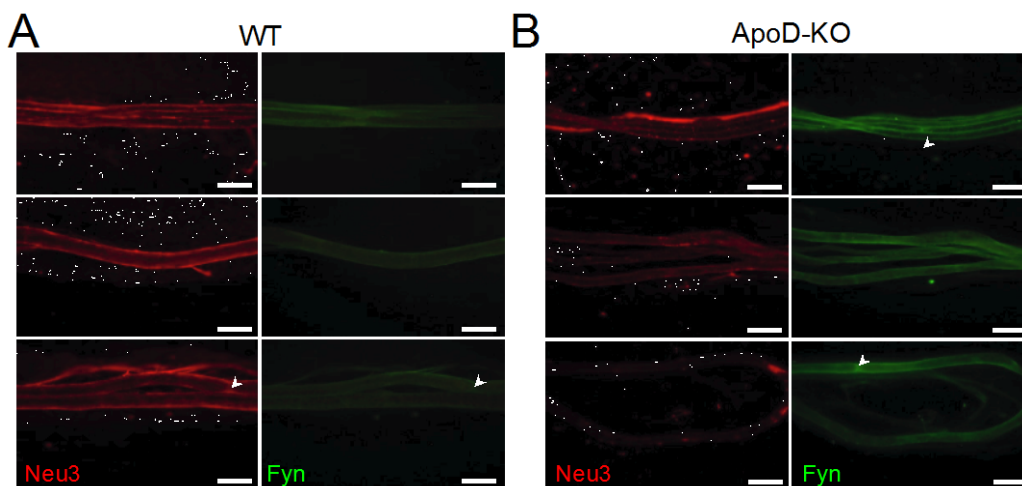
***Figure 39. Lack of ApoD alters trafficking of membrane Neu3 and Fyn kinase. A-B.** Neu3 and Fyn immunofluorescence images from teased WT (A) or ApoD-KO (B) nerve preparations. Neu3 labelling, which is apparent along the entire myelin coverage (arrowheads point to paranodes), decreases while Fyn kinase increases in ApoD-KO myelin sheaths. Representative images from three mice are shown. Calibration bars: 20 μm.*

In oligodendrocytes, membrane trafficking and sorting are known to take place through specialized endosome and lysosome-mediated recycling paths [170], and the key regulatory kinase Fyn has been proposed to regulate the lysosomal-mediated

trafficking determining adequate location of Plp in CNS myelin [171]. Fyn-specific antibody labeling reveals that while Neu3 decreases, Fyn increases in teased ApoD-KO nerves (Fig. 39B). The labeling pattern of Fyn suggests a myelin sheath location, and the complementary behavior of Neu3 and Fyn suggests a trafficking defect.

These results provide a strong indication that ApoD, by helping to preserve lysosomal membrane integrity, provides the necessary conditions to maintain an adequate activity of lysosomal sialidases and, at the same time, controls the adequate lysosomal-mediated trafficking of Neu3 and Fyn to and from myelin membrane, which is ultimately required for myelin complete compaction.

In addition to cell survival, ApoD affects biological processes in which optimal lysosomal function is important for glial cells. ApoD modifies the dynamics of myelin phagocytosis by astrocytes and favour the process of myelin glycocalyx removal adequating subcellular localization of lysosomal and membrane sialidases in Schwann cells.

CHAPTER 5: Lysosomal ApoD function rescues cells from neurodegenerative diseases of different origins.

5.1 ApoD-related Lipocalins rescue of proteinopathic neurodegeneration requires autophagosome-lysosome fusion.

5.2 Apolipoprotein D-mediated regulation of lysosomal membrane integrity preserve lysosomal function and promotes cell survival in Niemann-Pick Type A disease.

In this work, we have reported that ApoD is targeted to lysosomes and maintains their membrane stability and pH homeostasis. This lysosomal activity, and its overexpression under oxidative stress makes ApoD a perfect candidate for treatment of neurodegenerative diseases of different ethiology. We chose a polyglutamine-based neurodegeneration and a lysosomal storage disease to assess the effect of a loss of ApoD in both diseases, and also to test whether an exogenous addition of ApoD can minimize their symptoms and deleterious effects.

5.1 ApoD-related Lipocalins rescue of proteinopathic neurodegeneration requires autophagosome-lysosome fusion.

A diverse set of neurodegenerative disorders are caused by abnormal extensions of polyglutamine (poly-Q) stretches in various, functionally unrelated proteins. A common feature of these diseases is altered proteostasis. In this chapter we test whether ApoD also protects against poly-Q-triggered deterioration of protein quality control systems.

Using the Drosophila retina as a model system to assay neurodegeneration, our laboratory previously described that Type I Spinocerebellar Ataxia (SCA1) concurs with autophagic stress, showing an excessive or imbalanced induction of autophagy where autophagosome turnover is unable to keep pace with its formation [33]. GLaz, a Drosophila homologue of ApoD expressed by subsets of glial cells in the fly nervous system, has epistatic relationships with autophagy genes and optimizes clearance of aggregation-prone proteins such as the polyglutaminated form of human Ataxin 1 that

is responsible for the SCA1 phenotype [33]. GLaz rescues neurodegeneration by making autophagy more efficient, thus minimizing the negative effects of autophagic stress. It was also proposed that the Lipocalin-mediated control of lipid peroxide levels influences autophagy at several steps, slowing down the process and ultimately making it more efficient. However, the mechanism for such an optimization of autophagy was not completely discerned.

Here we want to prove if the rescue depends on a lysosomal function of GLaz. For that we evaluate retinal degeneration in the SCA1 fly retina model (Fig. 40I) using FLEYE, a method for unbiased quantification based on the acquisition of fly eye surface pictures [145]. We combined hATXN1^{82Q} expression with GLaz, and with DorRNAi, a knock-down of the HOPS complex subunit Vps18/Dor critical for tethering and fusing autophagosomes with lysosomes [144] (Fig. 40). GLaz neurodegeneration rescue (Fig. 40C-D), compare with controls in Fig. 40A-B) is completely abolished by DorRNAi expression (Fig. 40E,F), while Dor down-regulation neither produces neurodegeneration itself (Fig. 40G) not modifies significantly the neurodegeneration phenotype triggered by SCA1 in the fly retina (Fig. 40H). These results demonstrate that the lysosome-autophagosome fusion event is required for GLaz optimization of autophagy that finally results in an efficient clearance of misfolded proteins in neurodegenerative conditions *in vivo*.

These findings represent a novel function for ApoD, and for Lipocalins. Their active role in the lysosomal compartment provides a clear explanation for the mechanism of GLaz rescue of polyglutamine-based neurodegeneration [33]: it requires fusion of autophagosomes to healthy lysosomes to optimize autophagy (Fig. 40).
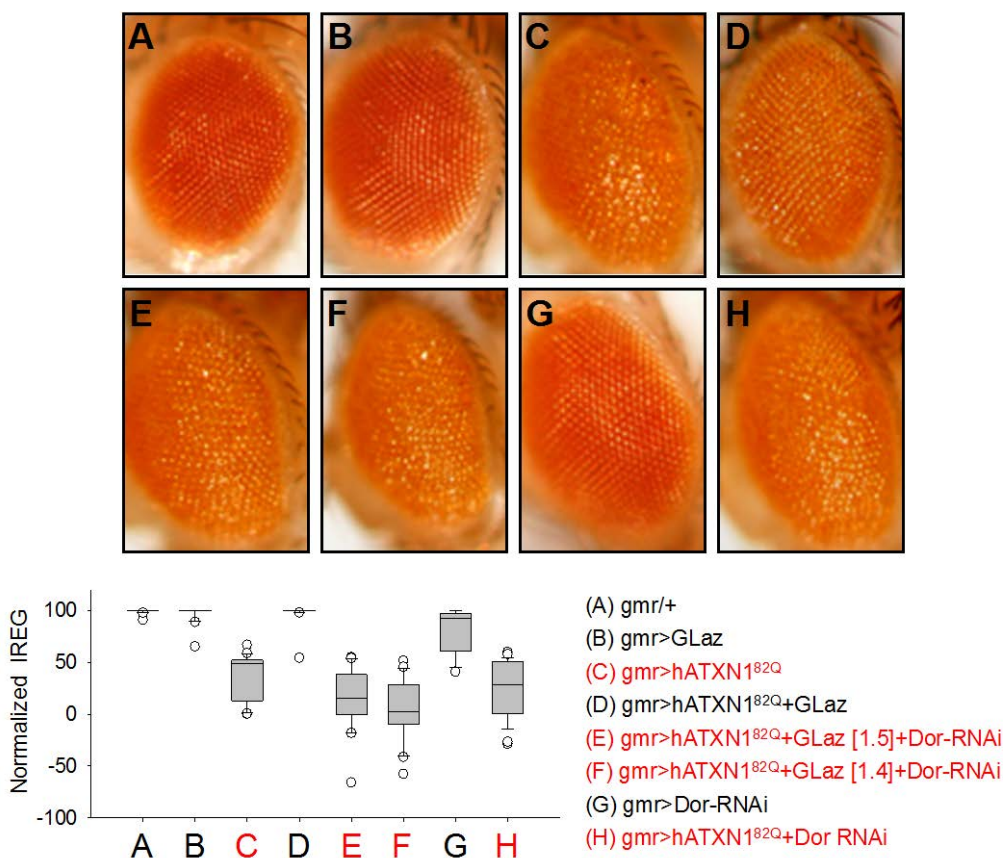
Figure 40. ApoD neuroprotection mechanism in polyglutamine-triggered neurodegeneration in Drosophila depends on lysosome-phagosome fusion in vivo. A-H. Representative examples of adult eye external morphology by light microscopy of the central eye surface region. The expression of all transgenes is directed by the gmr:Gal4 driver to photoreceptor neurons. Polyglutaminated human Ataxin 1 (UAS:hATXN1^{82Q}) is combined with UAS:GLaz and/or UAS:Dor-RNAi transgenes. *I.* Quantification of photoreceptor degeneration by computing a regularity index (IREG) using FLEYE. No rescue is detected when Dor is knocked-down (confirmed with two independent recombinant lines, E and F). Data normalized to the control genotype (gmr/+) are shown. N=20–30 flies/genotype. Statistical differences were assessed by ANOVA on Ranks and Tukey post-hoc correction. Genotypes C, E, F and H (degenerated) are significantly different from A, B, D, G (non-degenerated), p<0.001.

5.2 Apolipoprotein D-mediated regulation of lysosomal membrane integrity preserve lysosomal function and promotes cell survival in Niemann-Pick Type A disease.

The crucial role of ApoD within the lysosome led us to study the potential effects of ApoD on a particularly devastating LSD, the Niemann Pick type A disease (NPA), caused by loss of function mutations in the gene encoding for acid sphingomyelinase, which results in sphingomyelin (SM) accumulation in lysosomal and plasma membranes. The accumulation of sphingomyelin in NPA cells provoques the autophagy machinery to be blocked [127].

We here demonstrate that fibroblasts from patients with NPA express 40% less ApoD proteinthan healthy cells (Fig. 41).
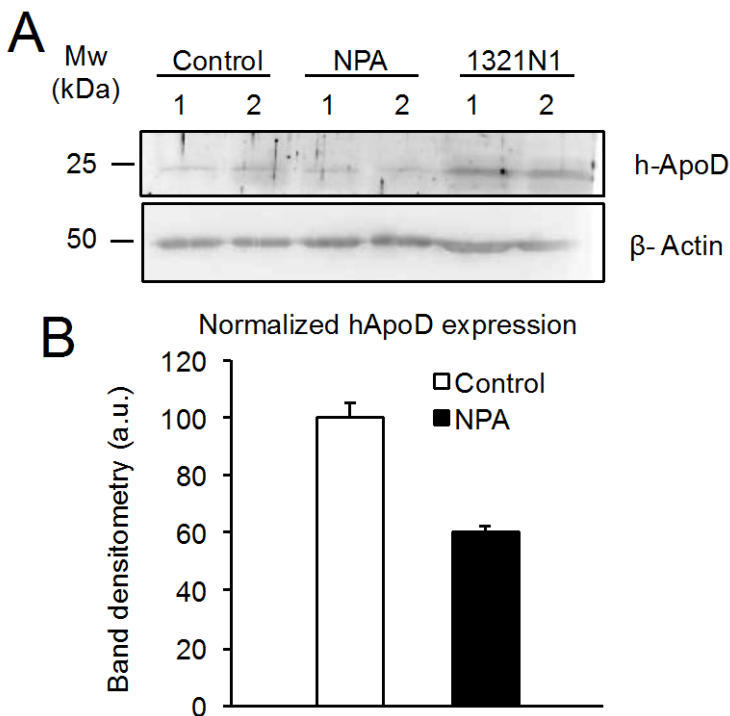
Figure 41. Fibroblasts from patients with Niemann-Pick Type A disease have decreased expression of ApoD. A. Immunoblot analyses of ApoD and β-Actin expression in fibroblast cells (two Control and two Niemann-Pick Type A (NPA) patients are shown. Two ApoD positive samples of 1321N1 astroglia were used as positive controls. B. ApoD content in Control and

NPA fibroblasts was quantified after protein levels were normalized to ²-actin signals. NPA fibroblasts express a lower amount of ApoD protein. Average ± SEM of two experiments using two cell lines derived from two un-related patients are shown. Fibroblast ID: WT: AG7323 and GM00969; NPA: GM13205 and GM00112.

This could be because the cell does not produce sufficient amounts of ApoD to protect itself from the large amounts of sphingomyelin that is accumulating in the cell, or because those large amounts of sphingomyelin are preventing the entry of ApoD into lysosomes that are responsible of sphinfomyelin degradation. To confirm any of these options, we added exogenous ApoD to fibroblast cultures, analyzing the co-localization of ApoD with Lamp-2. We have previously described that oxidative stress is a potent stimulus to target ApoD to lysosomes (Chapter 1, Fig. 14). Therefore, In cells of the nervous system, the entrance of ApoD is slow and is accentuated with the PQ treatment (Chapter 2, Fig. 21), that's why we performed conservative protocol of 24 h post-ApoD treatments, leaving enough time for ApoD to enter the lysosome, to test a change in co-localization (Fig. 42A).

As expected, we observe a slow (24 h) entry of ApoD to lysosomes after exogenous additionin healthy cells, which is accentuated by PQ-induced oxidative stress (Fig. 42B). However, NPA fibroblasts are able to target ApoD to the lysosomes during the 24 h period, oxidative stres doesn't favored this entry.

To check whether this increase over time in lysosomal ApoD observed in NPA cells is affecting the lysosome function, we studied proteolytic activity and stability of lysosomal membrane. We have described in Figure 36 (Chapter 4) that, in order to observe significant changes in the addition of ApoD, we need to perform exogenous human ApoD (hApoD) during a 7-day period (with replacement every 48–72 h) (Fig. 43A).
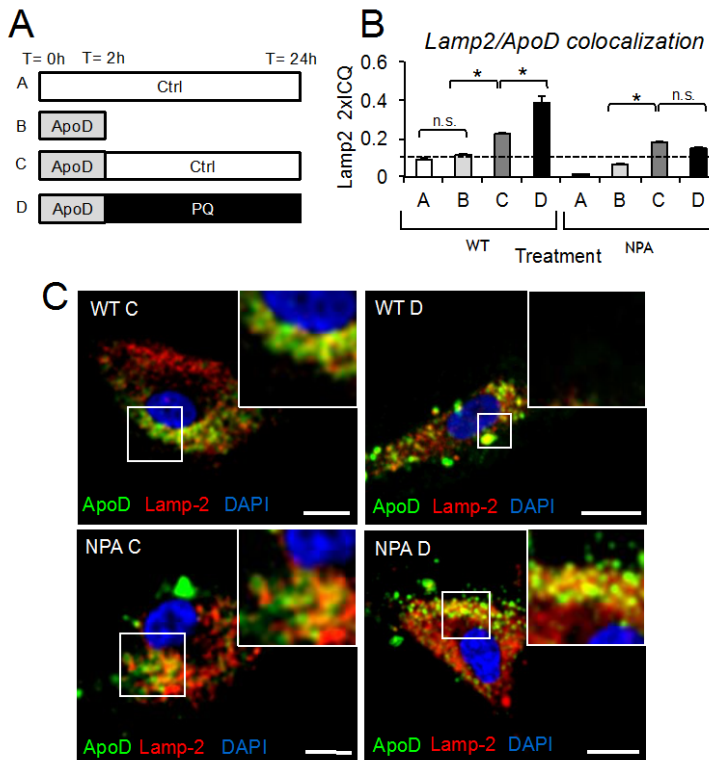
Figure 42. The regulated entry of ApoD to lysosomes is prevented in fibroblasts of NPA patients. *A. Graphic representation of cell treatment protocols used to analyze ApoD/Lamp-2 co-localization. **B.** Average co-localization index referenced to Lamp-2 signal (Lamp-2 2xICQ) for different treatments (n = 20 cells/condition from at least two independent experiments). NPA fibroblasts cannot redirect ApoD to their lysosomes upon oxidative stress (condition D). **C.** Representative confocal sections of fibroblasts labeled with ApoD (green) Lamp-2 (red) and DAPI (blue). With PQ-treatment (condition D), ApoD remains near the plasma membrane with minor co-localization with Lamp-2 in NPA cells. Insets at 2x magnifications are shown to appreciate changes in co-localization patterns. Statistical differences in B were assessed by two-way ANOVA (p<0.001), and Holm-Sidak post-hoc method (p<0.001). Calibration bars: 25 µm. Fibroblast ID: WT: AG7310; NPA: GM13205.*

Analyzing the lysosomal stability of WT and NPA cells, we can observe that NPA fibroblasts have lower Cathepsin B activity (Fig. 43B), possibly caused by permeabilization of the lysosomal membrane, which is also confirmed by the relocation of Gal3 in the lysosome (Fig. 43C). The exogenous addition of ApoD in

NPA fibroblasts, avoide the entry of Gal3 into the lysosomes, improving the lysosomal stability and consequently the activity of Cathepsin B.
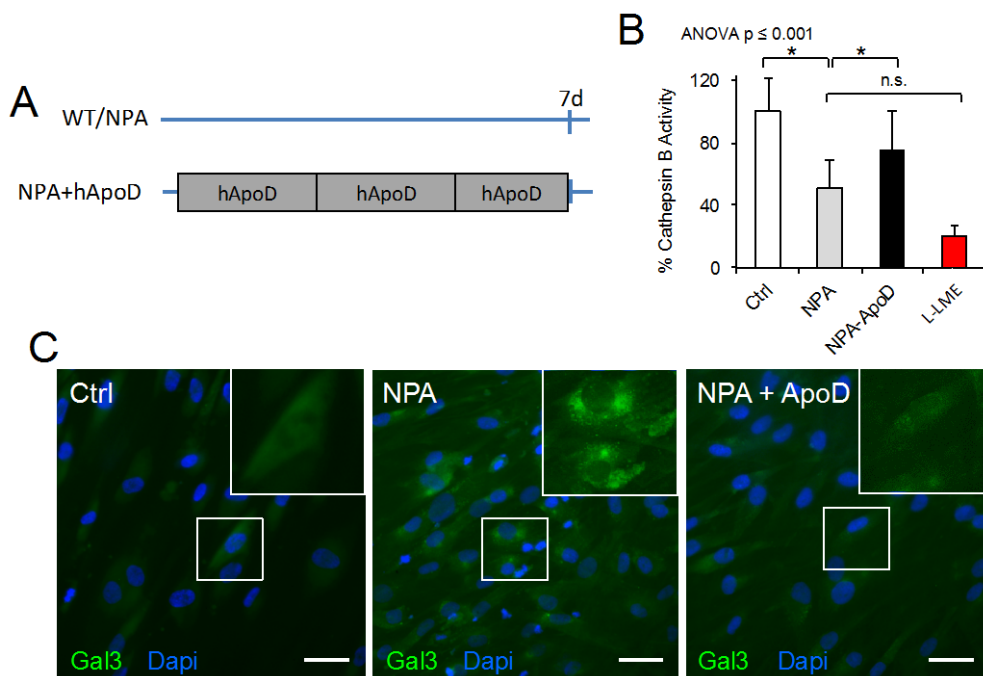
***Figure 43. ApoD improves lysosomal membranes, reducing their permeabilization, upon NPA disease. A.** Graphic representation of cell treatment protocols used to analyze lysosomal function. Treatment with exogenous hApoD was performed for 7 days (with replacement every 48–72 h).* ***B.** Cathepsin B activity monitored by Magic Red assay. L-leucyl-L-leucine methyl ester (L-LME) is used as positive control for lysosomal membrane rupture (n=3 independent experiments).* ***C.** Representative fluorescence microscopy images of Galectin-3 signal in WT, NPA and NPA+hApoD fibroblasts. Insets at 2x magnifications are shown to appreciate changes in labeling. A switch from vesicular (lysosomal) to cytoplasmic Galectin-3 labeling occurs under ApoD treatment. The punctate labeling of Galectin-3 is evident for NPA cells, and decreases under ApoD treatment. Calibration bars: 50 μm. Fibroblast ID: WT: GM00969; NPA: GM00112.*

These changes in the NPA lysosomes are also reflected in our analysis of lysosomal activity. Lipofuscin and peroxidized products are two of the compounds that will degrade in lysosomes. We can observe that NPA cells have a greater accumulation of lipofuscin in lysosomes (Fig. 44A,D). This amount decreases when ApoD is added

to the culture medium. Lipids peroxidized are detected with 4HNE. Although the exogenous addition of ApoD does not modify the net amounts of 4HNE, (Fig. 44B), its cellular distribution changes to a more punctate pattern after of ApoD increase (Fig. 44C, E) that results in a 4HNE-labeled area per cell similar to that in control conditions.

Accordingly, exogenous human ApoD (hApoD) during a 7-day period (with replacement every 48–72 h) improves the functionality of the lysosomes in NPA disease, favoring the redistribution and degradation of compounds such as lipofuscin and peroxidized lipids.
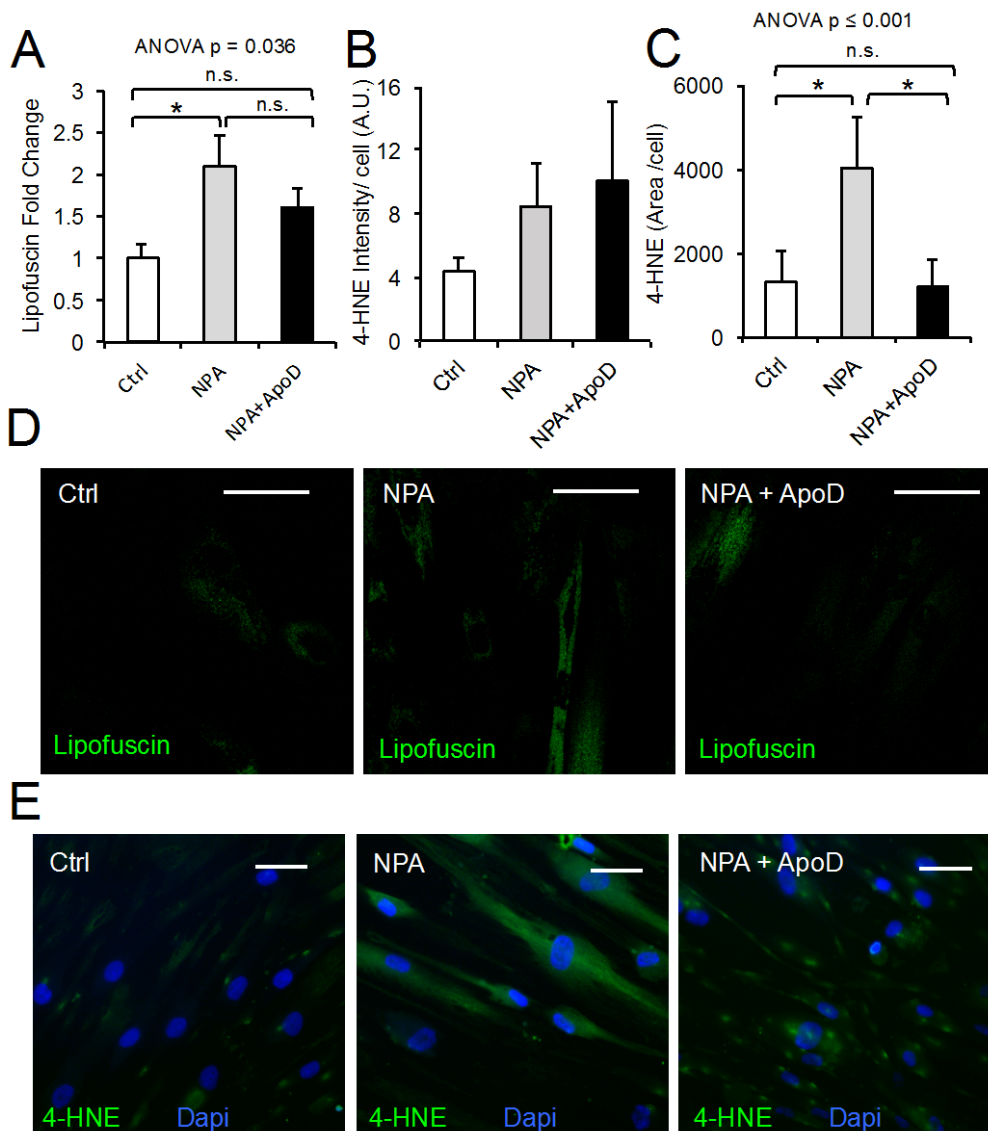
Figure 44. ApoD improves lysosomal antioxidant activity upon NPA disease. A. *Plot representing the fold change in lipofuscin intensity signal measured by confocal spectral analysis (n=10 cells/genotype from two independent experiments). NPA cells present a greater amount of accumulated Lipofuscin and the exogenous addition of ApoD significantly reduces it.* **B-C.** *Plot representing 4HNE intensity (B) and labeling area (C) per cell (n=10 cells/genotype from two independent experiments). Although the amount of 4HNE does not change with the treatment, the area occupied by 4HNE is significantly reduced with the ApoD treatment.* **D-E.** *Representative fluorescence microscopy images of lipofuscin (D) and 4HNE labeling signal (E) in WT and NPA fibroblasts under control conditions and after 7 d hApoD treatment. A clear*

change in 4HNE distribution can be observed. Treatment with exogenous hApoD was performed for 7 days (with replacement every 48–72 h). Calibration bars: 20 μm (C), 50 μm (D). Statistical differences in A and B were assessed by two-way ANOVA (p<0.001), and Holm-Sidak post-hoc method (p<0.001). Fibroblast ID: WT: GM00969; NPA: GM00112.

Using the MTT assay as an indicator of intracellular reduction potential to study cellular viability status. As we have analyzed [172], this test, in its standard format, is a measure of the net metabolic activity of the culture, without distinguishing whether the number of cells changes or the activity or viability of each one changes. Therefore, the results of this trial are described as "metabolic health" or "metabolic activity" of the fibroblasts. We observed that NPA cells show a reduced metabolic health caused by an increase in lysosomal pH (Fig. 45). When we treat NPA cells with ApoD, these cells are able to improve metabolic health (Fig. 45C) by acidifying their lysosomes (Fig. 45E). However, is the accumulation of sphingomyelin the cause of lysosomal and metabolic alterations of NPA cells? We performed sphingomyelin additions either 24 h before adding ApoD or simultaneously for 7 days (Fig. 45B) to healthy fibroblasts. This treatment mimics the effects observed with NPA cells. Sphingomyelin is the direct cause of lysosomal pH alkalinization and the consequent decrease in metabolic activity. The presence of sphingomyelin for 24 h models the NPA phenotype, and the damage is maintained for at least 7 days. ApoD is capable of improving both metabolic activity (Fig. 45D) and lysosomal pH (Fig. 45E) in the presence of an accumulation of sphingomyelin. However, a total recovery of lysosomal pH and, consequently, of cellular metabolic state was not achieved. (Fig. 45C,E). We also observed that a simultaneous treatment of ApoD with SM attains a larger recovery possibly due to ApoD ability to bind sphingomyelin.
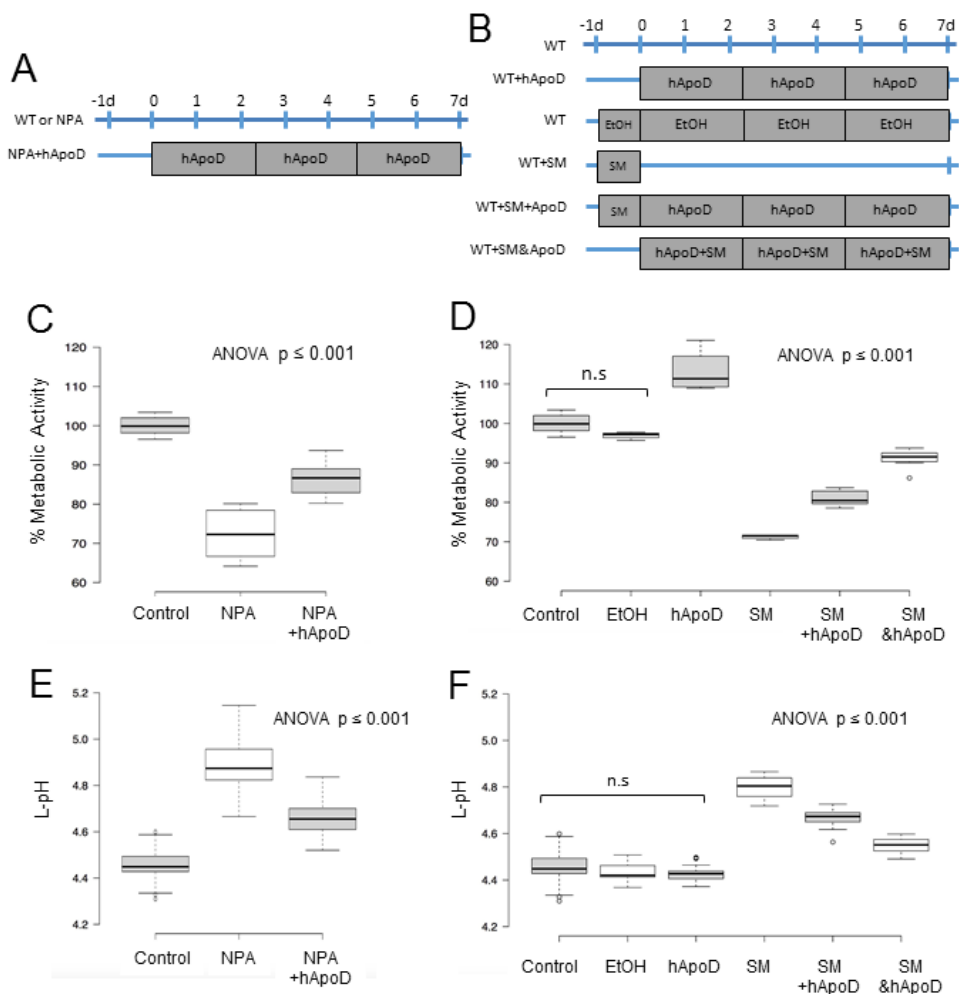
Figure 45. ApoD stabilizates lysosomal membranes in the NPA disease. A-B. *Graphic representation of treatment protocols used to analyze lysosomal functional state and cell metabolic health in WT and NPA fibroblasts. Treatment with exogenous hApoD or hApoD+sphingomyelin (SM) was performed for 7 days (with replacement every 48–72 h). In some cases, preceding 24 h incubation with SM was carried out. Ethanol (EtOH) was used as carrier control.* *C-F.* *Box plot representing % metabolic activity measured after 3 h MTT reduction to formazan (MTT-assay) (C-D) and lysosomal pH (L-pH) measured by LysoSensor ratiometric excitation analysis of (E-F) in fibroblast cell populations (WT or NPA) under different treatments. Center lines show median values; box limits indicate the 25th and 75thpercentiles as determined by R software; whiskers extend 1.5 times the interquartile range from the 25th and 75th percentiles, outliers are represented by dots; data points are plotted as open circles. n = 9 (C-D), 20 (E-F) cultures per condition from three independent experiments.*

The exogenous addition of ApoD improves the cellular metabolic activity and lysosomal pH modified by SM increase. No differences are found between the NPA models and exogenous addition of SM. The control samples are the same in C-D and in E-F. Fibroblast ID: WT: GM00969; NPA: GM00112.

Our results reveal that ApoD protection of lysosomal integrity is able to counteract biological deterioration in NPA cells, and open therapeutic opportunities for this devastating disease. ApoD is able to improve the function of lysosomes affected in the NPA disease. However, we must be aware that the direct cause of the disease, the mutation of Sphingomyelinase, is not solved and cell membranes will continue to be enriched in sphingomyelin.

Discussion

1. Identification of a new mechanism for preserving lysosomal functional integrity upon oxidative stress.

This study reveals for the first time a functionally complex stress-dependent trafficking of the Lipocalin ApoD (Fig. 46). While plasma membrane and endosomes are typical cellular locations for ApoD being secreted under basal conditions (Fig. 46A), lysosomes become an essential and stable niche for ApoD in a cell suffering from oxidative stress (Fig. 46B). After a fast protein secretion through the canonical RER-Golgi pathway, ApoD endocytosis is triggered by stress. Clathrin-dependent endocytosis is favored early under oxidative stress conditions. ApoD then moves through the early endosomal compartment to reach the LELC. Although the glycosylation of ApoD is not necessary for its endocytosis and its trafficking to lysosomes, the absence of glucidic residues in the protein causes rapid degradation, preventing ApoD from carrying out its function correctly. Subsequently, Lamp-2/ApoD-positive organelles either enter the autophagy pathway (early after oxidative stress stimulus), or ApoD is targeted back to the membrane at a late phase, possibly travelling within secretory lysosomes.
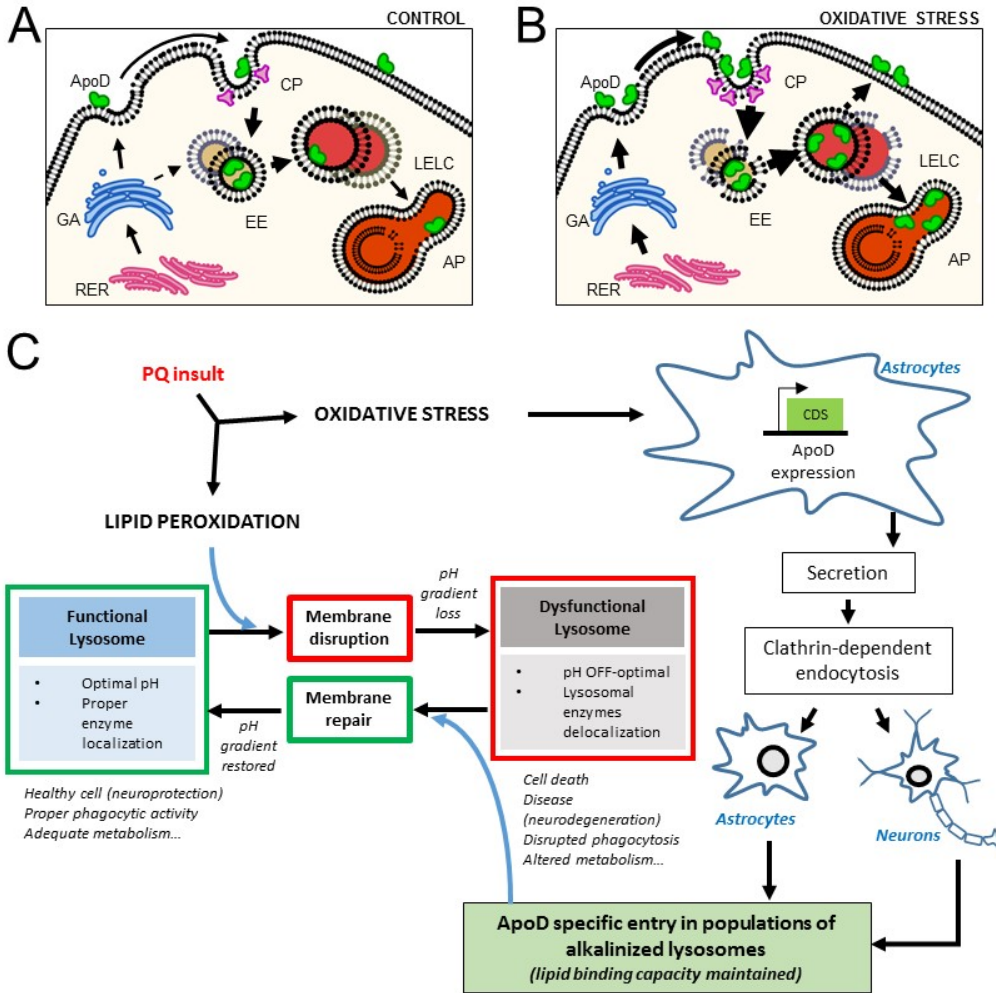
Figure 46. ApoD-dependent lysosomal integrity protection mechanism. A-B. *Model of oxidative stress-dependent cellular trafficking of ApoD. ApoD is depicted as a green molecule. Oxidized membranes are represented as broken lipid bilayers. ApoD enters only in a subset of lysosomes and restores their damaged membrane. Golgi apparatus (GA), Late endosomal-lysosomal compartment (LELC), Endoplasmic reticulum (RER) early endosomes (EE), Autophagosome (AP), Clathrin-coated pits (CP).* ***C.*** *PQ-triggered oxidative stress causes dysfunctions in a subset of vulnerable lysosomes, and, at the same time, induces expression, secretion, endocytosis and targeting of ApoD to that particular subset of lysosomes. ApoD is necessary and sufficient to restore lysosomal membrane and reinstates optimal lysosomal pH.*

Our results explain several aspects of the ApoD neuroprotective mechanism previously unanticipated. 1) ApoD locates in a subset of lysosomes particularly

sensitive to oxidative stress. These results support previous work reporting a functional heterogeneity of lysosomes according to their pH, vulnerability, pro-oxidative activity, or position within the cell [117, 121, 173]. 2) ApoD stability within lysosomes is dependent on its glycosylation state, which is functionally relevant given its reported heterogeneity in different tissues and cell types [174]. This result could also explain the absence of neuroprotective effect of bacterial recombinant ApoD against Aβ-challenged neuronal cells [175]. 3) ApoD targeting to lysosomes is a controlled process promoted by oxidative stress in ApoD-expressing astrocytes and ApoD-non-expressing neurons, which explains both autocrine and paracrine protective effects [60, 176]. 4) ApoD behaves as an acute phase protein, finely tuned through a JNK pathway-dependent transcriptional expression [60, 177] coordinated with a stress-dependent accelerated entry into lysosomes.

Another remarkable finding derived from our experiments is a functional link between the presence of intact ApoD within lysosomes and their pH. ApoD shows very low expression and seldom locates inside lysosomes of primary astrocytes cultured in control conditions. It is also found with more probability in endosomes than in lysosomes of control 1321N1 cells. However, it is rapidly up-regulated and mostly found in lysosomes upon oxidative stress. This situation is achieved in native cells after just 2 h of PQ treatment, though it occurs basally in rapidly proliferating cell lines like the 1321N1 astroglioma cells. Oxidative stress makes ApoD to translocate quickly and specifically to a subset of lysosomes with a slightly alkalinized pH in basal conditions and high sensitivity to oxidation. However, the presence of ApoD in these lysosomes is necessary and sufficient for restoring lysosomal pH to normal values after oxidation-dependent alkalinization, as confirmed by the stably alkalinized PQ-challenged ApoD-KO cells. This result holds for cells that endogenously express ApoD, like astrocytes, and for non-expressing cells exogenously supplied with ApoD, like neurons.

Lysosomal alkalinization is known to result from ROS-induced membrane permeabilization [178], and we find clear signs of lysosomal dysfunction and membrane permeabilization in ApoD-KO lysosomes (Chapter 2, Figs. 24 and 25) together with high levels of lipid peroxidation that can be counteracted only in the

presence of ApoD expression (Chapter 2, Fig. 23). Complex processes like bidirectional protein traffic along the endosome-lysosome compartments, can result in pH changes similar to the observed ones and should not be completely discarded. However, our current knowledge of the biochemical properties of ApoD, its lipid binding properties (preserved at acid pH in the range of ApoD-positive lysosomes; Chapter 2, Figs. 18 and 19), and its membrane association, including lysosomal membranes (Chapter 2, Fig. 17) lead to a most parsimonious mechanistic hypothesis for the lysosomal pH changes induced by ApoD. As a lipid peroxidation counteracting agent [179], ApoD restores the integrity of damaged lysosomal membranes.

It is of special interest to compare the beneficial repair of lysosomal function by ApoD with the effects of other extracellular lipid binding proteins known to have effects on lysosomes. The Lipocalin Lcn2 reduces lysosomal degradative activity, resulting in insulin resistance in cardiomyoblasts [180]. Apolipoprotein E (also expressed by astrocytes and consistently related to neurodegenerative phenotypes) has deleterious effects on lysosomal function, as the ApoE4 allele causes lysosomal leakage and apoptosis [181].

That ApoD helps to maintain H^+ gradients under oxidative stress in glial and neuronal lysosomes is a finding with high explanatory value in the understanding ApoD function. Lysosomal dysfunction does compromise cell resistance to oxidative stress, the major phenotypic hallmarks of all loss-of-function manipulations performed so far with ApoD and its related Lipocalins in animal models and cellular systems [42, 60, 176, 182, 183]. Moreover, a failure of lysosomal function is linked to inefficient toxic protein clearance in proteinopathies like SCA1 that ultimately leads to cell death and neurodegeneration. This study explains why neurodegeneration rescue by GLaz depends on the lysosome-autophagosome fusion (Chapter 5, Fig. 40), but also why phagocytosis resolution in astrocytes (Chapter 4, Fig. 30) and after PNS injury [142] is compromised. Interestingly, a recent report shows a similar delay in clearing myelin from injured nerves when lysosomal function is inhibited [184].

Summarizing, although previously considered to play a lipid transport function in various body fluids, the Lipocalin ApoD could now be recognized as a relevant acute

phase protein contributing to the nervous system response to stress, injury, neurodegeneration and aging by stabilizing the membrane of vulnerable lysosomes.

2. Study of extracellular vesicles derived from astroglia and its neuroprotection role on oxidative stress.

Besides a role in cell-cell communication during cellular homeostatis, extracellular vesicles are sheded by cells in response to pathological states (reviewed by [185, 186]). In the nervous system, glial EVs have been involved both in regulation of neuroinflammation [187-189], and in mechanisms triggering neuroprotection [190, 191].

The production of reactive oxygen species (ROS) and a concomitant inflammatory response have been classically considered a negative side-effect of tissue damage that hampers nervous system recovery upon aging and neurodegeneration. Consequently, great efforts have been made to identify antioxidants that can mediate neuroprotection through improvement of neuronal survival and axonal regeneration. However, a recent report has demonstrated that ROS can also play a positive pro-regenerative role upon neural damage by a mechanism based on glia-neuron EV-mediated Nox2-PI3K–pAkt signaling [192]. How can a cell control the side effects of ROS, and the levels that can be managed without tilting the equilibrium towards cell-death?

The Lipocalin ApoD has been demonstrated to be a neuroprotectant by controlling the levels of lipid peroxides (Chapter 2, Fig. 23) generated by ROS accumulation with aging or pathological conditions [42, 176, 182]. The neuroprotection exerted by ApoD not only influences ApoD-expressing cells such as astrocytes and myelinating glia, but also affects neurons in a paracrine manner (Chapter 2, Fig.22). The presence of a signal peptide in the unprocessed protein and the experimentally verified presence of the mature protein in organelles of the canonical secretion pathway (Chapter1. Fig 8) and in the extracellular milieu result in the annotation of ApoD as a secreted protein (UniProtKB-P51910/P05090). This property was assumed in the interpretation of our previous studies reporting ApoD trafficking in astrocytes and neurons under control or OS conditions (Chapter 2, Fig. 21).

The results presented in this work link ApoD trafficking to the extracellular vesicle compartment of astrocytes, where it appears as a very specific marker of the exosomal subtype of EVs (Chapter 3, Fig. 29) in comparison to classical exosome markers such as CD81 [193]. More importantly, the neuroprotective effect that ApoD exerts upon OS-challenged neurons must be entirely based on the protein present in the exosomes supplied by reactive astrocytes (Chapter 3, Fig. 33), since no incorporation of astrocyte-derived ApoD is detected when EVs have been removed from the astrocyte-conditioned medium.

This result agrees with other reports showing that non-neural cells exposed to ROS release EVs that carry OS response proteins and antioxidants [194, 195]. The fact that exosome-associated human ApoD is detected both as monomer and dimer (Chapter 3, Fig. 29), is a readout of its antioxidant activity, since it is known that a consequence of its lipid reducing activity is the formation of stable dimers [179], that have been found to accumulate in advanced stages of Alzheimer disease patients [196]. Since we know that the 1321N1 astrocytic cell line has a basal level of OS (Chapter 2, Fig. 23), it is not surprising that they are already targeting the redox pair reduced/oxidated-ApoD in exosomes.

Our results showing a lower concentration of EVs recovered from ApoD-KO astrocyte cultures are intriguing, but more work needs to be done to ascertain whether ApoD directly affects EV biogenesis in a direct manner. ApoD protection of membranes of the endolysosomal system (Chapter 2) might certainly condition the process of EV biogenesis. Also, we have recently discovered that ApoD protection mechanism is linked to the glycosylation state of membranes, by controlling the level of sialylated glycolipids and glycoproteins (Chapter 4, Fig. 36). Interestingly, EVs have been shown to bear distinctive glycan features [197]. Alternatively, a generally altered physiological state of ApoD-KO astrocytes might condition their EV production.

In summary, the discovery of ApoD in glia-derived EVs, and particularly in exosomes, reframes our understanding of the neuroprotective role of this Lipocalin. The capability of EVs to cross the blood-brain barrier [104] opens up new research

avenues to explore the use of systemically administered ApoD-positive exosomes to treat neurodegenerative diseases.

3. Functional consequences of ApoD glycocalyx management in health and disease.

Our data brings an unexpected key element to the already complex process of myelin biogenesis: ApoD, a lipid binding protein expressed by myelinating glia, whose function in the lysosomal compartment is required for the functional integrity of these intracellular organelles (Chapter 2, Figs. 24 and 25).

These data strongly support the following model. When ApoD is missing, glial lysosomes are partially permeabilized and two primary consequences follow: (1) lysosomal enzymes delocalize and/or are out of their optimal pH for efficient activity and (2) lysosome-myelin trafficking becomes dysfunctional. These primary defects may result in inefficient desialylation of glycoproteins by lysosomal Neu1, and inefficient trafficking of membrane Neu3, leading to an accumulation of sialylated glycolipids (gangliosides). The inability to remove the hydrophilic glycocalyx from the outer surface of myelin results in a very specific (only the IPL is affected), but generalized compaction defect that persists throughout life.

These defects in myelin glycocalyx removal eventually prevent completion of the extracellular leaflet compaction process. Our data support that two separate processes, the removal of repulsive structures and the expression of adhesive proteins to "lock the zip" (as proposed by [166]), can be dissociated. Thus, glycocalyx removal becomes a limiting factor for the completion of compact myelin.

Various functional consequences derive from the ApoD-KO "unfinished" myelin: (1) peripheral nerves decrease their conduction velocity by 40 weeks of age, without alterations in compound action potential amplitude or duration [55] and (2) cerebellum-dependent motor learning is compromised, without general locomotor deficits or alterations in other cognitive processes in the young adult (e.g., hippocampus-dependent object recognition tasks, [182]). Cognitive and motor deficits

do appear later upon further aging in ApoD-KO [42, 55, 182], suggesting defective myelin vulnerability to age-dependent deterioration.

Fyn kinase is also altered by the myelin recycling defect and gets anomalously enriched in PNS compact myelin domains. This finding is coherent with a specific alteration in lysosome-dependent (versus recycling endosome-dependent) myelin remodeling, and supports the proposal made by White and Kramer-Albers [171] for the CNS: Fyn could be a mediator between axonal signals and the lysosome-mediated traffic leading to a correct location of proteins in compact myelin. Particularly, Plp recycling is regulated by the small GTPase RhoA in response to axon signals [198, 199], and Fyn kinase is known to function upstream of RhoA (reviewed by [171, 200]). Furthermore, the effect of ApoD on Fyn subcellular localization in the PNS suggests that this membrane-bound kinase does traffic to and from myelin membrane, and predicts changes in downstream events, depending on its compartmentalization in membranes with different lipid-based structures [201].

The fact that ApoD is not present in peroxisomes (Fig 15G), also supports the specificity of the lysosome-dependent trafficking defects observed. Unlike in ApoD-KO mice, peroxisomal defective Schwann cells build myelin sheaths with unaltered thickness or periodicity [202], and a dysfunction of peroxisomes secondarily produces functional deficits in axons, with alterations in the amplitude of compound action potentials recorded both *ex vivo* and *in vivo*. This deficit neither is present in ApoD-KO nerves [55], nor we observe signs of axonal degeneration or damage in our EM analysis. Thus, the functional consequences of ApoD deficiency are restricted to the extracellular leaflet compaction defect, leaving ganglioside-enriched hydrophilic spaces that alter the insulating properties of myelin.

A major conclusion revealed by our findings is that a lipid binding protein of the Lipocalin family, typically described as lipid transporters, ultimately controls the glycocalyx of cells thanks to the maintenance of healthy lysosomal membranes, which conditions sialidases location and activity. An excessive glycocalyx results in a functionally suboptimal myelin cover, both in CNS and PNS.

Our current understanding of ApoD role in lysosome-mediated control of myelin glycocalyx provides new insights for understanding nerve injury progression: it would take longer to desialylate and opsonize a hypersialylated myelin and, once incorporated into the phagocytic cell, suboptimal lysosomal function would hinder myelin degradation by macrophages [56] as well as astrocytes (Chapter 4, Figs. 34 and 35).

4. Apolipoprotein D-mediated regulation of lysosomal membrane integrity preserves lysosomal function and promotes cell survival in Niemann-Pick Type A disease.

The Niemann-Pick type A disease is characterized by a mutation of the acid sphingomyelinase, which causes an accumulation of sphingomyelin in all cell membranes and a blocking in the degradation process. This accumulation of sphingomyelin is responsible for the modification of the permeability and basification of lysosomes and, as a consequence, a decrease in their function and cellular metabolic activity (Chapter 5, Fig. 45).

To date, many results describing NPA disease have been published [203]. However, it is the first time that it is described how the addition of a substance, in this case the protein ApoD, can improve the disease by reversing the effects of the accumulation of sphingomyelinat the cellular level. Our results reveal that ApoD protection of lysosomal integrity (Chapter 5, Figs. 43 and 44) is able to counteract biological deterioration in NPA cells, and open therapeutic opportunities for this devastating disease. Although many studies are needed to confirm the improvement of patients before this possible treatment, we could be at the beginning of finding an effective treatment against this disease. Althought, the evidence supports ApoD as an endogenous mechanism of protection, in the conditions in which that overexpression fails as a mechanism of neuroprotection, adding ApoD exogenously could solve the problem. And like any substance that is added exogenously, we will have to control the concentrations, since high amounts of ApoD could be harmful [38].

Understanding ApoD actions in lysosomes will open the possibility of developing a mechanism for therapeutic purposes. Using ApoD as a carrier to reach the lysosome,

not only helps NPA disease cells, but others neurodegenerative diseases such as proteinopathies could benefit from these studies.

5. The functionality of the lysosome as the core of ApoD membrane-management jobs.

When lysosomal dysfunction is the primary defect, it is not surprising that myelin defects follow, as it is the case in all lysosomal storage diseases known so far [204]. Thus, our reports on the cellular and molecular mechanisms of ApoD function should have important implications for the understanding of lysosomal storage diseases. They open the possibility for ApoD-based therapies for lysosomal diseases of diverse etiology.

Other pathological conditions in which cell membranes are hyperglycosylated might have two distinct outcomes. For cells like astrocytes, dealing with oxidative stress protective responses in the brain, a proper regulation of glycocalyx extent might contribute to their resilience. However, for phagocytic cells (microglia, Schwann cells after injury, or infiltrating macrophages), hypersialylated membranes might represent a problem.

Nomura et al. [205] have recently shown that when activated microglia are presented with dying or stressed neurons, they produce sialidases. Desialylation of membranes enables Galectin-3 (also produced by phagocytic microglia and Schwann cells) to bind and opsonize cells or cell parts (e.g., synapses), "marking" them for phagocytosis. Shahraz et al. [206] were able to control the extent of macrophage inflammatory response and oxidative outburst by using soluble polysialic chains as competitors of the sialylated glycocalyx of cellular debris from dying neurons.

Taking into account our current results, the mechanistic link between different apparently unrelated biological processes is clear: The direct control by ApoD of lysosomal function efficiency (Fig 47).
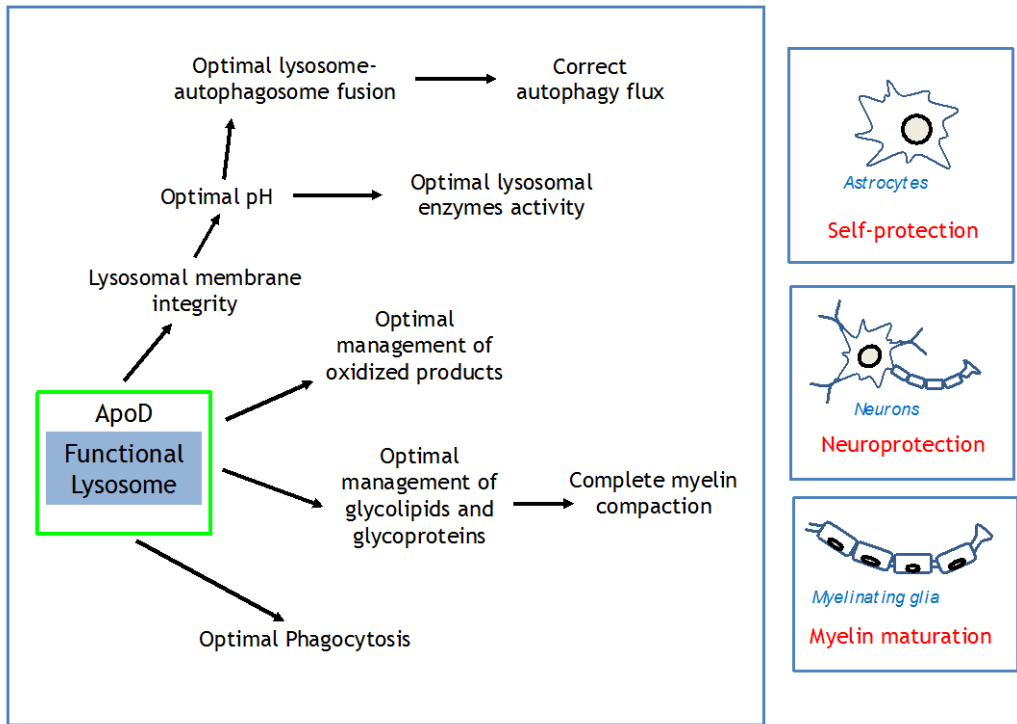
Figure. 47. A global view of ApoD membrane-management jobs. *ApoD acts through the maintenance of lysosome functionality, allowing maintenance of the integrity of lysosomal membrane, an optimal management of oxidized products, glycolipids and glycoproteins. All this would allow maintaining a correct flow of autophagy, an optimal lysosomal enzymes activity. Therefore, ApoD, through the control of the lysosomal function, will influence neuroprotection, as well as the maturation of myelin.*

In summary, in addition to the role for ApoD in myelin compaction, our data suggest that hypersialylated cells in the nervous system would condition phagocytosis efficiency not only upon injury or disease (where myelin phagocytosis is a limiting factor for axonal regeneration), but in normal conditions. Our plastic brain, where phagocytosis of excess neurons or synapses is paramount to normal development and influences whole life learning and memory, requires a fine control of the glycocalyx. ApoD contribution to such a control opens new research avenues to explore in the future. Moreover, we have reported a protective role for ApoD in the functional recovery of injured mammalian peripheral nerves by a mechanism regulating myelin phagocytosis efficiency [142] and the complete myelin compaction.

Conclusions

This thesis demonstrates that:

1. The lipid binding protein ApoD is endocytosed and targeted in a finely controlled way to subsets of lysosomes.

2. ApoD contributes significantly to the evolutionarily conserved mechanism of protecting cells by protecting their lysosomes. ApoD could be the first lysosomal marker known to be specific for a particular subset of lysosomes: the most vulnerable to oxidative stress.

3. The stable presence of ApoD in lysosomes is sufficient and necessary for lysosomes to recover from oxidation-induced membrane permeabilization and loss of proton gradients.

4. PQ promotes the entry of ApoD into lysosomes within a cell that expresses it, only to the lysosomes of the intermediate and external regions, while the perinuclear lysosomes are depleted of ApoD.

5. ApoD is present in glial-derived EVs and contributes, in this cell-cell communication format, to improve neuronal viability and function.

6. Hypersialylation in the absence of ApoD is a mechanism that can be generalized to ApoD-expressing glial cells, and targeting ApoD to lysosomes is sufficient for glial cells to control their glycocalyx. We need healthy lysosomes for the biogenesis of a healthy myelin and for myelin management upon injury or disease, and ApoD contributes significantly to both goals.

7. ApoD is a good candidate for the treatment of neurodegenerative diseases in which the lysosome is involved, such as: SCA1 and NPA.

8. ApoD neuroprotection mechanism in the neurodegeneration in SCA1 models depends on lysosome-phagosome fusion in vivo

9. Exogenously added ApoD is able to significantly reduce lysosomal permeabilization and NPA-promoted lysosomal alkalinization. ApoD addition reverts the accumulation of oxidized products in lysosomes and of lipid peroxidation in NPA cells, resulting in a significant increase in cell survival.

10. ApoD-mediated control of lysosomal membrane integrity represents a new cell protection mechanism at the hub of many cellular functions, and is critical for the outcome of a wide variety of neurodegenerative diseases.

References

1.   Do Carmo, S., et al., Neuroprotective effect of apolipoprotein D against human coronavirus OC43-induced encephalitis in mice. J Neurosci, 2008. 28(41): p. 10330-8.

2.   McConathy, W.J. and P. Alaupovic, Isolation and partial characterization of apolipoprotein D: a new protein moiety of the human plasma lipoprotein system. FEBS Lett, 1973. 37(2): p. 178-82.

3.   Rassart, E., et al., Apolipoprotein D. Biochim Biophys Acta, 2000. 1482(1-2): p. 185-98.

4.   Goessling, W. and S.D. Zucker, Role of apolipoprotein D in the transport of bilirubin in plasma. Am J Physiol Gastrointest Liver Physiol, 2000. 279(2): p. G356-65.

5.   Drayna, D., et al., Cloning and expression of human apolipoprotein D cDNA. J Biol Chem, 1986. 261(35): p. 16535-9.

6.   Sanchez, D., et al., Loss of glial lazarillo, a homolog of apolipoprotein D, reduces lifespan and stress resistance in Drosophila. Curr Biol, 2006. 16(7): p. 680-6.

7.   Flower, D.R., A.C. North, and C.E. Sansom, The lipocalin protein family: structural and sequence overview. Biochim Biophys Acta, 2000. 1482(1-2): p. 9-24.

8.   Gasymov, O.K., A.R. Abduragimov, and B.J. Glasgow, pH-Dependent conformational changes in tear lipocalin by site-directed tryptophan fluorescence. Biochemistry, 2010. 49(3): p. 582-90.

9.   Ganfornina, M.D., et al., A phylogenetic analysis of the lipocalin protein family. Mol Biol Evol, 2000. 17(1): p. 114-26.

10.   Seppala, M., et al., Glycosylation related actions of glycodelin: gamete, cumulus cell, immune cell and clinical associations. Hum Reprod Update, 2007. 13(3): p. 275-87.

11.   Wester, L., et al., Carbohydrate groups of alpha1-microglobulin are important for secretion and tissue localization but not for immunological properties. Glycobiology, 2000. 10(9): p. 891-900.

12.   Ruiz, M., et al., Lipid-binding properties of human ApoD and Lazarillo-related lipocalins: functional implications for cell differentiation. FEBS J, 2013. 280(16): p. 3928-43.

13.   Sanchez, D., et al., Molecular interactions of the neuronal GPI-anchored lipocalin Lazarillo. J Mol Recognit, 2008. 21(5): p. 313-23.

14.   Eichinger, A., et al., Structural insight into the dual ligand specificity and mode of high density lipoprotein association of apolipoprotein D. J Biol Chem, 2007. 282(42): p. 31068-75.

15.   Yang, C.Y., et al., Structure of human apolipoprotein D: locations of the intermolecular and intramolecular disulfide links. Biochemistry, 1994. 33(41): p. 12451-5.

16.   Morais Cabral, J.H., et al., Arachidonic acid binds to apolipoprotein D: implications for the protein's function. FEBS Lett, 1995. 366(1): p. 53-6.

17.   Breustedt, D.A., D.L. Schonfeld, and A. Skerra, Comparative ligand-binding analysis of ten human lipocalins. Biochim Biophys Acta, 2006. 1764(2): p. 161-73.

18.   Ruiz, M., et al., Ligand binding-dependent functions of the lipocalin NLaz: an in vivo study in Drosophila. FASEB J, 2013. 28(4): p. 1555-67.

19.   Schindler, P.A., et al., Site-specific detection and structural characterization of the glycosylation of human plasma proteins lecithin:cholesterol acyltransferase and apolipoprotein D using HPLC/electrospray mass spectrometry and sequential glycosidase digestion. Protein Sci, 1995. 4(4): p. 791-803.

20.   Zeng, C., et al., A human axillary odorant is carried by apolipoprotein D. Proc Natl Acad Sci U S A, 1996. 93(13): p. 6626-30.

21.   Seguin, D., M. Desforges, and E. Rassart, Molecular characterization and differential mRNA tissue distribution of mouse apolipoprotein D. Brain Res Mol Brain Res, 1995. 30(2): p. 242-50.

22.   Ganfornina, M.D., et al., Molecular characterization and developmental expression pattern of the chicken apolipoprotein D gene: implications for the evolution of vertebrate lipocalins. Dev Dyn, 2005. 232(1): p. 191-9.

23.   Navarro, A., E. Del Valle, and J. Tolivia, Differential expression of apolipoprotein d in human astroglial and oligodendroglial cells. J Histochem Cytochem, 2004. 52(8): p. 1031-6.

24.   Loerch, P.M., et al., Evolution of the aging brain transcriptome and synaptic regulation. PLoS One, 2008. 3(10): p. e3329.

25.   Sanchez, D., M.D. Ganfornina, and S. Martinez, Expression pattern of the lipocalin apolipoprotein D during mouse embryogenesis. Mech Dev, 2002. 110(1-2): p. 225-9.

26.   Boyles, J.K., L.M. Notterpek, and L.J. Anderson, Accumulation of apolipoproteins in the regenerating and remyelinating mammalian peripheral nerve. Identification of apolipoprotein D, apolipoprotein A-IV, apolipoprotein E, and apolipoprotein A-I. J Biol Chem, 1990. 265(29): p. 17805-15.

27.   Schaeren-Wiemers, N., et al., Identification of new oligodendrocyte- and myelin-specific genes by a differential screening approach. J Neurochem, 1995. 65(1): p. 10-22.

28.   Verheijen, M.H., et al., Local regulation of fat metabolism in peripheral nerves. Genes Dev, 2003. 17(19): p. 2450-64.

29.   Ong, W.Y., et al., Apolipoprotein D gene expression in the rat brain and light and electron microscopic immunocytochemistry of apolipoprotein D expression in the cerebellum of neonatal, immature and adult rats. Neuroscience, 1999. 90(3): p. 913-22.

30.   Ganfornina, M.D., D. Sanchez, and M.J. Bastiani, Lazarillo, a new GPI-linked surface lipocalin, is restricted to a subset of neurons in the grasshopper embryo. Development, 1995. 121(1): p. 123-34.

31.   Sanchez, D., M.D. Ganfornina, and M.J. Bastiani, Contributions of an orthopteran to the understanding of neuronal pathfinding. Immunol Cell Biol, 1995. 73(6): p. 565-74.

32.   Sanchez, D., et al., Characterization of two novel lipocalins expressed in the Drosophila embryonic nervous system. Int J Dev Biol, 2000. 44(4): p. 349-59.

33.   del Caño-Espinel, M., et al., Lazarillo-related Lipocalins confer long-term protection against type I Spinocerebellar Ataxia degeneration contributing to optimize selective autophagy. Mol Neurodegener, 2015. 10: p. 11.

34.   Ruiz, M., Lazarillo and related Lipocalins: ligands and functions., in Bioquímica y Biología Molecular y Fisiología. 2013, University of Valladolid: Valladolid.

35.   Thomas, E.A. and J.K. Yao, Clozapine specifically alters the arachidonic acid pathway in mice lacking apolipoprotein D. Schizophr Res, 2007. 89(1-3): p. 147-53.

36.   Thomas, E.A., R.C. George, and J.G. Sutcliffe, Apolipoprotein D modulates arachidonic acid signaling in cultured cells: implications for psychiatric disorders. Prostaglandins Leukot Essent Fatty Acids, 2003. 69(6): p. 421-7.

37.   Ordonez, C., et al., Apolipoprotein D expression in substantia nigra of Parkinson disease. Histol Histopathol, 2006. 21(4): p. 361-6.

38.   Bajo-Grañeras, R., et al., Expression and potential role of apolipoprotein D on the death-survival balance of human colorectal cancer cells under oxidative stress conditions. Int J Colorectal Dis, 2013. 28(6): p. 751-66.

39.   Ong, W.Y., C.Y. Hu, and S.C. Patel, Apolipoprotein D in the Niemann-Pick type C disease mouse brain: an ultrastructural immunocytochemical analysis. J Neurocytol, 2002. 31(2): p. 121-9.

40.   Dassati, S., A. Waldner, and R. Schweigreiter, Apolipoprotein D takes center stage in the stress response of the aging and degenerative brain. Neurobiol Aging, 2014. 35(7): p. 1632-42.

41.   Wang, L., et al., Characterization and expression of amphioxus ApoD gene encoding an archetype of vertebrate ApoD proteins. Cell Biol Int, 2007. 31(1): p. 74-81.

42.   Ganfornina, M.D., et al., Apolipoprotein D is involved in the mechanisms regulating protection from oxidative stress. Aging Cell, 2008. 7(4): p. 506-15.

43.   Bajo-Grañeras, R., et al., Apolipoprotein D mediates autocrine protection of astrocytes and controls their reactivity level, contributing to the functional maintenance of paraquat-challenged dopaminergic systems. Glia, 2011. 59(10): p. 1551-66.

44.   Fernandez-Funez, P., et al., Identification of genes that modify ataxin-1-induced neurodegeneration. Nature, 2000. 408(6808): p. 101-6.

45.   Heng, M.Y., et al., Early alterations of autophagy in Huntington disease-like mice. Autophagy. 6(8): p. 1206-8.

46.   Jimenez-Palomares, M., et al., Genetic deficiency of apolipoprotein D in the mouse is associated with nonfasting hypertriglyceridemia and hyperinsulinemia. Metabolism, 2011. 60(12): p. 1767-74.

47.   Wang, X. and E.K. Michaelis, Selective neuronal vulnerability to oxidative stress in the brain. Front Aging Neurosci, 2010. 2: p. 12.

48.   Adibhatla, R.M. and J.F. Hatcher, Altered lipid metabolism in brain injury and disorders. Subcell Biochem, 2008. 49: p. 241-68.

49.   Martin, L.J., et al., Neurodegeneration in excitotoxicity, global cerebral ischemia, and target deprivation: A perspective on the contributions of apoptosis and necrosis. Brain Res Bull, 1998. 46(4): p. 281-309.

50.   Stadtman, E.R., et al., Methionine oxidation and aging. Biochim Biophys Acta, 2005. 1703(2): p. 135-40.

51.   Shringarpure, R., et al., Ubiquitin conjugation is not required for the degradation of oxidized proteins by proteasome. J Biol Chem, 2003. 278(1): p. 311-8.

52.   Bus, J.S. and J.E. Gibson, Paraquat: model for oxidant-initiated toxicity. Environ Health Perspect, 1984. 55: p. 37-46.

53.   Bajo-Graneras, R., Estudio de los mecanismos moleculares y celulares de la función protectora de la Apolipoproteína D, in Bioquímica y Biología Molecular y Fisiología. 2012, University of Valladolid: Valladolid.

54.   Oakley, A.J., et al., Molecular dynamics analysis of apolipoprotein-D-lipid hydroperoxide interactions: mechanism for selective oxidation of Met-93. PLoS One, 2012. 7(3): p. e34057.

55.   Ganfornina, M.D., et al., ApoD, a glia-derived apolipoprotein, is required for peripheral nerve functional integrity and a timely response to injury. Glia, 2010. 58(11): p. 1320-34.

56.   Garcia-Mateo, N., et al., Schwann cell-derived Apolipoprotein D controls the dynamics of post-injury myelin recognition and degradation. Front Cell Neurosci, 2014. 8: p. 374.

57.   Garcia-Mateo, N., et al., Myelin extracellular leaflet compaction requires apolipoprotein D membrane management to optimize lysosomal-dependent recycling and glycocalyx removal. Glia, 2017.

58.   Najyb, O., L. Brissette, and E. Rassart, Apolipoprotein D Internalization Is a Basigin-dependent Mechanism. J Biol Chem, 2015. 290(26): p. 16077-87.

59.   Do Carmo, S., L.C. Levros, Jr., and E. Rassart, Modulation of apolipoprotein D expression and translocation under specific stress conditions. Biochim Biophys Acta, 2007. 1773(6): p. 954-69.

60.   Bajo-Grañeras, R., et al., Apolipoprotein D mediates autocrine protection of astrocytes and controls their reactivity level, contributing to the functional maintenance of paraquat-challenged dopaminergic systems. Glia, 2011. 59(10): p. 1551-66.

61.   Del Caño-Espinel, M., Relación de la Apolipoproteína D y sus homólogos en Drosophila con las membranas biológicas. Estudio de su función en diferentes procesos celulares y de su localización y efectos sobre las balsas lipídicas., in

Bioquímica y Biología Molecular y Fisiología. 2015, University of Valladolid: Valladolid.

62.   Pike, L.J., Lipid rafts: bringing order to chaos. J Lipid Res, 2003. 44(4): p. 655-67.

63.   Kirkham, M. and R.G. Parton, Clathrin-independent endocytosis: new insights into caveolae and non-caveolar lipid raft carriers. Biochim Biophys Acta, 2005. 1746(3): p. 349-63.

64.   Becker , K.L.J., Bertoni G. and Hardin J., The world of the cell. 9th ed. 2015: Pearson.

65.   Alberts B., J.A., Lewis J., Raff M., Roberts K., and Walter P., Molecular Biology of the cell. 4th ed. Garland Science. 2002.

66.   Beller, M., et al., Lipid droplets: a dynamic organelle moves into focus. FEBS Lett, 2010. 584(11): p. 2176-82.

67.   Glick, B.S. and A. Luini, Models for Golgi traffic: a critical assessment. Cold Spring Harb Perspect Biol, 2011. 3(11): p. a005215.

68.   Smith, J.J. and J.D. Aitchison, Peroxisomes take shape. Nat Rev Mol Cell Biol, 2013. 14(12): p. 803-17.

69.   Kiefel, B.R., P.R. Gilson, and P.L. Beech, Cell biology of mitochondrial dynamics. Int Rev Cytol, 2006. 254: p. 151-213.

70.   Klumperman, J. and G. Raposo, The complex ultrastructure of the endolysosomal system. Cold Spring Harb Perspect Biol, 2014. 6(10): p. a016857.

71.   Stoorvogel, W., V. Oorschot, and H.J. Geuze, A novel class of clathrin-coated vesicles budding from endosomes. J Cell Biol, 1996. 132(1-2): p. 21-33.

72.   Dikeakos, J.D. and T.L. Reudelhuber, Sending proteins to dense core secretory granules: still a lot to sort out. J Cell Biol, 2007. 177(2): p. 191-6.

73.   Cabrera, M. and C. Ungermann, Guiding endosomal maturation. Cell, 2010. 141(3): p. 404-6.

74.   Tanida, I., Autophagosome formation and molecular mechanism of autophagy. Antioxid Redox Signal, 2011. 14(11): p. 2201-14.

75. Neefjes, J., M.M.L. Jongsma, and I. Berlin, Stop or Go? Endosome Positioning in the Establishment of Compartment Architecture, Dynamics, and Function. Trends Cell Biol, 2017. 27(8): p. 580-594.

76. Thery, C., Exosomes: secreted vesicles and intercellular communications. F1000 Biol Rep, 2011. 3: p. 15.

77. DiCiccio, J.E. and B.E. Steinberg, Lysosomal pH and analysis of the counter ion pathways that support acidification. J Gen Physiol, 2011. 137(4): p. 385-90.

78. Sorkin, A. and M. von Zastrow, Endocytosis and signalling: intertwining molecular networks. Nat Rev Mol Cell Biol, 2009. 10(9): p. 609-22.

79. Hohn, A. and T. Grune, Lipofuscin: formation, effects and role of macroautophagy. Redox Biol, 2013. 1: p. 140-4.

80. Boya, P. and G. Kroemer, Lysosomal membrane permeabilization in cell death. Oncogene, 2008. 27(50): p. 6434-51.

81. Monti, E. and T. Miyagi, Structure and Function of Mammalian Sialidases. Top Curr Chem, 2015. 366: p. 183-208.

82. Li, J. and S.R. Pfeffer, Lysosomal membrane glycoproteins bind cholesterol and contribute to lysosomal cholesterol export. Elife, 2016. 5.

83. Shen, H.M. and N. Mizushima, At the end of the autophagic road: an emerging understanding of lysosomal functions in autophagy. Trends Biochem Sci, 2013. 39(2): p. 61-71.

84. Appelqvist, H., et al., The lysosome: from waste bag to potential therapeutic target. J Mol Cell Biol, 2013. 5(4): p. 214-26.

85. Huynh, C., et al., Defective lysosomal exocytosis and plasma membrane repair in Chediak-Higashi/beige cells. Proc Natl Acad Sci U S A, 2004. 101(48): p. 16795-800.

86. McNeil, P.L. and T. Kirchhausen, An emergency response team for membrane repair. Nat Rev Mol Cell Biol, 2005. 6(6): p. 499-505.

87. Blott, E.J. and G.M. Griffiths, Secretory lysosomes. Nat Rev Mol Cell Biol, 2002. 3(2): p. 122-31.

88. Hussain, M.M., Structural, biochemical and signaling properties of the low-density lipoprotein receptor gene family. Front Biosci, 2001. 6: p. D417-28.

89.   Schmitz, G. and G. Muller, Structure and function of lamellar bodies, lipid-protein complexes involved in storage and secretion of cellular lipids. J Lipid Res, 1991. 32(10): p. 1539-70.

90.   Romagnoli, G.G., et al., Dendritic Cell-Derived Exosomes may be a Tool for Cancer Immunotherapy by Converting Tumor Cells into Immunogenic Targets. Front Immunol, 2015. 5: p. 692.

91.   Fevrier, B., et al., Cells release prions in association with exosomes. Proc Natl Acad Sci U S A, 2004. 101(26): p. 9683-8.

92.   Valadi, H., et al., Exosome-mediated transfer of mRNAs and microRNAs is a novel mechanism of genetic exchange between cells. Nat Cell Biol, 2007. 9(6): p. 654-9.

93.   Basso, M. and V. Bonetto, Extracellular Vesicles and a Novel Form of Communication in the Brain. Front Neurosci, 2016. 10: p. 127.

94.   Fruhbeis, C., et al., Extracellular vesicles as mediators of neuron-glia communication. Front Cell Neurosci, 2013. 7: p. 182.

95.   Kramer-Albers, E.M., et al., Oligodendrocytes secrete exosomes containing major myelin and stress-protective proteins: Trophic support for axons? Proteomics Clin Appl, 2007. 1(11): p. 1446-61.

96.   Kalra, H., et al., Vesiclepedia: a compendium for extracellular vesicles with continuous community annotation. PLoS Biol, 2012. 10(12): p. e1001450.

97.   Keerthikumar, S., et al., ExoCarta: A Web-Based Compendium of Exosomal Cargo. J Mol Biol, 2015. 428(4): p. 688-692.

98.   Kim, D.K., et al., EVpedia: a community web portal for extracellular vesicles research. Bioinformatics, 2014. 31(6): p. 933-9.

99.   Gyorgy, B., et al., Membrane vesicles, current state-of-the-art: emerging role of extracellular vesicles. Cell Mol Life Sci, 2011. 68(16): p. 2667-88.

100.   Muller, G., Microvesicles/exosomes as potential novel biomarkers of metabolic diseases. Diabetes Metab Syndr Obes, 2012. 5: p. 247-82.

101.   Cheow, E.S., et al., Plasma-derived Extracellular Vesicles Contain Predictive Biomarkers and Potential Therapeutic Targets for Myocardial Ischemic (MI) Injury. Mol Cell Proteomics, 2016. 15(8): p. 2628-40.

102.   Rufino-Ramos, D., et al., Extracellular vesicles: Novel promising delivery systems for therapy of brain diseases. J Control Release, 2017. 262: p. 247-258.

103.   Andras, I.E. and M. Toborek, Extracellular vesicles of the blood-brain barrier. Tissue Barriers, 2016. 4(1): p. e1131804.

104.   Kramer-Albers, E.M., Ticket to Ride: Targeting Proteins to Exosomes for Brain Delivery. Mol Ther, 2017. 25(6): p. 1264-1266.

105.   Pandya, R.S., et al., Therapeutic neuroprotective agents for amyotrophic lateral sclerosis. Cell Mol Life Sci, 2013. 70(24): p. 4729-45.

106.   Spencer, B., et al., A neuroprotective brain-penetrating endopeptidase fusion protein ameliorates Alzheimer disease pathology and restores neurogenesis. J Biol Chem, 2014. 289(25): p. 17917-31.

107.   Bell, B.M., et al., Designer exosomes as next-generation cancer immunotherapy. Nanomedicine, 2015. 12(1): p. 163-9.

108.   Fruhbeis, C., et al., Neurotransmitter-triggered transfer of exosomes mediates oligodendrocyte-neuron communication. PLoS Biol, 2013. 11(7): p. e1001604.

109.   Falcon-Perez, J.M., S.C. Lu, and J.M. Mato, Sub-proteome approach to the knowledge of liver. Proteomics Clin Appl, 2010. 4(4): p. 407-15.

110.   Colombo, M., G. Raposo, and C. Thery, Biogenesis, secretion, and intercellular interactions of exosomes and other extracellular vesicles. Annu Rev Cell Dev Biol, 2014. 30: p. 255-89.

111.   Keller, S., et al., Exosomes: from biogenesis and secretion to biological function. Immunol Lett, 2006. 107(2): p. 102-8.

112.   Yanez-Mo, M., et al., Biological properties of extracellular vesicles and their physiological functions. J Extracell Vesicles, 2015. 4: p. 27066.

113.   Dreyer, F. and A. Baur, Biogenesis and Functions of Exosomes and Extracellular Vesicles. Methods Mol Biol, 2016. 1448: p. 201-16.

114.   Stoorvogel, W., et al., The biogenesis and functions of exosomes. Traffic, 2002. 3(5): p. 321-30.

115.   Johansson, A.C., et al., Regulation of apoptosis-associated lysosomal membrane permeabilization. Apoptosis, 2010. 15(5): p. 527-40.

116. Schwake, M., B. Schroder, and P. Saftig, Lysosomal membrane proteins and their central role in physiology. Traffic, 2013. 14(7): p. 739-48.

117. Nilsson, E., R. Ghassemifar, and U.T. Brunk, Lysosomal heterogeneity between and within cells with respect to resistance against oxidative stress. Histochem J, 1997. 29(11-12): p. 857-65.

118. Cesen, M.H., et al., Lysosomal pathways to cell death and their therapeutic applications. Exp Cell Res, 2012. 318(11): p. 1245-51.

119. Guha, S., et al., Approaches for detecting lysosomal alkalinization and impaired degradation in fresh and cultured RPE cells: evidence for a role in retinal degenerations. Exp Eye Res, 2014. 126: p. 68-76.

120. Coffey, E.E., et al., Lysosomal alkalization and dysfunction in human fibroblasts with the Alzheimer's disease-linked presenilin 1 A246E mutation can be reversed with cAMP. Neuroscience, 2014. 263: p. 111-24.

121. Chen, C.S., Phorbol ester induces elevated oxidative activity and alkalization in a subset of lysosomes. BMC Cell Biol, 2002. 3: p. 21.

122. Stoka, V., V. Turk, and B. Turk, Lysosomal cathepsins and their regulation in aging and neurodegeneration. Ageing Res Rev, 2016.

123. Colacurcio, D.J. and R.A. Nixon, Disorders of lysosomal acidification-The emerging role of v-ATPase in aging and neurodegenerative disease. Ageing Res Rev, 2016.

124. Perez-Canamas, A., et al., Sphingomyelin-induced inhibition of the plasma membrane calcium ATPase causes neurodegeneration in type A Niemann-Pick disease. Mol Psychiatry, 2016. 22(5): p. 711-723.

125. Galehdari, H., R. Tangestani, and S. Ghasemian, New Single Nucleotide Deletion In the SMPD1 Gene Causes Niemann Pick Disease Type A in a Child from Southwest Iran: A Case Report. Iran J Pediatr, 2013. 23(2): p. 233-6.

126. Schuchman, E.H. and R.J. Desnick, Types A and B Niemann-Pick disease. Mol Genet Metab, 2017. 120(1-2): p. 27-33.

127. Gabande-Rodriguez, E., et al., High sphingomyelin levels induce lysosomal damage and autophagy dysfunction in Niemann Pick disease type A. Cell Death Differ, 2014. 21(6): p. 864-75.

128.   Bu, J., et al., Merits of combination cortical, subcortical, and cerebellar injections for the treatment of Niemann-Pick disease type A. Mol Ther, 2012. 20(10): p. 1893-901.

129.   Horinouchi, K., et al., Acid sphingomyelinase deficient mice: a model of types A and B Niemann-Pick disease. Nat Genet, 1995. 10(3): p. 288-93.

130.   Macauley, S.L., et al., Neuropathology of the acid sphingomyelinase knockout mouse model of Niemann-Pick A disease including structure-function studies associated with cerebellar Purkinje cell degeneration. Exp Neurol, 2008. 214(2): p. 181-92.

131.   Marchiq, I., et al., Knock out of the BASIGIN/CD147 chaperone of lactate/H+ symporters disproves its pro-tumour action via extracellular matrix metalloproteases (MMPs) induction. Oncotarget, 2015. 6(28): p. 24636-48.

132.   Granja, S., et al., Gene disruption using zinc finger nuclease technology. Methods Mol Biol, 2014. 1165: p. 253-60.

133.   Krinke, G.J., N. Vidotto, and E. Weber, Teased-fiber technique for peripheral myelinated nerves: methodology and interpretation. Toxicol Pathol, 2000. 28(1): p. 113-21.

134.   Garcia-Mateo, N., Función de la ApolipoproteinaD en la mielinización y en la respuesta al saño en el sistema nerviosa periférico., in Bioquímica y Biología molecular y Fisiolgía. 2013, University of Valladolid: Valladolid.

135.   Nakamura, K., et al., Transiently increased colocalization of vesicular glutamate transporters 1 and 2 at single axon terminals during postnatal development of mouse neocortex: a quantitative analysis with correlation coefficient. Eur J Neurosci, 2007. 26(11): p. 3054-67.

136.   Li, Q., et al., A syntaxin 1, Galpha(o), and N-type calcium channel complex at a presynaptic nerve terminal: analysis by quantitative immunocolocalization. J Neurosci, 2004. 24(16): p. 4070-81.

137.   Manders, E.M.M., V.F. J., and A.J. A., Measurement of co-localization of objects in dual-colour confocal images. Journal of Microscopy Oxford, 1993. 169: p. 375-82.

138.   Baltazar, G.C., et al., Acidic nanoparticles are trafficked to lysosomes and restore an acidic lysosomal pH and degradative function to compromised ARPE-19 cells. PLoS One, 2013. 7(12): p. e49635.

139.   Guha, S., et al., Stimulation of the D5 dopamine receptor acidifies the lysosomal pH of retinal pigmented epithelial cells and decreases accumulation of autofluorescent photoreceptor debris. J Neurochem, 2013. 122(4): p. 823-33.

140.   Liu, J., et al., Cystic fibrosis transmembrane conductance regulator contributes to reacidification of alkalinized lysosomes in RPE cells. Am J Physiol Cell Physiol, 2012. 303(2): p. C160-9.

141.   Liu, J., et al., Restoration of lysosomal pH in RPE cells from cultured human and ABCA4(-/-) mice: pharmacologic approaches and functional recovery. Invest Ophthalmol Vis Sci, 2008. 49(2): p. 772-80.

142.   García-Mateo, N., et al., Schwann cell-derived Apolipoprotein D controls the dynamics of post-injury myelin recognition and degradation. Front Cell Neurosci, 2014. 8: p. 374.

143.   Norton, W.T. and S.E. Poduslo, Myelination in rat brain: method of myelin isolation. J Neurochem, 1973. 21(4): p. 749-57.

144.   Takats, S., et al., Interaction of the HOPS complex with Syntaxin 17 mediates autophagosome clearance in Drosophila. Mol Biol Cell, 2014. 25(8): p. 1338-54.

145.   Diez-Hermano, S., et al., An automated image analysis method to measure regularity in biological patterns: a case study in a Drosophila neurodegenerative model. Mol Neurodegener, 2015. 10: p. 9.

146.   Homewood, C.A., et al., Lysosomes, pH and the anti-malarial action of chloroquine. Nature, 1972. 235(5332): p. 50-2.

147.   Kundra, R. and S. Kornfeld, Asparagine-linked oligosaccharides protect Lamp-1 and Lamp-2 from intracellular proteolysis. J Biol Chem, 1999. 274(43): p. 31039-46.

148.   Dolman, N.J., J.A. Kilgore, and M.W. Davidson, A review of reagents for fluorescence microscopy of cellular compartments and structures, part I: BacMam labeling and reagents for vesicular structures. Curr Protoc Cytom, 2013. Chapter 12: p. Unit 12 30.

149.   Wolfe, D.M., et al., Autophagy failure in Alzheimer's disease and the role of defective lysosomal acidification. Eur J Neurosci, 2013. 37(12): p. 1949-61.

150.   Villeneuve, J., et al., Unconventional secretion of FABP4 by endosomes and secretory lysosomes. J Cell Biol, 2018. 217(2): p. 649-665.

151.   Jaiswal, J.K., N.W. Andrews, and S.M. Simon, Membrane proximal lysosomes are the major vesicles responsible for calcium-dependent exocytosis in nonsecretory cells. J Cell Biol, 2002. 159(4): p. 625-35.

152.   Rodriguez, A., et al., Lysosomes behave as Ca2+-regulated exocytic vesicles in fibroblasts and epithelial cells. J Cell Biol, 1997. 137(1): p. 93-104.

153.   Repnik, U., M. Hafner Cesen, and B. Turk, Lysosomal membrane permeabilization in cell death: concepts and challenges. Mitochondrion, 2014. 19 Pt A: p. 49-57.

154.   Holopainen, J.M., et al., Elevated lysosomal pH in neuronal ceroid lipofuscinoses (NCLs). Eur J Biochem, 2001. 268(22): p. 5851-6.

155.   Aits, S., et al., Sensitive detection of lysosomal membrane permeabilization by lysosomal galectin puncta assay. Autophagy, 2015. 11(8): p. 1408-24.

156.   Cheow, E.S., et al., Plasma-derived Extracellular Vesicles Contain Predictive Biomarkers and Potential Therapeutic Targets for Myocardial Ischemic (MI) Injury. Mol Cell Proteomics, 2015. 15(8): p. 2628-40.

157.   Przybycien-Szymanska, M.M., Y. Yang, and W.W. Ashley, Microparticle derived proteins as potential biomarkers for cerebral vasospasm post subarachnoid hemorrhage. A preliminary study. Clin Neurol Neurosurg, 2016. 141: p. 48-55.

158.   Escola, J.M., et al., Selective enrichment of tetraspan proteins on the internal vesicles of multivesicular endosomes and on exosomes secreted by human B-lymphocytes. J Biol Chem, 1998. 273(32): p. 20121-7.

159.   Pascua-Maestro, R., et al., Protecting cells by protecting their vulnerable lysosomes: Identification of a new mechanism for preserving lysosomal functional integrity upon oxidative stress. PLoS Genet, 2017. 13(2): p. e1006603.

160.   Baker, D.J., et al., Lysosomal and phagocytic activity is increased in astrocytes during disease progression in the SOD1 (G93A) mouse model of amyotrophic lateral sclerosis. Front Cell Neurosci, 2015. 9: p. 410.

161.   Chung, W.S., et al., Astrocytes mediate synapse elimination through MEGF10 and MERTK pathways. Nature, 2013. 504(7480): p. 394-400.

162.   Mills, E.A., et al., Astrocytes phagocytose focal dystrophies from shortening myelin segments in the optic nerve of Xenopus laevis at metamorphosis. Proc Natl Acad Sci U S A, 2015. 112(33): p. 10509-14.

163. Loov, C., et al., Slow degradation in phagocytic astrocytes can be enhanced by lysosomal acidification. Glia, 2015.

164. Siddiqui, T.A., S. Lively, and L.C. Schlichter, Complex molecular and functional outcomes of single versus sequential cytokine stimulation of rat microglia. J Neuroinflammation, 2016. 13(1): p. 66.

165. Simons, M. and J. Trotter, Wrapping it up: the cell biology of myelination. Curr Opin Neurobiol, 2007. 17(5): p. 533-40.

166. Bakhti, M., S. Aggarwal, and M. Simons, Myelin architecture: zippering membranes tightly together. Cell Mol Life Sci, 2014. 71(7): p. 1265-77.

167. Bakhti, M., et al., Loss of electrostatic cell-surface repulsion mediates myelin membrane adhesion and compaction in the central nervous system. Proc Natl Acad Sci U S A, 2013. 110(8): p. 3143-8.

168. Miyagi, T. and K. Yamaguchi, Mammalian sialidases: physiological and pathological roles in cellular functions. Glycobiology, 2012. 22(7): p. 880-96.

169. Kappagantula, S., et al., Neu3 sialidase-mediated ganglioside conversion is necessary for axon regeneration and is blocked in CNS axons. J Neurosci, 2014. 34(7): p. 2477-92.

170. Feldmann, A., et al., Transport of the major myelin proteolipid protein is directed by VAMP3 and VAMP7. J Neurosci, 2011. 31(15): p. 5659-72.

171. White, R. and E.M. Kramer-Albers, Axon-glia interaction and membrane traffic in myelin formation. Front Cell Neurosci, 2014. 7: p. 284.

172. Pascua-Maestro, R., et al., The MTT-formazan assay: Complementary technical approaches and in vivo validation in Drosophila larvae. Acta Histochem, 2018.

173. Johnson, D.E., et al., The position of lysosomes within the cell determines their luminal pH. J Cell Biol, 2016. 212(6): p. 677-92.

174. Li, H., et al., Cerebral Apolipoprotein-D Is Hypoglycosylated Compared to Peripheral Tissues and Is Variably Expressed in Mouse and Human Brain Regions. PLoS One, 2016. 11(2): p. e0148238.

175. Martinez, E., et al., Amyloid-beta25-35 induces apolipoprotein D Synthesis and growth arrest in HT22 hippocampal cells. J Alzheimers Dis, 2012. 30(2): p. 233-44.

176.   Li, H., et al., Apolipoprotein D modulates amyloid pathology in APP/PS1 Alzheimer's disease mice. Neurobiol Aging, 2015. 36(5): p. 1820-33.

177.   Hull-Thompson, J., et al., Control of metabolic homeostasis by stress signaling is mediated by the lipocalin NLaz. PLoS Genet, 2009. 5(4): p. e1000460.

178.   Porter, K., et al., Lysosomal basification and decreased autophagic flux in oxidatively stressed trabecular meshwork cells: implications for glaucoma pathogenesis. Autophagy, 2013. 9(4): p. 581-94.

179.   Bhatia, S., et al., Selective reduction of hydroperoxyeicosatetraenoic acids to their hydroxy derivatives by apolipoprotein D: implications for lipid antioxidant activity and Alzheimer's disease. Biochem J, 2012. 442(3): p. 713-21.

180.   Chan, Y.K., et al., Lipocalin-2 inhibits autophagy and induces insulin resistance in H9c2 cells. Mol Cell Endocrinol, 2016. 430: p. 68-76.

181.   Ji, Z.S., et al., Reactivity of apolipoprotein E4 and amyloid beta peptide: lysosomal stability and neurodegeneration. J Biol Chem, 2006. 281(5): p. 2683-92.

182.   Sanchez, D., et al., Aging without Apolipoprotein D: Molecular and cellular modifications in the hippocampus and cortex. Exp Gerontol, 2015. 67: p. 19-47.

183.   Navarro, J.A., et al., Altered lipid metabolism in a Drosophila model of Friedreich's ataxia. Human Molecular Genetics, 2010. 19(14): p. 2828-2840.

184.   Jang, S.Y., et al., Autophagic myelin destruction by Schwann cells during Wallerian degeneration and segmental demyelination. Glia, 2016. 64(5): p. 730-42.

185.   Holm, M.M., J. Kaiser, and M.E. Schwab, Extracellular Vesicles: Multimodal Envoys in Neural Maintenance and Repair. Trends Neurosci, 2018. 41(6): p. 360-372.

186.   Croese, T. and R. Furlan, Extracellular vesicles in neurodegenerative diseases. Mol Aspects Med, 2018. 60: p. 52-61.

187.   Kumar, A., et al., Microglial-derived microparticles mediate neuroinflammation after traumatic brain injury. J Neuroinflammation, 2017. 14(1): p. 47.

188.   Dickens, A.M., et al., Astrocyte-shed extracellular vesicles regulate the peripheral leukocyte response to inflammatory brain lesions. Sci Signal, 2017. 10(473).

189.   Wu, B., et al., Glutaminase 1 regulates the release of extracellular vesicles during neuroinflammation through key metabolic intermediate alpha-ketoglutarate. J Neuroinflammation, 2018. 15(1): p. 79.

190. Guitart, K., et al., Improvement of neuronal cell survival by astrocyte-derived exosomes under hypoxic and ischemic conditions depends on prion protein. Glia, 2016. 64(6): p. 896-910.

191. Lopez-Verrilli, M.A., F. Picou, and F.A. Court, Schwann cell-derived exosomes enhance axonal regeneration in the peripheral nervous system. Glia, 2013. 61(11): p. 1795-806.

192. Hervera, A., et al., Reactive oxygen species regulate axonal regeneration through the release of exosomal NADPH oxidase 2 complexes into injured axons. Nat Cell Biol, 2018. 20(3): p. 307-319.

193. Tkach, M., J. Kowal, and C. Thery, Why the need and how to approach the functional diversity of extracellular vesicles. Philos Trans R Soc Lond B Biol Sci, 2018. 373(1737).

194. Saeed-Zidane, M., et al., Cellular and exosome mediated molecular defense mechanism in bovine granulosa cells exposed to oxidative stress. PLoS One, 2017. 12(11): p. e0187569.

195. Chettimada, S., et al., Exosome markers associated with immune activation and oxidative stress in HIV patients on antiretroviral therapy. Sci Rep, 2018. 8(1): p. 7227.

196. Bhatia, S., et al., Increased apolipoprotein D dimer formation in Alzheimer's disease hippocampus is associated with lipid conjugated diene levels. J Alzheimers Dis, 2013. 35(3): p. 475-86.

197. Williams, C., et al., Glycosylation of extracellular vesicles: current knowledge, tools and clinical perspectives. J Extracell Vesicles, 2018. 7(1): p. 1442985.

198. Kippert, A., et al., Rho regulates membrane transport in the endocytic pathway to control plasma membrane specialization in oligodendroglial cells. J Neurosci, 2007. 27(13): p. 3560-70.

199. Simons, M. and K. Trajkovic, Neuron-glia communication in the control of oligodendrocyte function and myelin biogenesis. J Cell Sci, 2006. 119(Pt 21): p. 4381-9.

200. Baron, W. and D. Hoekstra, On the biogenesis of myelin membranes: sorting, trafficking and cell polarity. FEBS Lett, 2010. 584(9): p. 1760-70.

201. Kramer, E.M., et al., Compartmentation of Fyn kinase with glycosylphosphatidylinositol-anchored molecules in oligodendrocytes facilitates kinase activation during myelination. J Biol Chem, 1999. 274(41): p. 29042-9.

202. Kleinecke, S., et al., Peroxisomal dysfunctions cause lysosomal storage and axonal Kv1 channel redistribution in peripheral neuropathy. Elife, 2017. 6.

203. Torres, S., et al., Lysosomal and Mitochondrial Liaisons in Niemann-Pick Disease. Front Physiol, 2017. 8: p. 982.

204. Nave, K.A. and H.B. Werner, Myelination of the nervous system: mechanisms and functions. Annu Rev Cell Dev Biol, 2014. 30: p. 503-33.

205. Nomura, K., et al., Activated Microglia Desialylate and Phagocytose Cells via Neuraminidase, Galectin-3, and Mer Tyrosine Kinase. J Immunol, 2017. 198(12): p. 4792-4801.

206. Shahraz, A., et al., Anti-inflammatory activity of low molecular weight polysialic acid on human macrophages. Sci Rep, 2015. 5: p. 16800.

Notes

Aknowledgements

I want to thank all the help I have received over these years and that has allowed me to start and finish this doctoral thesis:

To my scientific parents: Diego and Lola. Thanks for everything, for letting me be part of this great family, for teaching me, for supporting me, and for trusting me. I have learned a lot, in every way. This thesis would not exist if it were not for you. Sorry for all my mistakes. Thank you Lola for the enthusiasm that you transmit to us every day and thanks Diego for putting sensibility in our moments of madness.

And we arrived at the Lazarillo lab. To all those who have shared some of their wisdom with me: Raquel, Mario, Judith, Espe, Bego, Nadia, Manuela, thank you all for your help. To my laboratory technicians, Carmen and Cándido, without whom I would not have been able to survive. Thanks Cándido for those game afternoons. Thanks to Miriam for bringing us new energy to the lab, I hope you do not go crazy about the triangle you've gotten into. And of course thanks to Sergio. We started together and although you are not in the laboratory now, you are part of our family. Thank you for your help and most of all for making us see that statistics can be fun.

To Lola who taught me the NPA world and trusted that ApoD could be a good therapy. To Sonia that helped me during my stay in Montreal and made me feel welcome on the other side of the globe.

We thank C. Sánchez-Vicente, Y. Noriega and A. Martín Muñoz at the IBGM Flow Citometry and Confocal Microscopy Service for technical assistance.

To my family and my sister who have supported me in my doctoral adventure. Thanks to my mother, who instilled in me the eagerness to know, for asking me the why of things and how everything works. I hope you are proud of me. Thanks to Mateo, for coming to our lives and filling them with color. I hope that one day you will realize how you have changed our lives.

And finally Rubén, my editing technician, my confidant,… my life. Thank you very much for coming to my life and changing it completely. For trusting in me and in this thesis more than myself. For accompanying me and giving me support in so many congresses, talks, stays, ... This thesis is more yours than mine. And thanks for giving me that little person who smiles us every day. You're the best thing that ever happened to me. *Maite zaitut (MZI).*

Thanks also to you for taking the time to read this thesis.